Decision Support System for Automated Detection of Glaucoma using Digital Fundus Imagery

Author

SALMAN MEHMOOD KHAN SHERWANI

NUST201362520MCEME35513F

Supervisor

Dr. Mohsin Islam Tiwana

DEPARTMENT OF MECHATRONICS ENGINEERING

COLLEGE OF ELECTRICAL & MECHANICAL ENGINEERING

NATIONAL UNIVERSITY OF SCIENCES AND TECHNOLOGY

ISLAMABAD

December, 2016

Decision Support System for Automated Detection of Glaucoma using Digital Fundus Imagery

Author

SALMAN MEHMOOD KHAN SHERWANI

NUST201362520MCEME35513F

A thesis submitted in partial fulfillment of the requirements for the degree of

MS Mechatronics Engineering

Thesis Supervisor:

Dr. Mohsin Islam Tiwana

Thesis Supervisor's Signature: _____

DEPARTMENT OF MECHATRONICS ENGINEERING

COLLEGE OF ELECTRICAL & MECHANICAL ENGINEERING

NATIONAL UNIVERSITY OF SCIENCES AND TECHNOLOGY, ISLAMABAD

December, 2016

Declaration

I certify that this research work titled "*Decision Support System for Automated Detection of Glaucoma using Digital Fundus Imagery"* is my own work. The work has not been presented elsewhere for assessment. The material that has been used from other sources has been properly acknowledged / referred.

Salman Mehmood Khan Sherwani

2013-NUST-MS-Mts-078

Language Correctness Certificate

This thesis has been read by an English expert and is free of typing, syntax, semantic, grammatical and spelling mistakes. Thesis is also according to the format given by the university.

Salman Mehmood Khan Sherwani
NUST201362520MCEME35513F

Dr. Mohsin Islam Tiwana
(Supervisor)

Copyright Statement

Acknowledgements

I am thankful to my Creator Allah Subhana-Watala to have guided me throughout this work at every step and for every new thought which You setup in my mind to improve it. Indeed I could have done nothing without Your priceless help and guidance. Whosoever helped me throughout the course of my thesis, whether my parents or any other individual was Your will, so indeed none be worthy of praise but You.

I am profusely thankful to my beloved parents who raised me when I was not capable of walking and continued to support me throughout in every department of my life.

I would also like to express special thanks to my supervisor Dr. Mohsin Islam Tiwana for his untiring help throughout my thesis. I am also thankful to Nigel H. Lowell, Fellow IEEE along with my supervisor for rendering an unprecedented support and guidance during the process of paper writing for international conference which ultimately got accepted in July 2015.

I would also like to pay special thanks to Dr. Usman Akram (Department of Computer Engineering) and Dr. Baber Attique (Senior Consultant, Ibrahim Eye Trust, Gujranwala) for their tremendous support and cooperation. Each time I got stuck in something, they came up with the solution. Without their help it wouldn't have been possible for me to complete my research work. I appreciate their patience and guidance throughout the task.

I would also like to pay my gratitude to Brig. Dr. Akhtar Nawaz Malik (Retd), Brig. Dr. Javaid Iqbal and Dr. Umar Shahbaz for being member of my thesis guidance and evaluation committee. I am also thankful to all my degree-fellows for their support and cooperation.

Finally, I would like to express my gratitude to all the individuals who have rendered valuable assistance to my study.

I specially dedicate this work to my late wife whose struggle during her ailment remained a source of inspiration for me during all hardships. I also dedicate it to my most respectable parents, caring wife and lovely children whose tremendous patience, support and cooperation enabled me to achieve this landmark.

Abstract

Glaucoma is one of the eye related diseases which cause permanent blindness if not diagnosed and cured timely. Well-timed diagnosis can only be possible if all the patients suspected of Glaucoma are thoroughly checked by classified ophthalmologist periodically. This activity of clinical examination is time consuming as well as entail more resources therefore an automated system is preferred which could support ophthalmologists in decision making.

Digital retinal fundus imaging is one of the sources available in Ophthalmology which could be used in detecting most of the eye related diseases including Glaucoma with the help of pattern recognition and image processing techniques.

In this research, the main aim remained to device an automated system capable of detecting Glaucoma using digital fundus image. The system will be able to carry out mass scale screening of eye patients without involvement of ophthalmologist. This process will segregate suspected Glaucomic patients from normal ones for detailed analysis hence reducing burden on limited availability of specialists.

Key Words: *Glaucoma, ISNT rule, Fundus, Segmentation, Vasculature displacement, Optic nerve head (ONH), Retina, Cup-to-disc ratio (CDR) and Adaptive thresholding.*

Table of Contents

List of Figures

List of Tables

CHAPTER – 1

INTRODUCTION

1.1 Overview

Application of non-invasive methods in automatic disease analysis has become an important area of research in medicines now-a-days. The information extracted from the analysis of digital images can be used to determine the existence of various diseases. Computerized Axial Tomography Scan (CT scan), Magnetic Resonance Imaging Scan (MRI scan), X-rays, OCT (Optical Coherence Tomography) and fundus imagery are few of the examples of those medical imageries on which medics rely heavily and play a vital role in clinical investigation of numerous ailments. If it is claimed that without medical imagery, timely and accurate diagnosis of major diseases are not possible in this modern world, there will be no point of exaggeration in it. Figure 1.1 depicts digital images which are the outcome of above mentioned techniques and used extensively in diagnosis and opinion making of different medical illnesses.

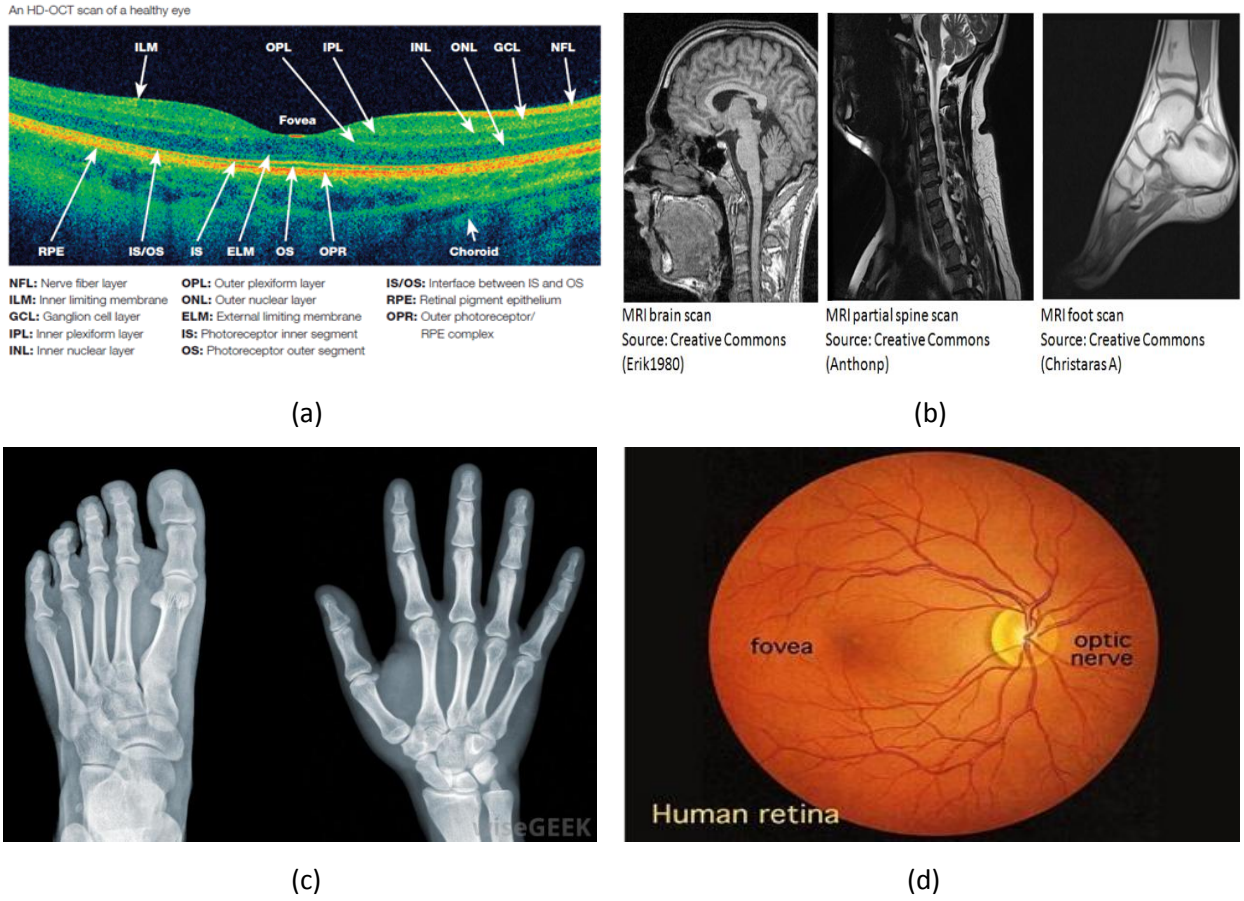

Figure 1.1: Medical Imageries (a) OCT [1] (b) MRI [2] (c) X-Ray [3] (d) Fundus Image [4]

Medical imaging incorporates diverse imaging techniques. These images are used for diagnosing diseases and used effectively for their treatment. It plays a paramount role to improve health conditions of general population of all age groups. These images are often used for follow-up cases as well in order to keep track of pre diagnosed and under treatment diseases. In public health and pre-emptive medicine as well as in remedial and pain-relieving upkeep of patients, correct diagnoses directly affects disease management procedure. Although medical findings has concrete evidence to treat any disease however use of investigative imaging tool is vital in confirmation, assessment, documentation of diseases and keep track of treatment response. To reduce unnecessary procedures and effective medical decision making, high quality imaging is important. For instance certain invasive procedures can be sidestepped if simple medical imaging facilities like CT scan, MRI and ultrasound are available.

Medical imaging is no doubt the fastest emerging field in medicines. It is useful in both clinical examination and R&D. Few of the vital benefits that are expected due to enhanced research work in this field are expected in [5]:

Enhanced Patient Care

• Individual based personalized disease management

• Effective evidence-based decision making in human healthcare

• Minimize surgery related difficulties

• Understanding the effect of drugs on ailments

Improved Fitness of People

• Screening of an entire / selected population

• Risk factor assessment and ease in disease inhibition

• Squeezed curing time due to enhanced treatment effectiveness

• Minimize relapse of illness

• Reduced death and sickness rate

Economical Healthcare

• Quick and precise findings

• Faster recovery from surgical procedure

• Early discharge from medical centers

• Economical use of expensive diagnostic and surgical equipment

Healthier Competitiveness of Health Business

• Research-based growth of advanced technology

• Cost-efficient healthcare through focus on user-friendly equipment

1.2 Motivation

Quigley claims that glaucoma is a second most dangerous ophthalmic pathology that causes loss of vision if not diagnosed timely [6]. Between 12 to 15 % of the total world population suffering from various stages of blindness is affected by glaucoma in its different stages [7]. Glaucoma is categorized due to damage of optic nerves and erosion of axons. Advancement of glaucoma is very sluggish and no glaring symptoms appeared in the initial stages. If glaucoma detection is not carried out timely, it causes irreversible damages to the optic nerves and visual field which ultimately lead to perpetual sightlessness.

According to summarized figures on glaucoma published by Michelson and Groh in 2001, the worldwide affected of glaucoma is about 67 million people, which are roughly 13% of all cases of blindness. Quigley further reports that less half of the patients affected with glaucoma remain unaware of their ailment in established countries. In the developing countries, awareness rate is even lower. The main reason behind high rate of affected patients and delayed commencement of treatment is the lengthy clinical procedures involved in the diagnosis of this disease. The procedures that contribute to the pre-diagnosis of glaucoma by the ophthalmologists include clinical history analysis of the affected person, intraocular pressure measurement, examination of changes in the optic disc and functional study of the visual field which is also known as Capimetry test.

Michelson et al also present an overview of the expenses incurred on treatment of glaucoma. Treatment cost of glaucoma in USA is approximately $400 million per year. Similarly statistics from UK shows expenditure of about £88.2 million. Low awareness coupled with high expenses connected to glaucoma are evident motives for introducing and implementing more advanced systems of screening and treatment for glaucoma.

Consequently, it is important to introduce novel methods for the effective detection of glaucoma. Lot of research work has been undertaken world over to incorporate digital medical imagery analysis for automated detection of such diseases for which timely diagnosis and in time commencement of correct treatment are the only effective and available options. The real motivation behind the study on this topic is to understand the problem in depth, carryout detailed

research on all the latest work that has been carried out so far to address this issue and then contribute towards the betterment and development of effective automated detection system for diagnosis of glaucoma.

1.3 Scope and Objectives of Research Work

1.3.1 Scope

Keeping in view the available statistical data and opportunities in the field of glaucoma diagnosis, the envisaged scope of this study is as under:-

- Make use of latest technology through which instead of examining retina by ophthalmologist in real time and take on spot decision (in time compressed environment) or taking aid of lengthy and expensive procedures like OCT, it is possible to save digital image of retina also known as fundus image. These images can be examined in detail in later time frame or through automation for accurate diagnosis of disease. It is pertinent to mention here that fundus images are acquired through specialized fundus camera which is a cheaper technology than OCT or IOP test.
- Low doctor to patient ratio also demands such solutions in which only potential candidates should have immediate access to ophthalmologist for more detailed examination and timely commencement of appropriate treatment.
- Make use of telematics to its optimum in health care sector in order to transfer true benefits of advancement in technology to population who do not have the facility of access to ophthalmologists and hospitals in their near vicinity.

1.3.2 Objectives

Following objectives were earmarked and aimed to be achieved during the course of this study on glaucoma detection:-

- Obtain digital fundus images using fundus camera of affected patients at mass level.
- Carryout automated screening of acquired fundus images for glaucoma using features which are presently examined clinically using ophthalmoscope or slit lamp bi-microscope.
- Finally the segregation of affected and normal patients hence reducing the burden over limited available resources in the country.

1.4 Challenges

In a very short span of time, the field of medical imaging has progressed remarkably in which pattern recognition as well as digital image processing has played the major role specifically in automation of disease diagnosis and subsequent utilization of its results in disease treatment. Digital fundus images are used for discovering retinal related aberrations. Numerous methods have been suggested by now for automated diagnosis of glaucoma but there always remain plenty of room for novelties and improvements until the system gets matured and implemented in its true sense. While implementing such techniques numerous challenges do come across. Similarly during the course of this research s well, few of the challenges being faced are as follows:

1.4.1 ROI Extraction

Copious dataset containing both glaucomic and normal fundus images are available online which are utilized for research purposes. Varying resolution and inclusion of redundant features of retina in fundus image made these datasets unable to be used directly in our algorithm. Acquisition of such regions which are free from unnecessary features was the first challenge in our study. In order to get rid of these redundant portions, a different technique comprising selection of brightest pixel value and analogous contiguous area known as optic nerve head (ONH) was adopted to extract region of interest.

1.4.2 Optic Disc (OD) Segmentation

Diagnosis of glaucoma using fundus images is mainly dependent upon correct and qualitative assessment of various parameters of optic disc. These parameters include thickness of neuro retinal rim (NRR), calculation of cup to disc ratio (CDR), enlargement of optic cup, displacement of blood vessels, optic disc atrophy, etc. The assessment of all these parameters is only possible if optic disc is correctly segmented out from digital fundus images. In this proposed method, adaptive thresholding technique is used for optic disc segmentation which proved to be an effective approach.

1.4.3 Diameter Calculation

Cup-to-disc ratio (CDR) which is amongst the basic parameters used to assess retinal fundus image for occurrence of glaucoma is usually calculated by measuring only vertical diameters of optic disc and cup for the purpose of ease. Horizontal diameter is all together neglected which leads to less accurate CDR calculation. Several studies are available in which

CDR is measured using only vertical measurements. A novel vector based approach is utilized in this proposed method for automated measurement of OD diameter which is close to actual size of the OD annotated by ophthalmologists hence contribute effectively in evaluation of OD for glaucoma.

1.4.4 Blood Vessel Extraction

Blood vessel pattern covers complete retina and is unique in every humanoid. Researchers working in the field of digital fundus images and automated pattern recognition make lot of use of this prominent feature for utilization in multiple applications. In glaucomic patients these blood vessels start displacing from central location inside optic disc towards its walls due to enlargement of optic cup. In this proposed method precise extraction of BV was of paramount importance. In order to overwhelm this challenge wavelet based technique was presented to accurately segment out BVs.

1.5 Research Methodology

- **Research proposal** of using digital retinal fundus imagery for automated detection of glaucoma was initiated.
- **Literature Review** was carried by incorporating / exploring following resources:-
  - Interaction with ophthalmologists.
  - Consulting recommended books on clinical examination of glaucoma.
  - Reading research articles on automated assessment of ONH (optic nerve head) for glaucoma.
- **Image Acquisition Protocol**
  - TRC-NW8F, Non-Mydriatic Retinal, 12.3 megapixel, high resolution, 45 deg FoV Camera (Topcon, Japan) was used.
  - Images of both eyes - 7 female & 8 male patients – age 38 to 65 years.
  - Ophthalmologists initially isolated patients with low vision & abnormal ONH appearance assessed through slit lamp.
  - Final selection for fundus imagery carried out on the basis of positive IOP Test.
- **Dataset Collection**
  - Glaucomic dataset of Pakistan based ethnic group was collected. Previously not available online.

- Fundus images of 15 glaucoma patients were collected from *Ibrahim Trust eye hospital, Gujranwala* with prior consent and approval of administration / patients.
- Images were stored in JPEG format with resolution of 3216x2136 pixels (High quality images).
- Images were then annotated by two different ophthalmologists that inculde marking of OD, OC and CDR judgment.

• **Algorithm development and Implementation Stage**

- An algorithm was formulated for automated features extraction and subsequent assessment of glaucoma.
- Devised algorithm was then implemented in Matlab using image processing toolbox and tested on acquired dataset.

• **Validation of Code.** In order to verify the efficacy of Matlab code, its validation was carried out using another dataset acquired from AFIO.

1.6 Thesis Organization

This study is organized in seven chapters. Chapter 2 covers the details of Glaucoma disease itself. This chapter is aimed at providing the insight of anatomy of human eye, structure of retina, causes of glaucoma and its type, evaluation procedure of optic nerve head (ONH) for glaucoma and finally few words on treatment procedure.

In chapter 3, brief history of digital fundus imagery is discussed followed by optical principles of fundus camera, its modes, indications, recording and interpretation and in the end few advantages / disadvantages are deliberated upon.

Chapter 4 summarizes previous work that has so far been carried out on automated detection of glaucoma by various researchers.

Chapter 5 explains the proposed methodology for automated detection of glaucoma. The details of experiments and their results are contained in chapter 6. Different graphs and tabular data are also depicted in the same part. Concluding remarks along with future work is encompassed in last chapter. Matlab code of developed algorithm is attached as appendix A.

CHAPTER 2

GLAUCOMA – AN OPHTHALMOLOGICAL DISORDER

The ideas and explanations of glaucoma have grown for last 100 years but till now they remain vague and focus remain on its technical qualifications. The word glaucoma originally means 'clouded' in the Greek language. It is defined as a disorder of the physical or functional reliability of the optic nerve that can typically be prevented or reduced by acceptable lowering of intraocular pressure (IOP). Before exploring types, causes, assessment procedures and management of glaucoma it is mandatory to understand the basic anatomy of human eye along with its working principles.

2.1 Anatomy of Human Eye

Although every organ has its unique importance in overall healthy functioning of human body however the human eye is graded by medical geniuses as the most intricate body part. Apparently small looking organ has multiple functioning parts. Complete understanding of human eye is even not claimed by classified ophthalmologists with surety however broad anatomy is discussed in subsequent paras in order to better understand impending concepts related to glaucoma.

2.1.1 Basis Definitions [8]

- **Lens.** It is a sphere-shaped object in the eye which is positioned behind the cornea and it focuses the light rays entering in eye on the retina.
- **Cornea.** It is clear part of the eye which cover the iris and pupil and allows the light to enter in eye is called Cornea. It permits an eye to provide sight.
- **Pupil.** Small circular dark center of an eye that adjusts itself as per necessity to control the amount of light that reaches retina is known as Pupil.
- **Iris.** It is Colored part of the eye which surrounds the pupil is Iris. It is like a pigmented membrane which lies between the cornea and the lens. This part of eye acts as a diaphragm which widen or narrow the pupil, thereby controlling amount of light that enters the eye.
- **Sclera.** It is outer coat of the eyeball which forms the visible white part of the eye and it surrounds the optic nerve which lie at the back of the eyeball

- **Retina.** It is sensory membrane which lines the eye; images formed by the lens is received by it and converted into signals and transmitted to brain through optic nerve.
- **Optic Nerve.** It carries electrical impulses from photoreceptor cells in the retina to the visual cortex which is in the brain.
- **Optic Nerve Head.** It is the circular area where the optic nerve enters to the retina, also the location of the eye's blind spot is known as optic nerve head. It is also known as optic disc.
- **Choroid.** It is layers of blood vessels which is located between the sclera and the retina; its functions is to provide nutrition to the back part of the eye.
- **Macula.** It is that portion of an eye which lie near the center of the retina that permits us to perceive the objects with great detail.
- **Fovea.** A depression in the retina that contains only cones and that provides acute eyesight.
- **Vitreous Body.** It is the portion of the eye which is between the lens and the retina comprising of a clear jelly called the vitreous humor.
- **Ciliary Body.** It is that part of the eye that exists between the iris and the choroid. Main functions of Ciliary body is to accommodate, aqueous hum or production and keeping the lens in place.
- **Aqueous Humor.** Is the fluid in between cornea and iris which is produced by ciliary body is called aqueous humor. Glaucoma roots trouble in draining this fluid and IOP build up.

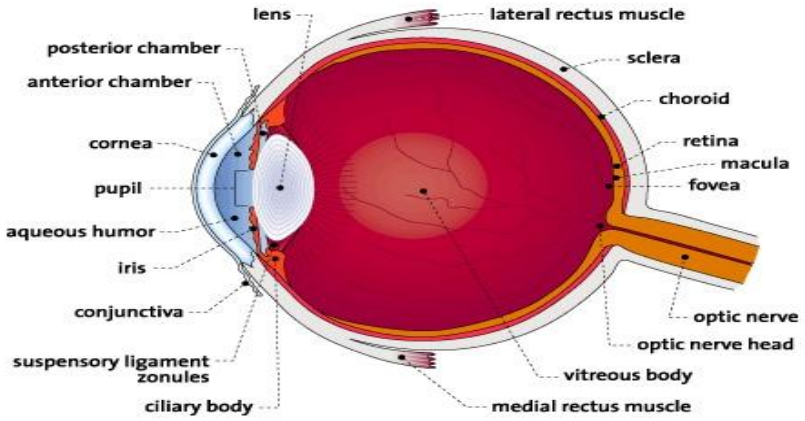

Figure 2.1: Human Eye Anatomy [8]

2.1.2 Working of an Eye

When we want to look at some object, our eyes necessarily focus the image on retina, which translate this optical image into electrical signals and transmit it to brain for interpretation. This is an astonishing and intricate procedure and we do it constantly without trying.

2.1.2.1 Image Creation on Retina

When light rebounds from any entity and reach back to the eye, it is required to be bent for rays to reach at the retina and a focused image of an object is seen. Four diverse planes causes the light rays to bend when it arrives to the eye: the cornea, the lens, the aqueous and the vitreous humors. Human optical system can visualize various things at different ranges with the help of ciliary muscles. When we look at distant object, the ciliary muscles contracts and the lens adopts trodden shape. On looking at close thing, these ciliary tissues again change shape and make the lens thickened. It makes the eye superior to the camera. Adjustment of the camera lens to focus on any object, we have to move the whole lens. Instead, lens in the eye only change its outline to adjust according to the distance of the object. In addition to focus the light, our eye can control the quantity of light entering into the eye. Iris controls the opening of pupil. In blurry light, iris makes the pupil to dilate more, permitting maximum light rays into an eye and vice versa.

2.1.2.2 Conversion into Electrical Signal

When focused light enters the retinal portion of an eye, a chemical reaction occurs in rod and cone cells which are light-sensitive. The rods contain a substance known as **rhodopsin** and cones contain a substance known as **color pigments**. These substances endure an alteration which generates electrical impulses which is then sent to the brain via optic nerve.

2.1.2.3 Brain Interpretation

As soon as the electrical signals reaches to the brain it initially examines the information about light and its color. Brain then invert the received image and fills missing information if required. This complete action occurs spontaneously without disturbing human vision. Brain contain a visual reflex system that also receives few of the information from the retina. This reflex system helps in reacting quickly to all the visual threats. When we observe some object approaching head on, this visual reflex system start processing and give signals to the body to react timely in order to avoid any damage.

2.2 Retinal Diseases

Vigorous and accurate vision can only be ensured through healthy retina. Light coming from various object first arrives into the human eye through iris. Iris control the amount of light and retina which is a thin membrane forming rear part of an eye collects it and focus onto the retina. It is the retina that converts this focused image into electrical impulses and optic nerves transmit them to the head.

To inspect the retina, an ophthalmologist usually dilate the pupil during clinical examination using different medicines [9]. Then the ophthalmologist uses a special magnifying lens for retinal inspection. Dilation converses after few hours.

The human eye is considered as the only body part where doctors can directly observe arteries and deep veins with the help of ophthalmoscope. Studying these blood vessels the doctors can examine the effects of diseases like hypertension and atherosclerosis on blood vessels in the body. Retinal disorders are numerous in number having several causes to ensue. Most commonly occurring retinal diseases are discussed very briefly in following part:-

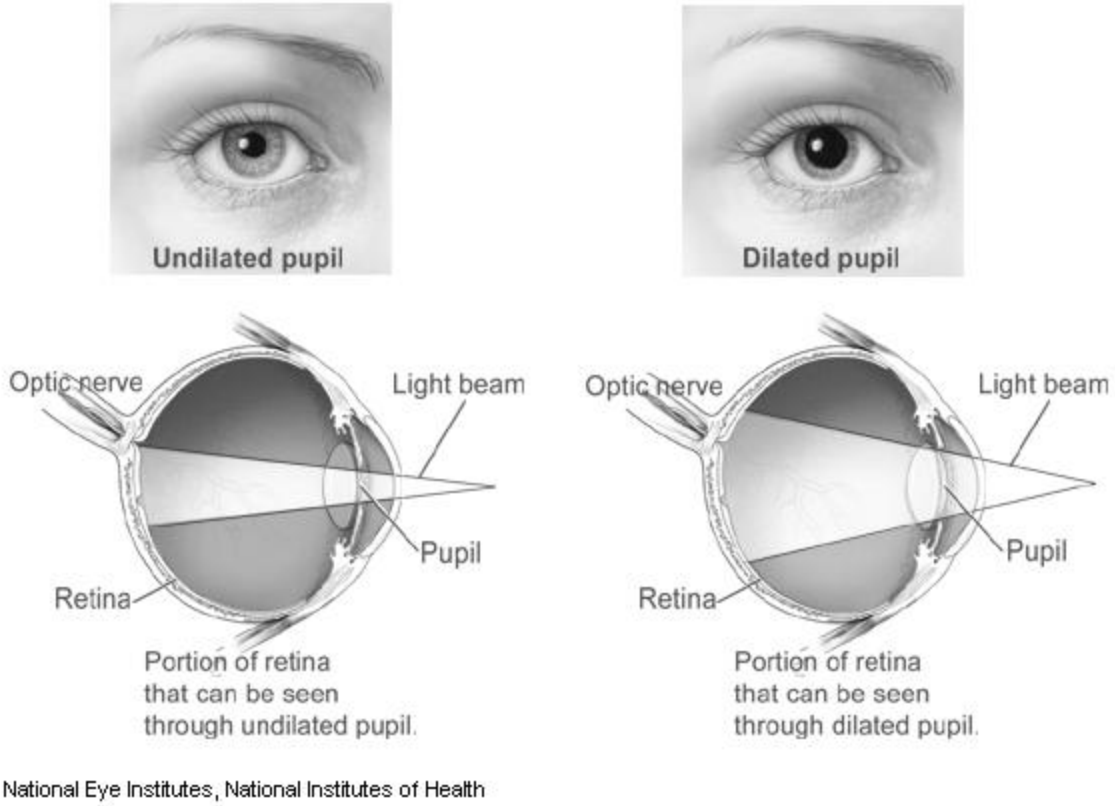

Figure 2.2: Dilated and Un-dilated Eyes [10]

2.2.1 Age-related Macular Degeneration (AMD)

Amongst elderly population, age related macular degeneration is considered as the most common cause of permanent central vision loss. It is such a disease that is equally common amongst male and female patients. This disease progressively deteriorate the macula which is the most sensitive part of the retina and lies in the middle. It completely wash out the central vision and straight lines starts appearing wavy. Specialized equipment is used by ophthalmologists to characterize macular degeneration. Fast progression of this disease can be controlled with the help of dietary supplements [11].

2.2.2 Hypertensive Retinopathy (HR)

Retina can be damaged due to high blood pressure. Hypertension could affect the small blood arteries spread all over the retina which will cause their walls to get thick and resultantly reduce the blood flow. It will reduce the blood supply to the retina causing damage to the patches of the retina due to insufficient blood supply. As hypertensive retinopathy develops, blood may drip into the retina. These deviations lead to a slow loss of vision, especially if they affect the macula. Mild hypertension could damage the retinal blood vessels if it is not treated for long time [12/80].

2.2.3 Diabetic Retinopathy (DR)

This disease usually occur amongst working-age adults suffering from diabetes. People having diabetes who are also patient of high blood pressure are more prone to diabetic retinopathy as both ailments could cause impairment of retina. Repeated occurrence of high sugar (glucose) level in the blood could affect the blood vessels walls and making them weaker causing damage to them. Blood could get leaked from these impaired retinal blood vessels. Usually diabetic retinopathy (DR) appears 5 years in the eyes after suffering type 1 diabetes.

2.2.4 Choroidal Melanoma

It is a cancer which comes from the pigment-producing cells (melanocytes) of the choroid. Categorized as frequently originating cancer in the human eye. It happens most often between the ages 55 to 60. In initial phases, it does not restrict the vision but on later stage it may be the reason of blurred vision or retinal detachment with symptoms like flashes of light, a shroud or screen

across the visual field. Melanomas, mostly if large, may spread into the orbit or spread through the bloodstream (metastasize) to other parts of the human body and may be lethal.

2.2.5 Glaucoma

It is a multifaceted eye illness with precise features such as damaged optic nerves and irreversible loss of visual field. In glaucoma the bordering vision is usually affected in initial stage. The variations in vision may be so slow that they are not noticed till a lot of vision loss has already happened. If the glaucoma is not treated in time then central vision will also be reduced and finally vanished. Visual impairment from glaucoma is most often noticed in such manner. The positive thing is that glaucoma can be managed if spotted early and with treatment most people with glaucoma can avoid losing their vision.

2.3 Causes of Glaucoma

It was general opinion in past that high pressure inside the eye is the primary cause of optic nerves damage, also known as intra-ocular pressure or IOP. Though IOP is an obvious risk factor however research shows that there are other factors as well that are involved because even those people having normal IOP also experience vision loss due to glaucoma [13/71]. Other common causes include:-

- Family history
- Injury to eye that damage iris
- After effect of medication
- Iris inflammation or tumor

2.4 Types of Glaucoma

An individual with raised IOP is a glaucoma *suspect*, as the high eye pressure might cause glaucoma. Glaucoma *suspect* also include those who have other indications that may now or at any time in the future, give rise to glaucoma. E.g., a strong family history of glaucoma or a suspicious optic nerve may make someone susceptible to glaucoma.

Glaucoma result in loss of vision when the eye pressure increases to a point that it causes irreversible damage to the optic nerve while first effecting the peripheral (side) vision. The vision loss may be slow and unnoticeable till a substantial loss of vision has already taken place.

Glaucoma can be classified into three major types that can be further divided into primary and secondary categories. These include:-

a) Open angle glaucoma
b) Close angle glaucoma
c) Developmental glaucoma

2.4.1 Open-Angle Glaucoma

The most common type of glaucoma is considered to be the Open angle glaucoma that accounts for at least 90% of all glaucoma cases. It results from the gradual blockage of drainage canals, causing an increase in eye pressure (Figure 2.3). It has a wide and open angle between the cornea and the iris (Figure 2.4). Development of Open angle glaucoma is slow and a lifelong condition. Symptoms and damage of this type of glaucoma goes unnoticed until onset of vision loss.

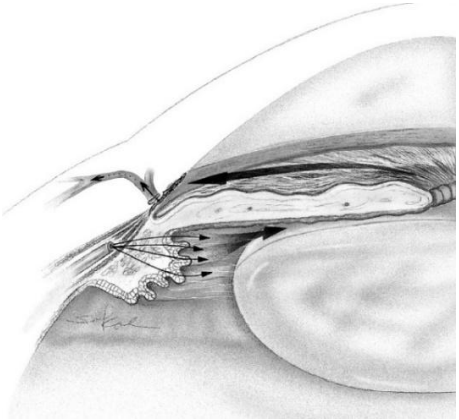

Figure 2.3: Open-Angle Glaucoma - reduced aqueous humor flow from Schlemm's canal [13]

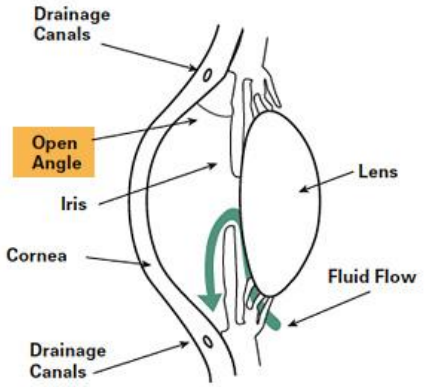

Figure 2.4: Open-Angle Glaucoma [14]

The width of an angle between the iris and cornea in Open angle type remain as per the normal specification therefore it is called Open angle. It is also known as primary or chronic glaucoma. Further subdivision of this type of glaucoma is as under:-

1. Chronic open-angle glaucoma
    a. Intraocular pressure (IOP) higher than normal
    b. Intraocular pressure (IOP) within normal range
2. Secondary open-angle glaucoma
    a. Pigmentary glaucoma
    b. Steroid glaucoma
    c. Lens-induced glaucoma
    e. Glaucoma after cataract surgery
    f. Glaucoma after trauma
    g. Glaucoma associated with intraocular hemorrhage
    h. Glaucoma associated with retinal detachment
    k. Glaucoma with intraocular tumors

2.4.2 Angle-Closure Glaucoma

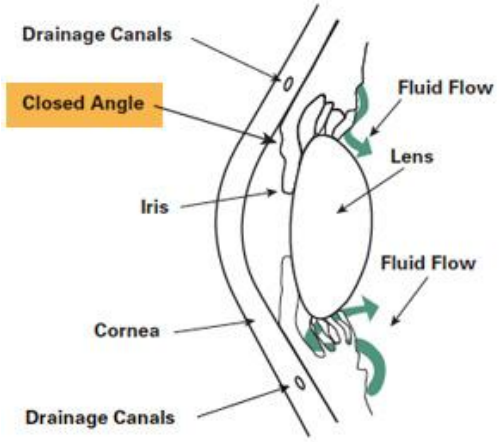

Figure 2.5: Angle-Closure Glaucoma [14]

Another type of glaucoma which is somewhat less common amongst masses is Angle-closure glaucoma. Trabecular meshwork is blocked that result in a sudden rise in IOP. Angle between cornea and iris gets narrower in this kind of glaucoma. The Angle-closure glaucoma progresses quickly and the resulting symptoms and damage is very noticeable thus needing immediate medical attention.

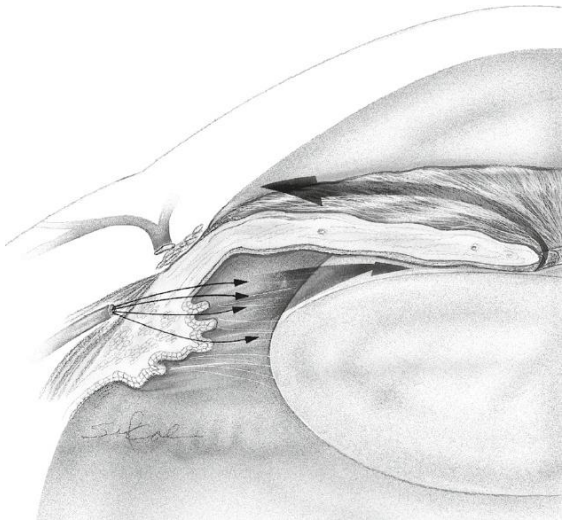

Figure 2.6: Angle-Closure Glaucoma - Iris covers the drainage canals – Outflow of aqueous humor is obstructed [13]

Angle-Closure Glaucoma is also called narrow-angle glaucoma or acute glaucoma. Angle-closure glaucoma is due to the narrowness of angle between the iris and cornea. Subdivision of angle-closure glaucoma is as under:-

1. Primary angle-closure disease. Contact between iris and trabecular meshwork is the only cause of primary angle closure disease, restricting aqueous outflow. It can be conceptualized in two complimentary schemes:
    a. Natural history
        (1) Primary angle closure *suspect*
        (2) Primary angle *closure*
        (3) Primary angle-closure *glaucoma*
    b. Front segment mechanisms of closure
        (1) Iris–pupil obstruction
        (2) Ciliary body anomalies
        (3) Lens–pupil block (swollen lens)
2. Secondary angle-closures
    a. Front ‘pulling mechanism’. Due to the contraction of membrane, the iris is pulled forward and obstruct fluid flow.
        (1) Neovascular glaucoma
        (2) Irido-corneal endothelial syndromes

(3) Posterior polymorphous dystrophy

(4) Epithelial down growth

(5) Fibrous ingrowth

(6) Flat anterior chamber

(7) Inflammation

(8) Penetrating keratoplasty

(9) Aniridia

b. Posterior 'pushing mechanism'. Due to increased pressure in vitreous humor the pressure behind the lens also increases hence push the iris and lens both in forward direction.

(1) Malignant glaucoma

(2) Cysts of the iris and ciliary body

(3) Intraocular tumors

(4) Nanophthalmos

(5) Suprachoroidal hemorrhage

(6) Intravitreal air injection

(7) Ciliochoroidal effusions

(8) Scleral buckling procedure

(9) Retrolental fibroplasias

2.4.3 Developmental Glaucoma

Developmental glaucoma, also called infantile or pediatric glaucoma, occurs in young children and babies. It is diagnosed usually quite early i-e during first year after birth. This is an unusual condition which is caused by improper growth of drainage system of an eye before birth and could be hereditary. This leads to increased IOP, which then harms the nerve fibers. Symptoms of this kind of glaucoma include:-

- Vagueness of the cornea
- Photosensitivity, and
- Enlarged eyes

The breakdown of developmental glaucoma is as under:-

1. Primary inherited glaucoma
    a. Hereditary glaucoma

b. Autosomal dominant juvenile glaucoma
c. Glaucoma related to systemic abnormalities
d. Glaucoma related to ocular abnormalities

2. Secondary glaucoma
a. Traumatic glaucoma
b. Glaucoma with intraocular neoplasm
c. Uveitis glaucoma
d. Lens-induced glaucoma
e. Glaucoma after inherited cataract surgery
f. Steroid-induced glaucoma
g. Neovascular glaucoma
h. Secondary angle-closure glaucoma
j. Glaucoma secondary to intraocular infection

2.4.4 Normal-Tension Glaucoma (NTG)

Normal-Tension Glaucoma sometimes also referred as low-tension glaucoma. In this type of glaucoma the optic nerve gets damaged despite the absence of high eye pressure. The reasons of nerve fiber damage due to this type of glaucoma is still not known even though the IOP is normal. Population who is at high risk to be affected by this kind of glaucoma are:

- Populaces of Japanese origin
- Individuals with a history of heart disease
- Persons having family history

2.5 Optic Nerve Head and its Evaluation Procedure [15]

Glaucomatous optic neuropathy is involved in all the types of glaucoma. In order to detect and manage glaucoma it is pertinent to comprehend that how the optic nerve head (ONH) is examined.

2.5.1 Clinical Examination of ONH

There are several instruments available used by ophthalmologists for examining ONH which mainly includes direct and indirect ophthalmoscope or lens along with a slit lamp as shown in Figure 2.7. A health professional with appropriate training can assess the ONH accurately. ONH examination being the uncomfortable procedure for the affectees, the time window available for

viewing the optic nerve head is often short, therefore the examiner should be quick to make key observations. Pupil dilation helps in improving the correctness of investigation with all instruments. More advanced technology and devices are also available like confocal scanning laser ophthalmoscopy, OCT and scanning laser polarimetry which always augment the clinical examination of retina and provide quantitative measurements.

(a) **(b)** **(c)**

Figure 2.7: (a) & (b) Direct & Indirect Ophthalmoscopes, **(c)** Slit lamp & posterior pole lens [16]

2.5.2 Characteristics of Normal ONH

Optic nerve head (ONH) is an oval shaped feature placed on retina having orange complexion, beneath which nerve fibers approximately millions in number pass through a mesh-like layer which is called lamina cribrosa. These fibers are then bundled together at the backof an eye to make an optic nerve which takes the signal to the brain. These optic nerve fibers are distributed unequally over the retinal surface as a thin layer having 'feathery' appearance, which can be observed closely in the surrounding areas of an optic disc specifically above and below the disc. As the nerve fibers converge on the boundary of the optic disc they discharge over the scleral ring and then go down its inner surface. This compressed packing of nerve fibers in between optic disc and optic cup is referred as the neuro-retinal rim. The optic cup is the central yellowish region of optic disc. The cup boundary can be best segmented out with the help of blood vessels bends which occur due to entrance of these vessels into the cup. This neuro-retinal rim obeys ISNT rule which tells that width of NRR is maximum on inferior side than superior side followed by nasal side and thinnest on the temporal side. (Figure 2.8).

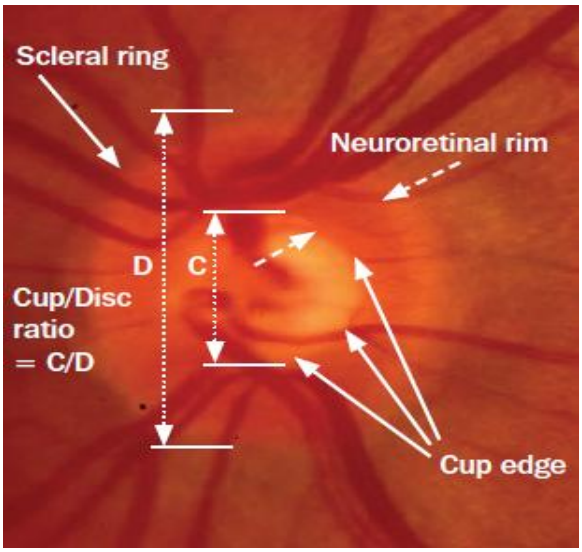

Figure 2.8: Normal optic nerve head [15]

2.5.3 Appearance of Glaucomatous ONH

Normal optic nerve head when affected with glaucoma is called Glaucomatous optic nerves head. Such ONH contain some peculiar features which can easily be assessed using available clinical instruments by ophthalmologists. Gist of such features are as under:-

- Generalized / focal expansion of the cup. Increased cup to disc ratio (CDR)
- Disc hemorrhage
- Diminishing of neuro-retinal rim
- Irregularity of excavation between two eyes
- Damage of optic nerve fiber layer
- Para-papillary atrophy
- Displacement of vascular bundle towards nasal side [7]

2.5.4 Distinguishing Glaucomatous ONH from Normal

In the light of above mentioned characteristics, ophthalmologists distinguish normal and glaucomatous ONH using following protocol:-

- Pupil dilation is carried out
- Recognize optic disc boundary and optic cup margins in order to identify retinal rim
- Is neuro retinal rim follow the famous rule of ISNT
- Does hemorrhage visible or not?

- Vertical cup to disc ratio (CDR) is estimated
- Optic nerve head size is measured
- Evaluate RNFL (retinal nerve fiber layer)
- Annotation of the ONH is carried out
- Qualitatively inspect the displacement of vessel bundle towards nasal side

2.6 Screening of Glaucoma and its Importance

2.6.1 Clinical Procedure

In order to correctly diagnose glaucoma, an ophthalmologist or optometrist get assistance of certain clinical tests for comprehensive examination of an eye. For glaucoma suspects or patients are always advised to undergo dilated pupil eye examination at least once in one to two years. Importance of screening cannot be ignored as it is the only possible way of avoiding glaucoma progression. This examination may include following clinical tests:

2.6.1.1 Tonometry

This is considered as the basic test for glaucoma in which inside pressure of eyes are measured also known as intraocular pressure (IOP). Examples of tonometers include:

- A puff of air is emitted using ***noncontact tonometer***. Resistance offered by an eye is used to calculate the eye pressure.
- Other method usually used for the same purpose is ***applanation tonometer.*** An eye surface is touched after making it numbed and pressure is measured that is essential to flatten the cornea. This tonometer is considered as the most sensitive one.
- Digital pen like instrument is used which directly come in contact with anesthetized eyes to measure the eye pressure. It is also known as ***electronic indentation method***.

2.6.1.2 Pupil Dilation

Under normal circumstances the pupil has a very small opening which is adjusted as per external light conditions. Through this opening light enters into the eye and make image of an object at retina. As this opening is very limited hence very limited portion of retina is exposed to be examined by ophthalmologist for any abnormality. Therefore peculiar eye drops are used for enlargement of pupils on temporary basis so that retina can be completely seen during examination of an eye.

2.6.1.3 Visual Field Testing

As glaucoma hampers the vision gradually starting from periphery towards center therefore visual field testing is carried to assess the area seen by forward looking eye. A spot is displayed to the patient and on the basis of dimmest intensity being seen in an area the ophthalmologist document it and find out the state of vision. A patient responds whenever blinking of a light is seen that is visible in front.

2.6.1.4 Visual Acuity Test

Sharpness of an eyesight is measured with the help of this test at varied distances. Visual charts are made to be read by patients from a distance of 20-25 feet using various lens sizes.

2.6.1.5 Pachymetry

It is another method of evaluating the pressure inside an eye. An instrument producing ultrasonic waves is used for the purpose through which cornea thickness is determined.

2.6.1.6 Ophthalmoscopy

Direct or indirect ophthalmoscopes are the instruments used in this screening method to examine the internal surface of an eye through pupil. This test help in detecting any impairment of optic nerve head caused by glaucoma.

2.6.1.7 Gonioscopy

In closed-angle glaucoma iris gets closer to the back of cornea. Gonioscopy is a procedure in which a specialized instrument is used to diagnose glaucoma in closed-angle by viewing the front part of the eye (anterior chamber). It determines position of an iris that weather it is closer than normal or not.

2.6.1.8 Optic Nerve Imaging

Medical imaging is a technique being used in medical science to document various diseases during diagnosis and prognosis process. With the passage of time optic nerve head experience physical changes due to presence of abnormalities. Existing imaging techniques used in ophthalmology to document these changes include:-

- Stereo photographs of ONH
- Heidelberg Retinal Tomography or HRT
- Scanning laser polarimetry
- Fundus imagery

- Optical coherence tomography (OCT)

Above mentioned techniques are noninvasive hence painless. On the basis of condition of glaucoma an ophthalmologist determines suitable method(s) to be utilized.

2.6.2 Automated Procedure

Medical imagery is a technique used extensively in recent days to register existing condition of ONH instead of examining retina in real time and recognize / diagnose abnormality in limited time frame. These medical imagery provide ophthalmologists an opportunity to document and compare disease progression in optic nerve head. Also researchers are working on getting maximum benefits of these medical images in automated detection of those diseases whose physical appearance can be segmented out and recognized using different pattern / feature recognition techniques.

Automated procedure of screening glaucoma can help ophthalmologists by carrying out mass level screening of patients and segregating suspected eyes with normal ones. This approach will not only reduce the burden over limited number of available ophthalmologists in the society but also play an effective role in early detection of glaucoma affected patients which is the only solution available to avoid this irreversible disease.

2.7 Treatment of Glaucoma

Treatment of glaucoma solely depends upon type of glaucoma with which patient being diagnosed, its severity and response given by patient to specific treatment.

Management of glaucoma can be carried by adopting different treatment methods. Most commonly used treatment options prescribed by ophthalmologists in ascending order are as under:-

- **Medication**
  - Primary medication - using eye drops
  - Secondary medication - that include use of pills / tablets
- **Surgical Procedures**
  - Non-invasive or Laser surgery
  - Invasive or traditional surgery
- **Combination of above mentioned methods**

Prompt and regular glaucoma management is crucial for preventing vision-threatening damage. Every medication has some probable after effects yet exceptions are always there who

experience little or no side effects hence it is mutual effort which is to undertaken by patient and consultant to fight effectively against glaucoma during the course of this battle.

2.7.1 Medication

All types of treatment used for glaucoma are mainly targeted at reducing IOP hence regular medication is the main key. Eye drops are initially used that absorbed into the bloodstream. Under certain circumstances if eye drops are not effective healing pills could be resorted to in addition to eye drops. These pills aid to turn down the eye's outlet and reduces the creation of fluid.

2.7.2 Surgical Measures

Sometimes use of medicine do not produce anticipated consequences or have insufferable side effects then ophthalmologist go to subsequent phase and that include surgical procedure.

Laser surgery is an intermediate step between medication and conventional surgical procedures. It has become increasingly popular though the lasting success rates are inconstant. Laser surgery is relatively a simpler procedure hence can be undertaken in either clinic or outpatient facility. It is normally completed within 10 to 15 minutes and is painless. The most common types of laser surgery being carried out for glaucoma are as under:-

- Argon Laser Trabeculoplasty (ALT)
- Selective Laser Trabeculoplasty (SLT)
- Laser Peripheral Iridotomy (LPI)

When medications and therapies based on laser do not sufficiently lower eye pressure then as a last resort consultants recommend traditional therapies. In this practice the main target of any specialist is to drain excessive fluid inside the eye by creating a passage in the sclera which resultantly reduce inside pressure and avoid nerve damage. The most common of these operations are as under:-

- Trabeculectomy
- Drainage Implant Surgery
- Nonpenetrating Surgery

Conventional therapy is a painful procedure however around 50% affectees recovers effectively from glaucoma after undergoing surgical treatment and even no longer require medications for substantial length of time [17].

CHAPTER – 3
DIGITAL FUNDUS IMAGERY

Literary meaning of fundus is ‘bottom’. The part of a hollow organ (such as the uterus or the gall bladder) that is farthest from the opening and the upper element of the stomach, forms a bulge above the opening level of the Oesophagus (farthest away from the Pylorus) comes under the category of fundus. *In ophthalmology the part of an eyeball opposite to the pupil is referred as the fundus.*

Taking an image of the rear far end of an eye that is also called fundus comes under purview of fundus photography. Specialized fundus cameras are used in fundus photography which includes a complex microscope attached to a flash enabled camera. The main structures of eye i.e. the complete retina, optic nerve head and macula can be visualized on a fundus photo. Colored filters or specialized dyes may be used in fundus photography.

Due to evolution in technology during last century the fundus photography has also seen lot of improvements in its technique. Since the sophisticated equipment is involved in fundus photography and more challenging to manufacturers to develop it to clinical criteria therefore limited number of companies are available in market that produce this equipment. Topcon, Canon, Nidek, Kowa, Zeiss, CSO and Center Vue are amongst those few manufacturers of fundus camera.

Figure 3.1: Fundus Images - (left) right eye, (right) left eye [18]

Figure 3.1 depicts normal fundus images of both eyes seen from front. All the images in which blood vessels are bundled towards right side are images of person's right eye. Each fundus has no sign of disease or pathology. In every image the macula always lie in the

middle of the retina whereas the optic disc is located towards the nasal side. Fundus photography documents the retina. The photography of retina can be performed directly as the pupil is used as an entrance and exit point for light rays coming from fundus camera into the eye.

3.1 Brief History

For about 75 years a concerted efforts were made by specialists to clearly take the image of fundus. Many ophthalmologists worked day and night to overcome the problems encountered. Friedrich Dimmer finally succeeded in early 20th century and published his photographs in 1921. The fundus camera used by Dimmer was state of the art research tool, which was developed in 1904. In 1926, Stockholm's Johan Nordenson and the Zeiss Camera Company jointly developed the first modern fundus camera and made commercially available for use by practitioners.

Since 1926, the features of fundus cameras have been improved drastically. Most significant features are non-mydriatic imaging, electronically controlled illumination system, automatic alignment between eye and lens and high-resolution digital images. These developments paved a way forward for making fundus photography a regular practice for documenting retinal disease.

Figure 3.2: Fundus Camera [19]

3.2 Optical Principle of Fundus Camera

Fundus camera is basically a specific optical microscope coupled with typical optical arrangement [2]. Its ocular design is based on the technique known in ophthalmology as indirect ophthalmoscope. Angle of view of the lens is an important parameter in fundus cameras. Normal angle of view (30°), creates a film image 2.5 times magnified than original one whereas wide angle fundus cameras capture images ranging 45° to 140°. Wide angle fundus cameras provide

proportionately less retinal magnification. Range of angle of view of narrow angle fundus camera is 20° or less.

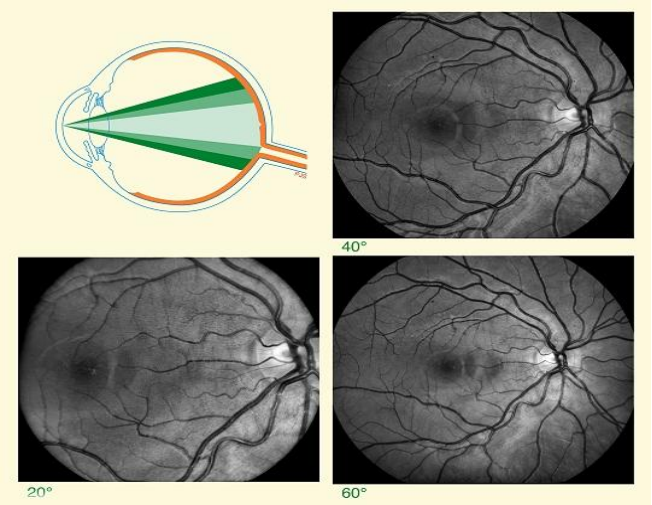

Figure 3.3: Angle of View – Fundus Camera [20]

Electronic flash is used to create light, which is passed through a set of filters and projected onto a circular reflective glass. Series of lenses are used to focus this light which is reflected by the mirror. Uppermost lens has a mask, which shapes the light into doughnut like shape. This doughnut shaped light is then reflected onto the circular reflective glass with a central aperture, exits the camera through the objective lens and enters into the eye through the pupil. Most important consideration in this procedure is that the illumination system and the object required to be photographed are accurately aligned and focused. The resultant image of retina follow the central un-illuminated portion of the doughnut and exits the cornea. The light continues through the central aperture of the previously described mirror, through the astigmatic correction device and the diopter compensation lenses, and then back to the single lens reflex camera system which redirects the light onto the capturing medium, whether it is film or a digital CCD.

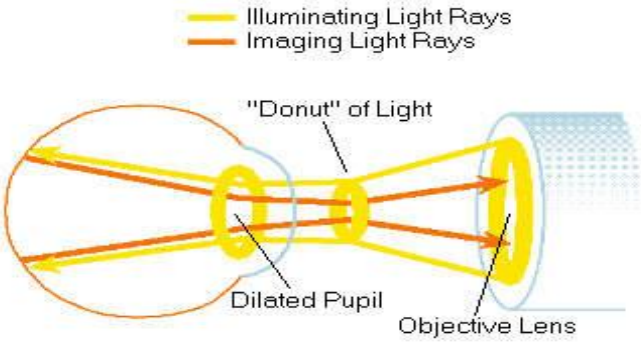

Figure 3.4: Doughnut of Light Formation [20]

3.3 Modes – Resolve Artifacts in Imageries

Commercial instruments used for digital fundus imagery, carryout following modes of investigation.

3.3.1 Color

In this mode of examination, retina is examined in color however the illumination of retina is carried out by white light.

3.3.2 Red Free Fundus Imagery

Different filters are used to examine lesions and abnormalities that occur onto the retina or in its surroundings. Green filter (~540-570 nm) is used to block the wavelengths of red light. It creates an image which has better contrast for observing blood vessels and hemorrhages, soft lesions like drusen and exudates, and delicate features such as RNFL defects and epi-retinal membranes. Usage of Red free imagery prior to angiography, is also being followed regularly as a base line image.

3.3.3 Angiography

It is a technique in which fluorescent dye is injected into the blood stream to make it prominent for imaging / capturing blood vessels flow on the retina and neighboring tissues. This dye shines a different color when light of particular wavelength reaches it. With the help of this technique the movement and pooling of blood vessels in different phases can be captured as the dye flows through the retina and choroid.

3.3.4 Sodium Fluorescein Angiography

This technique is used for the imaging of retinal vascular disease and utilizes blue excitation light of ~490 nm and fluoresces a yellow light of ~530 nm. It is regularly being used to image Cystoid Macular edema and Diabetic Retinopathy among others.

3.3.5 Indocyanine Green Angiography

Near IR diode laser of 805 mm and filters that allow light with wavelength of 500 – 810 nm are used in this method for photography. This technique is primarily utilized for imaging deeper choroidal diseases. Indocyanine Green Angiography is useful for observing choroidal vessel out

pouching, abnormal vessels supplying ocular tumors and hyper permeable vessels amongst other diseases.

3.3.6 Stereo Fundus Photography

Recent advancements in digital imagery and 3-dimensional monitors have attracted the attention of makers to incorporate this technology in photographic gadgetry. The recent development has made simultaneous photography of retina from various angles possible which results in generating 3-dimensional image. By using this technique, image can provide enhanced information about surface appearances of the retina and results in better analysis.

3.3.8 Resolution of Artifacts in Fundus Imagery

Artifact errors do occur in fundus imagery while capturing retinal images which are not desirable. As these artifacts affect image quality therefore patient support in this regard is of vital importance to minimize artifacts. Before capturing images, clinicians must educate the patient about Dos and Donts. They must also ensure that alignment and camera controls setting and decision making regarding film choice is correct. Besides taking all these precautions, there still exist some artifacts which are not very prominent and cannot be identified until imaging is taken place. Usually such artifacts occur due to a mechanical problems in the camera or naturally small sized pupil of patient.

Another reason of blur images could be the dry eyes of patient. In such cases measures like blinking of an eye several times must be taken to lubricate the eye before taking images. The examiner capturing the image has to be vigilant and scrupulous in confirming precise alignment. White dots must be in clear focus and aligned with the pupil before pressing the alignment button. Joystick should be used effectively to focus the retinal image. Once the image is clearly focused only then process is completed and image can be captured.

3.4 Indications of Diseases

Medical professionals (Optometrists, Ophthalmologists, Orthoptists) use fundus photographs to record anomalies affecting the eye, diagnose correct disease and use them in follow up to check the effectiveness of treatment. Diabetes, glaucoma, age related macular degeneration, neoplasm of the choroid etc. are few of the diseases that indicate symptoms on the fundus.

In many cases, regular fundus screening is of utmost importance as the same can avoid aggravation of such diseases which could cause vision loss if left untreated for a longer period of time. For example diabetic retinopathy (DR) can be prevented by laser treatment if disease is diagnosed early.

Fundus imagery could also be a useful tool in diagnosing abnormal diastolic pressure in patients having constant headaches and often misrelate it to the weakness of eyesight.

Glaucoma is a disease in which patient do not realize retinal nerve fiber damage till initiation of sudden visual loss. Only cheap and non-invasive solution available to avoid this disease is periodic retinal screening through fundus photography and control over intraocular pressure through timely medication. Vascular displacement in optic nerve heads are one of the indications of glaucoma.

Similarly patients prone to severe headaches can be identified through fundus images by discovering swollen optic discs on fundus images. This sign depicts increased intracranial pressure which could occur due to brain tumor.

Arterial high blood pressure may diagnose with the help of fundus images. Hypertensive changes of the retina visible in fundus images closely mimic those in the brain and may indicate or predict strokes.

3.5 Recording & Interpretation

To capture fundus image, patients place chin at the rest available in the front and adjust forehead against the bar of the fundus camera. Then the camera operator carryout necessary alignment and focus the retina. On pressing the shutter button a flash is fired that ultimately captures the fundus image.

Fundus imagery is the record of retinal appearance. One fundus image is equivalent to hundreds of words that an ophthalmologist is required to describe any specific disease of a patient. These imageries allow the specialists to deeply go into the details of such diseases in which instantaneous decision could lead towards wrong diagnoses. It also provides an opportunity to the doctors to consult coworkers those cases in which retinal findings are complicated.

Fundus imagery is advised in number of cases where ophthalmic conditions are needed to be deeply studied. It is an effective source of developing initial understanding of an issue. Fundus photographs remain very helpful in better planning and subsequent disease management. Record

of all kinds of medical imaging must be kept in an orderly manner in order to allow clinicians to compare results from different timelines. It is also a useful tool in objectively documenting and recording disease progression. Although fundus photography has become a mature field now-a-days however still regarded as the tool to complement gold standard for fundus investigation i-e indirect ophthalmoscopy. The main purpose of fundus imagery is to observe the development of a retinal disorder. Presently researchers are making use of these fundus photographs to automate process of retinal disease detection.

3.6 Advantages & Disadvantages

Being an advanced technology where there are numerous advantages of fundus imagery, there are few limitations as well. Both are briefly mentioned below:-

3.6.1 Advantages

- Easy to handle therefore do not require any special training to master
- Larger area of retina can be observed as compared to ophthalmoscopy
- No dilation of pupil takes place.
- Lesser invasive technique than other available methods
- Better patient acquiescence
- Images can be stored in database for subsequent use
- Development of diseases can be monitored over time and helpful for better management plans
- Different filters and dyes commercially available to allow for different types of tests

3.6.2 Disadvantages

- Image produced by fundus camera is 2-dimensional
- Difficulty in observing and assessing abnormalities (e.g. cotton wool spots) due to lack of depth appreciation on images
- Low magnification and clarity in images as compared to ophthalmoscopy
- Certain opacities in eye which may be a result of any disease like cataract affects image quality
- Artifact usually cause weird images

3.7 Future Advancements

Fundus photography is proven to be decisive in diagnosing and treating patients in Ophthalmology. Recent research work has showed that computer-aided disease detection and analysis of human retinal fundus has remained a useful tool for the ophthalmologists. It has not only acted as a complement to the existing techniques but also reduces the burden of less available specialist as compared to the number of patients. In future it would be considered as a useful resource for automated detection of diseases and mass screening of patients for early diagnoses of various hazardous disorders.

CHAPTER – 4

AUTOMATED GLAUCOMA DETECTION – REPORTED TECHNIQUES

4.1 Introduction

In retinal diseases where risk of vision loss has higher probability and the same can only be avoided if medication starts timely, early detection and correct diagnosis of ailment plays a vital role. Traditionally manual methods are usually used for observation and identification of any retinal disorder. Direct and indirect ophthalmoscopy, scanning laser ophthalmoscopy (SLO) or state of the art fundus cameras are used for acquisition of retinal images. Optometrists and ophthalmologists regularly depend on picture operations, for example, change of complexity and zooming to decipher these pictures and analyze outcomes in the light of their own involvement and space information. In case, particular variations from the norm are detected, ophthalmologists may perform Optical Coherence Tomography (OCT) or Fluorescein Angiography for further examination. These indicative methods are tedious and obtrusive. Computerized strategies of analysis anticipate that more patients will be screened and more reliable results can be given in relatively lesser time.

Glaucoma are the eye ailments that have basic characteristics, for instance, regular vision loss, higher eye pressure and damaged Optic Nerve Head. It influences fringe vision and in the longer run prompts to visual impairment, if left untreated. The available techniques for identification of Glaucoma incorporate estimation of Intra-Ocular Pressure (IOP) utilizing Gonioscopy, Tonometer, Pachymetry, and so on which are performed physically by the doctors. These tests are generally trailed by examining the appearance of Optic Nerve Head (ONH) for giving the conclusive verdict about occurrence of Glaucoma. These conclusions are required to be observed consistently, which is an exorbitant and tedious procedure. The exactness and unwavering quality of the findings is restricted by the related information possessed by various ophthalmologists. Thus, programmed or automatic analysis of Glaucoma is considered to be more important nowadays.

Several automated detection techniques are available in which fundus retinal images are used to identify those features which are altered due to the occurrence of Glaucoma. Both segmentation and non-segmentation based methods have been developed by researchers so far to perform this automated task. Optic Nerve Head (ONH) being the prime feature of retina that is

affected by glaucoma remains the main focus of analysis. Due to same very reason maximum techniques follow the procedure of extracting ONH and its surrounding region of interest. However at the same time other vital features like RNFL erosion, peripapillary atrophy and vasculature shift also remain under study and methods have been devised to detect these changes in order to diagnose Glaucoma without using segmentation method of Optic Disc. This part reviews the best available programmed extraction of anatomical components from retinal fundus pictures so as to help early identification of the Glaucoma. Existing extraction techniques that depend on the elements including Retinal Nerve Fiber Layer (RNFL), Optic Cup to Disk Ratio (CDR), Peripapillary Atrophy (PPA), Vasculature Shift, Neuroretinal Rim Notching, and so on, have been studied which contributes to extraction of proficient elements related with the diagnosis of Glaucoma. [21]

4.2 Segmentation Based Feature Detection for Glaucoma

Techniques discussed under this part are categorized in an order that has been followed in proposed method to achieve the desired results. Image processing methods which are segmentation based and introduced by numerous researchers of this field are as under:-.

4.2.1 Extraction of ROI – Optic Nerve Head

The Localization of ONH is the underlying stride keeping in mind the end goal to find other anatomical structures, vessel following and enrolling changes inside Optic Disk area. In case any pixel is found inside the Optic Disk limit, it can encourage the extraction of the Optic Disk limit. There are three principle groups in which analysts have worked and contrived approaches for the restriction of the Optic Disk limits which are examined in the subsequent subsections.

4.2.1.1 Detection of ONH Using Brightest Point Method

The main group depends on figuring out the pixels intensity in shaded and grayscale pictures. Under typical conditions optic disc area is the brightest locale in retinal picture. Accordingly it can be distinguished by margining out the pixels with the power values beneath a specific limit [22].

Sinthanayothin et al. [23] confined optic disc utilizing Local Contrast Color Enhancement as a part of Intensity-Hue-Saturation space. The difference picture subsequent to changing over back to RGB space will increase optic disc when contrasted with rest of the picture. The algorithm brought about higher exactness in their related datasets though, others have discovered its high disappointment rate in the pictures with an expansive number of white scratches, light relics or

unequivocally noticeable choroidal vessels [24]. The utilization of preprocessing steps, for instance, picture sifting for evacuating ancient relics brighter than the Optic Disk may bring about change in the outcomes.

By using mathematical morphology Sekhar et al. [25] enhanced the strategy, to apply the shade adjustment on the retinal picture. Analysis of the geometrical structures in the picture by changing their shape and form is known as mathematical morphology [26].The biggest region of the shape remedied retinal picture was considered as Optic Disk district. The shade revision albeit enhanced the confinement exactness when contrasted with the past technique, its part in finding the Optic Disk district is unverifiable. Circular Hough Transform [27] is used by both researchers to locate the optic disk which plans to discover roundabout examples inside a picture.

4.2.1.2 Matching Template Method

. The second class depends on arrangement of layout representing to the Optic Disk and coordinating the format in a test picture. The outcomes were relatively precise when contrasted with first one to the detriment of the computational time. An effective algorithmic strategy is introduced for decreasing the computational time.

Li et al. [28] demonstrated the Optic Disk surface utilizing Principal Component Analysis (PCA). The Optic Disk in a test picture was confined by partitioning the test picture into sub-pictures and Euclidean separation from the PCA-model was ascertained for every sub-picture. The sub-picture with the Optic Disk at the middle will have slightest Euclidean separation from the PCA display. The outcomes were precise yet the inquiry technique was computationally expensive. By reducing the resolution of the image computational time can also be reduced but it will lead to in missing some important information due to which accurate localization will be difficult

For comparing template image and the region of interest in his research Osareh et al. [29] assessed the standardized connection coefficient. After averaging the 16 color normalized retinal image which leads to the template. The strategy just recognized the area in light of most elevated estimation of standardized connection coefficient which does not really mean the Optic Disk focus. They additionally enhanced their layout by isolating the Optic Disk into lighter portions and selecting the biggest section which is estimated to a half circle and the locale is not blocked by veins. The logic took after the iterative strategy for minimizing the error between the arrangement of pixels in the circular segment points and the assessed curve.

Directional matched filter is used by Yousiff et al. [30] in order to investigate the vasculature structure. At that point a mask of 9x9 from the test picture was compared with the pixels related with the vasculature bundle which can be resized in view of the magnitude of the picture. The pixel which is carrying minimum aggregate distance was taken as a center of optic disc.

4.2.1.3 Optic Disc Center Using Blood Vasculature Pattern

The midpoint of the ONH is the place where all the blood vessels converges in the retina is the basis of the third type. Delocalization of the Optic Disk as the majority of the retinal veins join inside the ONH district can be avoided by considering this assumption. Besides if the retinal vasculature structure is segmented out precisely, it can likewise maintain a strategic distance from the discovery disappointment of Optic Disk focus because of layout coordinating.

A. Usman et al [31] proposed a robust segmentation method which can detect OD using vasculature structure even in the presence of retinal abnormalities and noise. Candidate OD regions were segmented out by applying Laplacian of Gaussian (LoG) kernel in frequency domain. Brightest regions were enhanced and selected for further investigation. Connected component algorithm was used to label the detected regions and subsequently assessing the size of the region. Regions with reasonable size were segregated from smaller ones and vessel segmentation carried out. In final stage of the algorithm, vessel density was checked within each candidate region and the one with maximum density was declared as OD region.

For determining the point of intersection Hoover et al. [32] segmented out the blood vessels. A voting procedure was utilized to identify the point where all the blood vessels converges and the point with greatest votes was viewed as ONH center. For determining the distinctive region in the retinal picture illumination equalization was applied which leads to the diverse brilliant spots on retina. At last theory was created in light of locale size and if just a single region was characterized out, it was considered as Optic Disk region.

Tensor voting technique is utilized by park et al. [33] to dig out vasculature structure. Geometrical features based voting procedure of the expected candidates. The picture was at first contrast enhanced before use of tensor voting process. Mean shift procedure is utilized to identify the Optic Disk which focuses towards the point of the largest thickness (blood vessels converging point).

4.2.2 Segmentation of ONH

Appearance of ONH has a vital importance in diagnosis of glaucoma. There are several indications that appear inside or around ONH which depicts initiation of disease and ophthalmologists use them for clinical assessment. There are two major features which makes ONH one is Optic disc and other is optic cup. Optic nerve damage is one of the main factors which leads to the glaucoma and this damage has a direct effect on above discussed features hence in automated detection of glaucoma segmentation of these landmarks further open up avenues to reach at firm conclusions which differentiate any 2D retinal or ONH fundus image as glaucomic or normal. Several methods have so far been developed for segmentation of optic disc and optic cup which are discussed separately in succeeding paragraphs.

4.2.2.1 Optic Disc (OD) Segmentation

Optic disc can be extracted using various methods. They can be subdivided into two categories:-

- **Non-prototypical based methodologies.** Different image processing techniques are used in this category for OD extraction.
- **Prototypical based methodologies.** OD boundary is extracted using mathematical models.

4.2.2.1.1 Non-prototypical (Non-model) Based Methodologies

For a non-model based methodologies, the Optic Disk was either segmented out utilizing distinctive thresholding procedures or morphological operations; or approximated as circular and elliptical area. At start for segmentation of optic disc morphological techniques were used as it requires a little background knowledge of image processing. Since the state of Optic Disk is as shut bend, in this way the structure was approximated with round and curved shapes.

Noor Elaiza et al [34] in this paper discussed a new approach for segmentation of optic disc using Fuzzy c-Means (FCM) clustering method. Standard RGB fundus image was passed through preprocessing and processing stages to acquire optic disc feature. In preprocessing stage original images were reduced to region of interest (ROI) containing OD portion only in order to reduce computational cost. This step was followed by color channel analysis in which red, green and blue channels were segregated. Due to enhanced contrast and bright image as compared to other color channels, green channel was used in processing stage. In the presence of inhomogeneity

in intensity values FCM can accurately segment out prominent features. This algorithm assigned cluster membership to each pixel on the basis of its minimum distance from the center of clusters. Depending upon the member of cluster image can be easily segregated into different segments and the one closely depicting shape of optic disc is the desired feature. The most critical part of FCM algorithm is deciding number of clusters. Sensitivity of 0.876 was achieved which indicates satisfactory performance of the proposed method.

In his research Walter et al [35] depicted a methodology in which RGB picture was changed over to Hue-Luminance-Saturation (HLS) space. A thresholding was connected to confine the Optic Disk focus in the luminance channel. Watershed transform is used to determine the exact boundary of the optic disk by utilizing the red channel of the RGB picture which involves morphological preprocessing of the gradient image. After Watershed Transform, the picture is separated into little portions called super pixels. The red plane was chosen as Optic Disk boundary is more noticeable here. To decide the Optic Disk, the Watershed change is obliged by markers got from a formerly computed Optic Disk center. The process to identify the optic disc boundary had a few issues because of veins impediment.

In his research Zhu et al. [36] utilized Hough Transform. They applied this technique on edge map that was obtained from applying morphological operations on the Luminance gray scale of the image. By normalizing each component of RGB space luminance grayscale can be achieved. This technique is approximately associated with primary converging of retinal veins. The creators cautioned that because of feeble edge data their technique disappointment on low quality pictures as round Hough space may be misinformed. Aquino et al. [37] approximated the Optic Disk limit utilizing Circular Hough change on the angle picture got after expulsion of veins. It is acquired from the ophthalmologists that the outcomes were contrasted and ’Roundabout Gold Standards’ (benchmarks). They associated that roundabout estimates could beaten by the execution with curved guess and deformable methodologies.

Carmona et al. [38] acquired an arrangement of speculation focuses that spoke to force levels and geometric properties like ONH shape pixels. At that point a hereditary calculation was connected keeping in mind the end goal to discover a circle approximating the limit of ONH. The technique was connected on DRION-DB database and the exactness was accounted for regarding pixel distinction.

In his research Babu and Shenbagadevi [39] utilized k-means clustering subsequent to changing over the picture into YUV shading space (one luma Y and two chrominance UV segments) in view of Commission Internationale de Éclairage (CIE) format. They computed the CDR by taking the rectangular zone estimations of both the Optic Disk and Optic Cup. The general exactness of the strategy was dictated by contrasting CDR values and those got from Gold Standard qualities from the Ophthalmologists.

In his research Daniel Welfer et al [40] portrayed a versatile morphological technique for the instinctive detection of the optic disc in computerized shading eye fundus pictures. This strategy was intended to distinguish the optic disc center focus and the optic circle rim. For representing the color input retinal image perceptually uniform Luv color space was selected. The method which is discussed in the research has the ability to detect the center of optic disc is accurate up to 100 % and 97.75% using DRIVE and DIARETDB1 databases. The method has the ability to correct all the optic disc regions which is being detected which is within the premises of optic disc marked manually. The proposed method has sensitivity 83.54% and specificity 99.81% for identifying rim of optic disc which is in the DRIVE database, whereas DIARETDB1 database had the specificity 99.76% and sensitivity 92.51%.

In the non-model based methodologies for extricating out Optic Disc, the measures, for example, vertical length or horizontal length were utilized as a part of deciding CDR after digging out Optic Cup. For diagnosing Glaucoma one of the important features is CDR it is not crucial for Glaucoma documentation [41] as some of the patients can have large size of ONH. In this way it is adequate to decide different symptoms, for example, neuro-retinal edge loss and PPA which require correct division of Optic Disk and Optic Cup. In this way, Model based methodologies can be utilized as a part of deciding out correct limits of Optic Disk and are clarified in the accompanying segments.

4.2.2.1.2 Prototypical (Model) Based Methodologies

The prototypical or model based methodologies can be further categorized into two main types [83] on the basis of technique being utilized:-

- Freeform modeling
- Statistical shape modeling

No unequivocal structure of format aside from a few limitations is there in Freeform Modeling. Active Contour Modeling (ACM) [42] has been generally applied for segmentation of

optic disc perimeter in this specific class. It changes its shape comparing to the properties of an image based contour properties and/or knowledge based constraints. Energy functions both internal and external are responsible for behavior of classical parametric active contours. The region that contain model which is derived by image features is determined by external energies. Whereas, the curve of the model serving as smoothness limitations to resist any distortion is determined by internal energies (e.g. elasticity and rigidity). The contour is moved towards the target shape by reduction of energy function. Mendels et al [84] utilized morphological processes on YIQ fundus images along with active contour to extract optic disc. Gradient Vector Flow (GVF) derived from edge maps was used to fit the contour to the rim of the disc [41/31]. The ultimate position of the delineation was not dependent on initialization values. Nine retinal images were used to test this technique. As opposed to use original grayscale images directly, morphological pre-processing has proven effective.

Xu et al. [43] defined the vector of control points by modifying the energy function of contour. Circular Hough Transform was used to initialize the contour. Moreover, weighted k-means algorithm was used in which the contour points position was updated automatically. The contour points then grouped into clusters of edge point and uncertain point. The edge points are retained near to their initial locations and the uncertain points are updated to their correct positions by this operation. Optic Disc segmentation has overall high accuracy but the images having Peripapillary Atrophy (PPA) resulted in algorithm failure due to less coverage of energy function.

P S Mittapalli et al [44] have proposed a method in which optic disc contour was detected using implicit region based active contour model which acquired 0.975 of F-score when implemented on 59 2D retinal fundus images. This method is used after getting inspired from state of the art local binary fitting energy active contour model (LBF). Information of local image is incorporated at each point of interest which gives boost to the LBF active contour model. Features like texture, intensity and color were used for the purpose which resulted in high accuracy for all types of optic disc including disc affected by peripapillary atrophy. No constraint on change of shape is imposed on fundamental model in this method and therefore a relatively better solution for segmentation of optic disc. This novel contour recognition method for optic disc is typically dependent on inherent active contour model that is region based. Detection on the range of OD instances is improved by considering information about image at point of interest. Method initially

defines an energy function. Two vectors approximated the feature values of contour from outside as well as inside. Optimal values are selected for two vectors which minimizes the energy function centered at selected point when the contour C is exactly on the object boundary.

Joshi et al. [45] adopted a level set approach where zero-level set represented the contour of an optic disc similar to the one used in Lipschitz function. Based on appropriately selected initialization parameters a good accuracy has been achieved compromising computational efficiency. Yu et al used an information of region intensity in level set module that made its implementation fast however accuracy was compromised. MESSIDOR dataset with erased blood vessels was used for implementation of proposed methodology.

As compared to Non-model based techniques, higher accuracies were achieved in segmenting optic disc by using ACM. In case of test images where atrophies or textural alterations are involved, the ACM gave more errors. Moreover, robustness of these techniques is questionable as they were applied on local dataset only. Proposed algorithm is required to be tested on publicly available databases to check its robustness.

An offline process of training is adopted in ***Statistical Shape Modeling*** in order to determine any shape. In this category, Optic Disc boundary has been extracted using ASM. Using statistical based model, ASM approximates the shape of an object. Optic disc boundary is reflected in ways which are matching to the orientation depicted in training dataset by deforming ASM. Li et al [46] proposed a method in which they utilized ASM technique to get the optic disc boundary segmented out by differentiating the edges of OD on the basis of image gradient from rest of the features. Subsequently the acquired results were compared with annotated images obtained from ophthalmologists using mean distance to closest point.

Fengshou et al [47] searched the most appropriate candidate point during search for an edge by using minimum Mahalanobis distance from the mean profile vector. Additional information of Gradient was augmented with Mahalanobis distance function to add weight into it. The results were evaluated with benchmark that included other assessment measures along with mean distance to the closest point. The exploration space was constrained by defining the search outline on the image gradient for defining the boundary of an optic disc [48]. The method could give more improved results by erasing blood vessels inside optic disc region.

Warp Kim et al. [49] after selecting ONH as brightest point defined the imaginary circle. The technique of random sample consensus was implemented. In this technique a pretended ring

was changed into a rectangular shape which then inversely perverted into a circular shape in order to locate ONH boundary. The shape changing was implemented by applying threshold on the grayscale image. The threshold value mainly dictated the fate of boundary pixels. The author achieved higher accuracy through Random Sample Consensus (RANSAC).

Statistical shape modelling as compared to freeform modelling did not achieve higher segmentation accuracy reason being fewer factors were used for training dataset construction. For bringing more accuracy in segmentation results statistical measures may be included in training set and even energy information may be contoured. It could be fairly helpful in differentiating PPA and optic disc regions by incorporating previous statistics in the training set. Moreover, through diminishing blood vessels overlapping effect, segmentation accuracy could be improved.

4.2.2.2 Optic Cup (OC) Segmentation

Optic cup segmentation is the next important step after successful segmentation of optic disc in the process of diagnosing glaucoma. Optic disc is a sort of excavation in the optic disc through which blood vessels and optic nerves are passing and its detection is an essential step in glaucoma assessment. Although it is challenging to identify optic cup in 2-D fundus image however these two features are used extensively in investigating and determining some of the key indicators like cup to disc ratio, neuroretinal rim and deviation from ISNT rule. Similar to boundary extraction of Optic Disc, several methods have been proposed and implemented to determine the Optic Cup boundary. Some of the automated techniques for extraction of Optic Cup boundary using 2-Dimensional fundus image covered in the literature are discussed as follows.

Nayak et al. segmented out the optic cup region by applying erosion and dilation operations on green plane of RGB images.

Babu et al. [50] after erasing vascular pattern from OD utilized Fuzzy C-means clustering technique on the green plane image transformed using wavelet method. Same technique was used for segmentation of optic disc as well. However red plane image was used, as optic disc gives better contrast in red plane as compared to optic cup which becomes more prominent in green plane.

Ophthalmologists often use kinks in blood vessels during clinical examination of glaucoma to determine the location of optic cup. Wong et al [51] applied same technique of locating kinks in their proposed method to find out the initiation point of optic cup. Kinks are basically the bends which occur in blood vessels as they negotiate the boundary of optic cup. In this proposed method

small areas called patches are extracted within the optic disc. Out of these patches certain features like segment-based wavelet, edge and color are generated for vessel candidates. Subsequently these candidates were classified using SVM technique. A shifting multi-scale window interval is used to detect and localize kinking through probing the blood vessels along its length. The pallor-based information was then combined with obtained kinks to determine the OC. It was determined empirically that places where blood vessels bent greater than 20^{o} were the Optic Cup boundary. Experiments on a sample data set showed promising results for the proposed method.

Joshi et al. [45] determined the Optic Cup boundary by interpolating the vessels kinks and the Optic Cup boundary in the 3rd dimension using spline interpolation by using the same information of blood vessel kinks at the edge of Optic Cup. The cup boundary was approximated by utilizing clinical knowledge of ophthalmologists obtained from direct3D cup examination.

Malay et al [52] used double threshold method for segmentation of optic cup. Blood vessels were removed by using first threshold and super intensity pixels contained by optic cup were segmented by using second threshold. In comparison to the other parts of the Fundus image optic cup and optic disk region have brighter intensity pixels. These pixels are therefore termed as super pixels. For obtaining the optic cup by segmenting these high intensity super pixels this method was used. The size of the input image was then calculated and grayscale image of the same was obtained if the colour band was more than 1. The number of pixels is counted and is called the pixel count from all the grey levels from the histogram of input image. Then the bar graph of pixel count is drawn and the middle column is computed for the bar graph. The bar graph is then divided into two halves, left half and right half. The number of pixels in left half (PL) and right half (PR) is computed. Further the difference of pixel count of left half and right half is calculated and is called the resultant pixels count (PRP). This resultant pixel count contains pixels which belong to the region of interest. From the resultant pixel count we need to segment the super pixels to detect the optic cup. For this a threshold was defined to differentiate the super pixels from the remaining pixels of the fundus image for proper segmentation of the optic cup. The threshold was obtained by calculating the absolute sum of the resultant pixel count and $1/40^{th}$ part of this absolute sum was used in case of optic cup segmentation. The corresponding grey-level is utilized as a threshold. This was found empirically true for most of the fundus images. The optic cup is segmented using this threshold and green channel of the image. Optic cup is the brightest part of the optic nerve

head (ONH) which is clearly identified in green channel of the input. Furthermore Hough Transform was used for calculating the radius of the optic cup.

Pardha et al [53] proposed an unusual optic cup segmentation method which was based on the structural and grey level properties of optic cup. Most commonly used visual signs for approximation of optic cup boundary from fundus image are change in intensity level near boundary of optic disc and cup and secondly blood vessel bends. On the basis of same clues this clustering based thresholding method has been proposed. A thresholding technique based on SWFCM algorithm [54] is implemented which can preserve the spatial structures in thresholded image. As usual the same green channel in RGB space is used in this method as it provides better information about optic cup. An iterative FCM algorithm is employed which is clustering based method and minimizes the weighted sum. Due to inherent drawback of taking more time by FCM, a grey level histogram of image is employed for calculating parameters followed by performing threshold function with a threshold value of average of maximum and minimum grey level intensities. This gives the initial detection of optic cup which although does not resemble with actual cup due to blood vessel obstructing nasal side and close value of intensities of both disc and cup on temporal side however give good estimation. To address these issues certain morphological techniques like convex hull, opening and closing are used. Employment of these morphological operations help in smoothening the boundary of optic cup towards temporal side however could not perform well on nasal side. Subsequently the information on nasal side was estimated by using symmetrical properties of the cup in both horizontal as well as vertical directions with respect to the center of the cup. Final cup boundary points were then detected by calculating major and minor axes in the orientation of initial cup obtained through clustering. Finally the detected cup boundary was found to be accurate and corresponds with clues normally used by ophthalmologists.

Different from most of the methods previously explained in the collected works, to get better accuracy, method proposed by Kavitha et al [55] differs by preliminary detection of optic cup region followed by blood vessels evasion. To distinguish the optic cup region from neighboring region, the research group established a method containing color space examination, histogram scrutiny based segmentation and k means clustering followed by morphological operations. K-Means clustering is a technique that lies under unsupervised learning category. On the basis of inherent distance from each other, it principally classifies the input data into several clusters. The algorithm firstly envisages that the data features form a vector space and iteratively

tries to discover regular clustering. As it is known that color space transformation plays a considerable role in image processing, color information is incorporated into the segmentation process through this step, where the original RGB image is altered to different color spaces and it has been established that L*a*b* space consisting of a luminosity layer 'L*', chromaticity layer 'a*' indicating where color falls along the red-green axis, and chromaticity-layer 'b*' indicating where the color falls along the blue-yellow axis. 'a*' and 'b*' layers have all the color information. When compared with the other color spaces, Optic cup is clearly obtained in this color space. These spaces serve as feature vectors for k means clustering. Color difference is measured with the help of Euclidean distance metric. On the basis of domain knowledge, the number of clusters manually selected in proposed method is four (K=4) as the optic disc region contained four prominent features that include optic cup, blood vessels, inner portion of optic disc and outer optic disc.

4.2.2.3 Calculation of CDR

Cup-to-disc ratio measurement is one of the regularly used techniques adopted by ophthalmologists while clinically assessing glaucoma. Ratio of diameters between optic disc (outer portion of ONH) and optic cup (inner portion of ONH) measured in vertical direction as ONH is vertically oval or elliptical. 0.4 to 0.5 is usually considered as the acceptable range of cup-to-disc ratio and shows that ONH is normal. Anything greater than 0.5 gives an indication towards suspicious ONH that could be suffering from glaucoma. As it is one of the integral clinical test carried out in glaucoma assessment hence lot of study has so far carried out to automate the calculation of this ratio using digital fundus image. Automated CDR calculation could assist consultants in segregating glaucomatous images from normal ones in shorter period of time and concentrate more on affected cases. Summary of research carried out in this field by different researchers is discussed in succeeding paragraphs.

K-means algorithm, an iterative technique used to partition the ROI image into K clusters and subsequently measure cup to disc ratio were used by K. Narasimhan et al [56]. In this technique, K value is chosen as 3 since ROI mainly covers the entire optic disc, optic cup and a small portion of other regions of the image. The cluster which contains the border region out of these three clusters belongs to the other region of the ROI image that does not contain the optic disc and optic cup. Therefore, it is removed for the extraction of optic disc and the optic disc region is formed by remaining two clusters. The cluster in the center of the image forms the optic cup,

since it is clearly known that the optic cup is inside the optic disc. Finally, to fill the holes and small region inside optic disc clusters and optic cup cluster, morphological operation is performed. Connected components technique is applied after extracting optic disc to form the rectangle that contains the whole disc region and cup region. An inscribed ellipse is drawn from the center of the rectangle. $A = \pi ab$ is used to calculate area of the ellipse as well as area of the optic disc, where a and b are major and minor axis length respectively i.e. half of the rectangle width and half of the rectangle height. Similarly, area of optic cup is also calculated. Ratio between area of the optic cup and area of the optic disc is computed as The CDR, which is used as one of the features for the detection of glaucoma.

Yuji Hatanaka et al [57] explained that presence of glaucoma is often diagnosed through measuring cup-to-disc ratio by ophthalmologists; though, determining cup area on the basis of computational algorithm is a very difficult task. Measurement of cup-to-disc ratio using a vertical profile on the optic disc has been devised and proposed as more comprehensive and relatively easily implementable method. Afterwards, to detect the edge of optic disc, Canny edge detection filter was used and profile of center of the optic disc was obtained. Successively, through classification of the profiles based on zero-crossing method, the edges of the cup area were determined. Vertical cup-to-disc ratio was calculated in the end. As against the normal cases, Glaucoma cases tend to have enlarged cup regions. In many cases, the bright region is extended. Contrast of the cup and the rim regions was also found high. During comparison of optic disc profiles, profile for glaucoma case appears as a broad mountain with short skirts while that of normal cases tends to appear as an arrow mountain with long skirts. AUC of 0.947 was achieved when 45 images including 23 glaucoma images were utilized for assessment of this method.

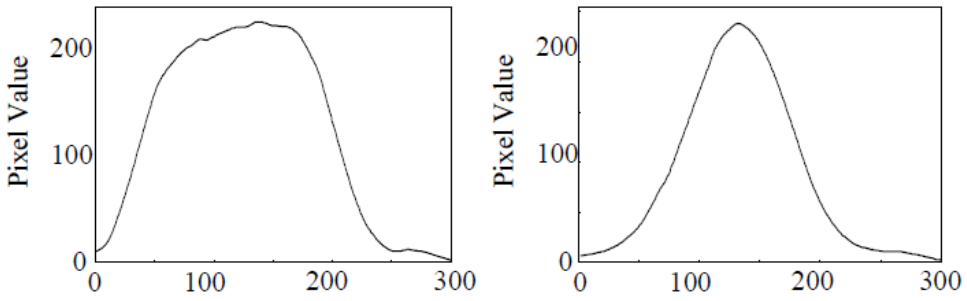

Figure 4.1: (Left) Glaucomatous eye profile, (Right) Normal eye profile. [58]

A. Poshtyar et al [59] adopted a different approach for assessment of CDR. Instead of measuring diameters of optic cup and disc features they presented an approach of automatic calculation of CDR using automated segmentation of these features followed by quantitative determination of areas by selecting related pixels using fundus image and subsequently taking their ratio. For coarse and accurate localization of optic cup and disc, Green band of colored fundus image in RGB model was used. 12x12 pixel size square template was convolved over the image for assessing max average intensity value. Using threshold technique based on criteria set through empirical calculation, pixels were labelled and segregated as optic disc or optic cup. To determine the edge values, AND Logic Operation was used on each sequence pixels. Once the edges were defined the areas of both the features were measured and ratio was obtained. With the help of proposed method, 111 out of 120 fundus images with glaucoma with a success rate of 0.92% were correctly classified.

4.2.3 Parapapillary Atrophy

To examine the region adjacent to the optic disc for the presence of Parapapillary atrophy is one of the rules for assessment of optic disc for glaucoma. It is the thinning out of chorioretinal tissue present near the outer side of optic disc which is closely associated to the initiation of glaucoma. In ophthalmic language, alpha and zone beta are the two zones in which Parapapillary atrophy can be divided. Figure 4.2 clearly depicts these two areas. Zone alpha is characterized as irregular pigmentation available in lower as well as upper portion of the optic disc. Both normal as well as glaucomatous eyes generally have this zone. However, in context of glaucoma, zone beta is of vital importance which is caused by atrophy of retinal nerve fiber layer and choriocapillaries that leads towards enlarged choroidal vessels and sclera become more visible. Zone alpha will always border zone beta in case of such eyes where both zones are present. Eye suffering from glaucoma will have extensive zone beta as compared to healthy eyes. The area around optic disc that is affected by PPA is closely related to neuroretinal rim loss pattern. Generally the atrophy appears to be largest on that side of neuroretinal rim where its thickness is minimum.

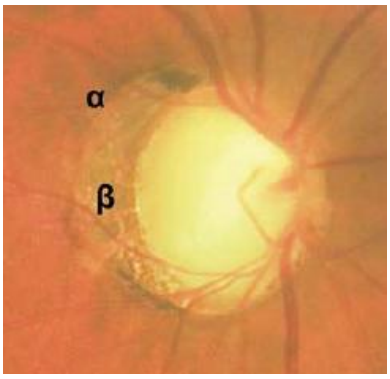

Figure 4.2: Zones of Parapapillary Atrophy. [60]

Several researchers have used this feature of retinal images for automated detection of glaucoma. Tan et al [61] proposed variational level set method for detecting PPA boundary. Horizontal and vertical elliptical curves were initialized inside as well as outside the OD boundary respectively. The horizontal curve is meant to diminish the impact of retinal blood vessels impact and allow level set function to nurture outward till the time accurate OD boundary is reached or searched. On the other side its vertical counterpart is initialized externally and shrink inward to represents the closest physical shape of the OD. Once both the boundaries of OD are earmarked by the algorithm then subsequently the difference of these two contours is taken followed by thresholding that difference in the HSV color space to broadly segment out the PPA area. The proposed method claim the accuracy of 95% for localization of PPA.

In another attempt for segmentation of PPA area, the texture based statistical features like mean, variance, standard deviation, correlation and contrast were found out by Muramatsu et al [62] to make a feature vector of precisely 63 diverse features. On the basis of this feature vector PPA and non-PPA pixels were segregated from each other. Linear discriminate analysis (LDA) [63] was used by Smola et al. for classification of pixels after carrying out training of proposed algorithm using both normal and glaucomatous images. The proposed method was applied over 58 glaucomatous images having moderate to severe PPA and results remained satisfactory. Importance of correct segmentation of PPA can never be ignored as it not only assists in diagnosis of glaucoma but also remained helpful in accurate assessment of optic disc boundary.

4.2.4 Retinal Nerve Fiber Layer Defect Analysis

After ONH (optical nerve head), RNFL (retinal nerve fiber layer) is the most important component of retina that get structurally affected by glaucoma. Optic nerve fiber layer is

progressively degenerated during the course of this disease. Correct quantitative analysis of RNFL defects using image processing techniques on digital retinal fundus image can assist in early diagnosis of glaucoma. This aspect has also been covered amply by researchers in applying computer aided diagnosis algorithms which are briefly highlighted in this part.

Prageeth et al [64] has developed a system for glaucoma screening that utilizes fundus images for processing and compare results with examination of ophthalmic field test. The proposed method assimilates a number of glaucoma detection techniques and creates an automated system. This automated system uses a database of fundus images to attain high sensitivity and global accuracy. In fundus image the reflection reduces due to RNFL atrophy. That decrease in reflection caused decrease of brightness in retina. The degree of atrophy was evaluated in this system by quantitative analysis of low contrast area around OD and other regions of an image. After image pre-processing the optic disc was localized using thresholding and canny edge detection algorithm with a purpose to define area to be analyzed. Since area affected by RNFL atrophy looks dark in complexion than remaining portion of the retinal image therefore intensity of all the pixels around optic disc and outer edge of fundus image was estimated for quantitative analysis. Intensity of pixels was taken out at definite degree interval and plotted against the distance from optic disc and outer edge respectively. If the number of white pixels exceed predetermined threshold around optic disc and edge portion then that image was put under the category of suspected case for glaucoma. Total 829 images were included in dataset that was analyzed (300 normal and 529 glaucomatous) with size of 768 × 576 pixels. The proposed system had 91.5% successful rate of performance.

Acharya et al. [65] proposed a method to analyze the RNFL texture using higher order spectra, run-length and co-occurrence matrices. The method was tested on 60 images (30 normal and 30 glaucomatous) having a size of (560 × 720 pixels). The authors used several supervised classification techniques to classify normal and glaucomatous images. Although, the classification accuracies were more than 80%, the article does not thoroughly explain the process of feature extraction and which area of the image was analyzed.

Progressive atrophy results in reduction of RNFL thickness [66]. A novel approach was introduced by Jan Odstrcilik et al in which textural appearance of RNFL in colored retinal fundus image was automatedly analyzed to capture these variations in thickness. Proposed method used the features based on Gaussian Markov random fields and local binary patterns, together with various regression models for prediction of the RNFL thickness. The approach allows description

of the changes in RNFL texture, directly reflecting variations in the RNFL thickness. 16 normal and 8 glaucoma affected fundus images were used for evaluation of the effectiveness of devised method. Correlation of 0.72 and 0.58 respectively was achieved between values of output of proposed method and RNFL thickness measured through optical coherence tomography (OCT) which is considered as the standard and authentic devise for detection of glaucoma.

Dharmanna Lamani et al [67] suggested another method for RNFL analysis which was based on Texture and Fractal feature description. These extracted features then subsequently undergone through well-known support vector machine (SVM) classifier for segregation into normal and glaucomatous images. The suggested method utilized color fundus images having resolution of 530x720 pixels. It was presented that there is deep correlation between Texture & Fractal dimensions. Estimated correlation coefficient of 0.35 was observed for healthy RNFL. Similarly linear correlation coefficient values estimated for medium loss was 0.57 and 0.87 was the value evaluated for severe loss of RNFL. These texture and fractal features were measured at 303 different regions in near vicinity of peripapillary area. 50 fundus images of normal individuals whereas 24 glaucomic images were used in the study.

4.2.5 Vasculature Shift

Optic disc (OD) also known as optic papilla is the most prominent part of retinal fundus image. In all normal eyes, the blood vessels network or vasculature bundle arises from the choroids and lie in the middle of the nervous fibers that creates the optic nerve. This optic nerve passes through optic cup and ultimately reaches the brain after passing through a tube like structure. The same anatomy can be clearly seen in digital fundus imagery taken through fundus camera. As soon as the intraocular pressure exceeds normal limit which is the basic cause of glaucoma, it immediately starts damaging the optic nerves hence results in increased size of optic cup commonly known as excavation. This cupping thicken the walls of the papilla due to which the blood vessels enclosed inside the boundary of optic disc are pushed towards the nasal side.

Few of the visible changes that are the outcome of glaucoma and on the basis of same ophthalmologists differentiate between normal and affected eyes include increased size of optic disc and in some cases asymmetric excavation in both eyes, thinning of optic nerves, existence of notches in blood vessels inside perimeter of optic cup, loss of retinal nerve fiber layer mainly from inferior and superior regions, parapapillary atrophy, non-adherence to ISNT rule by neuroretinal rim and vasculature shift. Mostly the assessment of cup-to-disc ratio and deviation from ISNT rule

are used as the key features by ophthalmologists while diagnosing glaucoma. Vasculature shift is also one of the prominent yard stick which can be utilized for the assessment of optic disc in relation to the occurrence of glaucoma.

J.A.d.l. Fuente-Arriaga et al [7] offered a novel approach for classification of digital retinal fundus imagery affected with glaucoma. The proposed method analyzes the alterations inside the optic papilla. The method is formulated on the basis of close connection found between the blood vessels displacement and the optic cup growth inside the boundary of optic disc mainly in three zones less temporal region. The algorithm works in the following sequence: (1) Acquisition of colored digital fundus images; (2) automated extraction of the optic papilla or optic disc region; (3) recognition of a reference mark in the temporal region of optic disc near boundary of optic cup; (4) finding the centroids of vascular bundles in remaining three zones; (5) measurement of the displacement between three centroids and the reference mark selected on the cup boundary; (6) comparing the measured lengths with already set threshold and segregating normal images from glaucomatous ones if distance exceeds threshold value. The method was applied upon 67 images out of which 62 fundus images gave accurate results. The overall sensitivity of this reported method were found out to be 93.02%, specificity of 91.66% and accuracy remained 91.34%.

4.3 Non Segmentation Based Detection of Glaucoma

Although there are few efforts available reflecting the classification between Normal and Glaucomatous patients based on features that do not require segmentation of retinal structures. These methods can serve as prior knowledge for measuring different Glaucomatous symptoms associated with retinal segmentation. Some of those methods are discussed as follows:-

In non-segmentation based methods, Bock has major contribution [68, 69, 70]. Initially they used Pixel Intensity Values on which they applied Principal Component Analysis (PCA) [50] for dimensionality reduction. As a pre-processing step, they corrected illumination and intensity inhomogeneity then in-painted vasculature area after segmenting them out. Later on they added features such as Image Texture, FFT Coefficients, Histogram Models and B-Spline coefficients. Based on these features they calculated Glaucoma Risk Index (GRI). They used classifiers such as Naïve Based Classifier, k-Nearest Neighbor Classifier and Support Vector Machines (SVM) to classify between healthy and Glaucomatous images and they found SVM to be less prone to sparsely sampled feature space.

Dua et al. [65] used Wavelet-Based Energy Features and compared the performance of different classifiers including the previously mentioned classifiers, Random Forests and Sequential minimal optimization (SMO). From SMO they obtained the maximum classification accuracy.

Non-segmentation based methods are not validated by the ophthalmologists in order to distinguish among Normal and Glaucomatous images as in the case of segmentation based methods. If these methods are used in conjunction with segmentation based methods, they cannot only be quite effective in increasing the classification accuracy among different stages of Glaucoma but also can serve as a bench mark for development of further automatic classification methods.

4.4 Glaucoma Related Public Databases for Investigation

A general overview of the public databases being utilized by different researchers discussed in this literature review is given in this part. Below mentioned datasets were mostly constructed for automated extraction of features of Diabetic Retinopathy (DR) however due to the similar nature of anatomical structures used for detection of glaucoma like optic cup and optic disc, these databases were also used for diagnosis of glaucoma as well. Few of the datasets were solely compiled for automated extraction of features for diagnosis of glaucoma.

1. STARE (STructured Analysis of the REtina)

The database called STARE was introduced at University of California by Michael Goldbaum back in 1975. The database contained 81 digital fundus imageries out of which 50 were affected with various pathologies like exudates and hemorrhages and 31 were normal. Top Con TRV-50 fundus camera at 35^0 FOV was utilized for image acquisition that gave an image resolution of 605 × 700 pixels.

2. DRIVE (Digital Retinal Images for Vessel Extraction)

The images for this database were attained from a diabetic retinopathy screening program conducted in Netherlands. 400 diabetic patients were screened between 25-90 years of age. Canon CR5 non-mydriatic (which does not cause dilation) camera with a 45 degree field of view (FOV) was used for image acquisition that gave an image resolution of 768 x 584 pixels.

3. DIARETDB0 (Standard Diabetic Retinopathy Database Calibration Level 0)

A public database used as gold standard for detection of diabetic retinopathy from digital fundus images. It contains 130 color fundus images of size 1500 x 1152 pixels out of which 20 are Normal and 110 contain signs of the diabetic retinopathy. While taking these images no calibration

is performed and the imaging was performed with unknown amount of imaging parameters therefore this dataset is denoted as "calibration level 0 fundus images."

4. DIARETDB1 (Standard Diabetic Retinopathy Database Calibration Level 1)

This dataset have same properties as of DIARTDB0 as far as size, acquisition camera and benchmarking is concerned. Difference lies only in quantity of images (89 colour fundus images out of which 84 with mild Microaneurysms and 5 are Normal) and presence of imaging noise and optical aberrations at the time of capturing due to which this data set is referred to as "calibration level 1 fundus images."

5. MESSIDOR

It is an abbreviation of *Méthodes d'Evaluation de Systèmes de Segmentation et d'Indexation Dédiées à l'Ophtalmologie Rétinienne*. MESSIDOR was a project funded by the French Ministry of Research and Defense in 2004 TECHNO-VISION program. It is composed of 1200 color retinal images out of which 800 images were captured with dilated pupil and 400 without dilation. 540 images are normal and 660 images correspond to patients affected by DR. Topcon TRC NW6 non-mydriatic fundus camera with 45 degree field of view was used for capturing images of size 1440 × 960, 2240 × 1488 or 2304 × 1536 pixels and 8-bits per color plane in TIFF format. The Optic Disc rim was manually annotated by ophthalmologists making it a gold standard set.

6. DRION-DB (Digital Retinal Images for Optic Nerve Segmentation Database)

A joint collaboration of three Spanish organizations, i.e. Universidad Complutense, Hospital Miguel Servet and Universidad Nacional de Educación a Distancia resulted in composition of this dataset. It contain 110 retinal images with the resolution of 600 × 400 pixels. Two different ophthalmologists made annotation of Optic Disc in these images with 36 landmarks. The images were acquired using analog fundus camera which was subsequently converted into digital format using HP-PhotoSmart-S20 high-resolution scanner.

7. RIM-ONE (An Open Retinal Image Database for Optic Nerve Evaluation)

The images for this database are collected from three different Spanish hospitals. This database is collected with exclusive focus on ONH segmentation. It contains 169 images of high-resolution out of which 118 images are non-glaucomic, 12 belong to early glaucoma, 14 with moderate glaucoma, another 14 with deep glaucoma and 11 images are affected with Ocular Hypertension (OHT). More than five experts were employed for manual annotation of images that

makes this database a reliable gold standards and helps the researchers in developing highly accurate segmentation algorithms. Compilation of images from diversified sources is also an assurance of acquiring representative and mixed dataset. All the images of this dataset are captured through non-mydriatic fundus camera.

4.5 Retinal Feature Extraction for Biometric Identification

Over the past few years the trend of automated personnel identification using biometric has increased manifolds. Those fields where uniqueness in identity is of utmost importance, biometric has been incorporated in order to make the system secure and authentic. Widely used biometric systems use numerous physiological features of human body for recognition purpose. Finger prints, iris, speech recognition and face recognition are the most commonly utilized physiological biometrics these days being easily accessible externally. Accepting the fact that developed systems are highly mature and accurate however majority can easily be forged. Keeping this loophole in view a need of an alternate system using such physiological features which are less prone to be tempered or altered cannot be overruled. Unlike traditional biometrics, human retina provides this opportunity to utilize unique features contained in it. Retina is located at a place in human eye which is not accessible externally hence cannot be forged. System uses retina for personnel identification differs from those based on the recognition of iris in which pattern of iris is accessed for distinctiveness. The basis of such retinal recognition system is optic nerve head (ONH) shape and blood vessels pattern distributed all over the retina.

Digital fundus imagery is a useful source for researchers in automated personnel identification systems. Such images can be acquired using digital fundus camera used by ophthalmologists for assessment of retinal condition whether affected by any disease or not. Although this biometric system has the property of being highly secure, reliable and most suitable for security of sensitive installations however acquisition method of fundus image which is the main component on which success of such system is based upon is still awaiting major breakthrough.

Numerous studies have so far been reported on biometric recognition using retinal scan for analysis of capillary blood vessels located on the fundus of an eye. These vessel are extracted using different algorithms and then it is compared with test images in order to build correlation. In most cases the target area remained the extraction of blood vessels and its analysis due to its uniqueness. M. Ortega et al. [71] used a feature point based biometric pattern for retinal recognition. Z. W. Xu et al. [72] focuses on vessel bifurcation and crossover points as key features in retinal

identification. K. Fukuta et al. [73] worked on cross correlation coefficient based identification of human retina. Image registration of input image is carried out in initial stage followed by matching it with reference image by correlating the vessels layout. Usman Akram et al. [74] proposed a three stage method of retinal recognition. Feature vector containing validated feature points of vascular pattern is formed which is subsequently matched using mahalanobis distances.

CHAPTER - 5

PROPOSED METHODOLOGY

5.1 Basic Concept

- ***Cup-to-disc ratio (CDR) & ISNT rule*** is the most accepted physiological parameters for diagnosing glaucoma however accuracy depends upon correct segmentation & measurement of optic disc (OD) and optic cup (OC) in both cases.
- Automated segmentation of OC remains a challenge due to overlapping of blood vessels (BV), poor color contrast, less prominence due to pathological disorders hence affect accuracy of method.
- To overcome this inherent problem of BV occlusion, instead of using CDR a parameter of ***Vasculature Alteration*** was adopted for detailed analysis and assessment of glaucoma.
- Adopted sequence is as under:-
    1. OD segmentation and reference point detection
    2. Vasculature displacement measurement
    3. Biometric approach

5.2 Optic Disc Segmentation

Cup-to-disc ratio (CDR) is one of the most accepted physiological parameters used for diagnosing glaucoma. The accuracy of CDR depends upon correct segmentation of both the optic disc (OD) and the optic cup (OC). Automated detection of this parameter using digital fundus images is extensively used by researchers however many shortcomings like pathological disorders, luminance, poor contrast and blood vessels occlusion are associated with it. This study is aimed at extracting the optic disc region from the retinal fundus image coupled with vasculature displacement measurement and enhanced accuracy through biometric approach for diagnosis of glaucoma. A thresholding technique augmented with a connected component algorithm and morphological operations was used for OD segmentation. Furthermore, a novel vector based approach was utilized for automated measurement of OD diameter which formed basis of biometric approach. A dataset of 25 glaucomic images annotated by certified ophthalmologists was used to assess the performance. An accuracy of 97.32% was achieved in optic disc segmentation part followed by an overall accuracy of 93.9%.

Vision is the most complex and richest of the senses. However blinding diseases such as glaucoma can deprive the people of this remarkable sense due to late diagnosis and the non-curable nature of the disease at advanced stages. Due to clandestine nature of its proliferation and late disclosure it is also identified as a 'silent killer of vision'. Glaucoma mostly affects people aged 40 years and above. Also the noticeable symptoms of glaucoma like vision loss only starts appearing at an advanced stage. Being non-curable at this point of time the option normally left for ophthalmologist is to stop further damage however damage to the optic nerves and associated vision loss cannot be reverted.

Due to non-existence of explicit symptoms, proactive mass level screening systems are necessary to segregate affected patients for detailed health checks followed by appropriate disease management. CDR is a widely accepted index for the diagnosis of glaucoma amongst ophthalmologists however its manual assessment remains inconsistent and fluctuates with observer. This part is mainly focused on automated segmentation of the optic disc along with diameter calculation using a novel approach. Numerous studies have so far been reported on automated segmentation of the optic disc. As examples, Gagnon et al. [75] used a Canny edge detector for the identification of the optic disc edge followed by using template matching technique to match a circular template with edge map. Noor et al. [76] employed color multi thresholding on fundus images to segment the optic disc (OD) for assessment of CDR. The OD boundary was modeled using a circular Hough transform and superpixel classification based OD segmentation was carried out by Thorat et al. [77]. Liu and Chen proposed mathematical morphology and a snake model based approach to distinguish the OD [78]. Success rates of 96.7% and 95.1% were reported for OD localization and OD rim detection respectively. Ashish et al. [79] presented segmentation technique of optic disc based on adaptive thresholding using mean and standard deviation of image to remove information other than optic nerve head (ONH). Ting Yu et al. [80] extracted OD boundary using distance regularized narrow band level set evolution (DRLSE) based on combination of vessel convergence and intensity.

The optic nerve head is the brightest feature in the human retina. It comprises the OD which is a pale colored oval portion and forms the outline of the ONH, an inner orange pink portion is optic cup and the region in between these two features is termed as neuro-retinal rim (NRR). Retinal blood vessels and optic nerves enter into the retina through the ONH which acts as a reference point for other features present in the retinal fundus image. Parametric changes of ONH

are a source of indication for numerous ophthalmic disorders amongst which glaucoma is the most significant. An initial step for understanding and analyzing the ONH is correct detection and segmentation of the OD region. Keeping this in view the under discussion part of proposed method is primarily focused on OD detection which facilitates the extraction of other features and ultimately leads towards the automated screening of the disease. The different steps adopted in proposed method are represented in Figure 5.1.

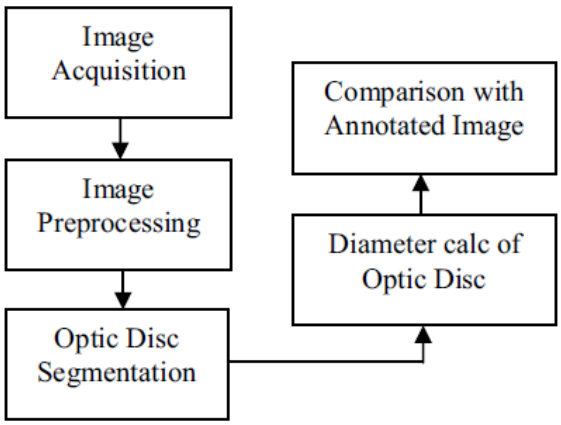

Figure 5.1: Different steps adopted in proposed method.

5.2.1 Fundus Image Acquisition

5.2.1.1 Data Collection

While copious online datasets are accessible online, those containing only glaucomic images are rarely available. With reference to this study an effort has been made to create a comprehensive glaucomic dataset comprising a Pakistan-based ethnic group to fill this gap. Apart from becoming an addition to the existing archive, it could also be used by other researchers in their future work.

Digital fundus images of glaucoma patients were collected from the Ibrahim trust eye hospital, Gujranwala over the period of almost two months. Fundus images of 15 patients were captured with their prior consent and with institutional ethics committee approval. Images were stored in JPEG format and had a resolution of 3216x2136 pixels. All the images were later separately annotated by two different ophthalmologists. Annotation included marking of the OD, optic cup and CDR judgment.

5.2.1.2 Method of Image Acquisition

A fundus camera is a specific type of low power microscope with camera attached. The optical design of the fundus camera is based on the indirect ophthalmoscope whereby a camera registers the retinal image. A TRC-NW8F, Non-Mydriatic Retinal Camera (Topcon, Japan) was used for said purpose. This 12.3 megapixel camera provides high resolution images with 45^{O} field of view. Images of both eyes of seven female and eight male patients between 38 to 65 years of age were taken. A diagnosis of glaucoma is dependent on various confirmatory examinations like visual field test, intraocular pressure (IOP) measurement and optical coherence tomography (OCT) therefore segregating such patients from others took time. Ophthalmologists initially set the criteria for isolating patients with low vision as well as having abnormal ONH appearance during routine checkup using a slit lamp. Once confirmed on the basis of IOP testing the patient was finally selected for fundus imagery.

5.2.2 Preprocessing Stage

Inter technician proficiency, inability of patients to focus on external targets given by the observer, media opacities mainly due to different diseases and large image size affected the image eminence. Preprocessing stage made the image data more practical to be utilized in subsequent study.

5.2.2.1 Contrast Enhancement

A number of fundus images were very low in contrast resulting in poor visibility and merging of the ONH with the retinal background. Under such conditions it becomes difficult for the naked eye to differentiate between different retinal features hence contrast enhancement is used to distribute intensity values uniformly over a broad range to enhance image quality.

5.2.2.2 ROI Extraction

Different steps included in extraction of region of interest (ROI) from the original image are shown in Figure 5.2. The original image acquired through the fundus camera typically comprises of whole retina including macula, fovea, retinal nerve fiber layer and blood vessels. In this study information other than optic disc region was redundant for segmentation. The input fundus image was of size 3216x2136 however the area of interest occupied approximately 700x700 pixels. The OD is the portion of the fundus image having the highest brightness as

compared to the rest of image. The brightest point inside the optic cup using all three color channels was picked. The

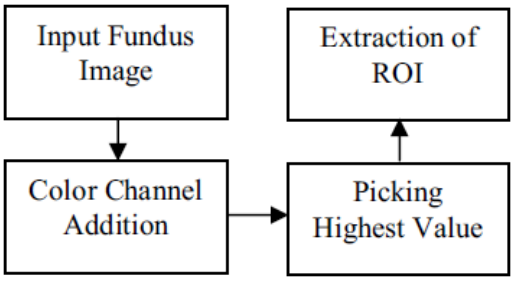

Figure 5.2: Extraction stages for ROI.

ROI was extracted covering the complete OD region as well as surrounding portion using brightest point as the midpoint of ROI square. Figure 5.3 depicts the original input fundus image and extracted ROI.

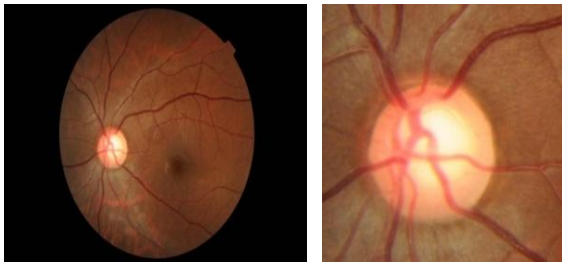

Figure 5.3: Original and ROI extracted images.

Due to variation in size of OD features, it was mandatory to select some standard size of ROI so that OD remains fully detectable and in the middle of all ROI images. To fulfill this constraint different image sizes were tested on dataset. After analysis, a size of 600x600 was found out to be the optimum for ROI as all the images contained a full OD region prominently visible with appropriate clearance from edges (Figure 5.4).

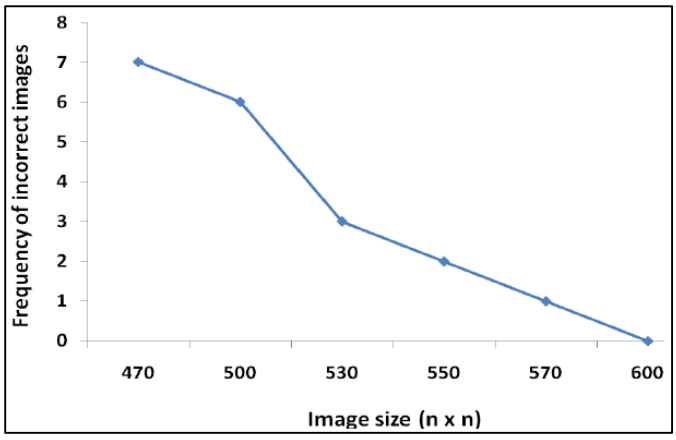

Figure 5.4: ROI size analysis.

5.2.3 Processing Stage

5.2.3.1 Optic Disc Segmentation

The extracted ROI image is the combination of red, green and blue components in the RGB space. The green plane gives better contrast for optic cup whereas the OD has better contrast in the red plane [58/67]. The same technique was implemented on ROI images in this dataset to find out the color plane that gave an optimal contrast result for OD segmentation. The colored image was converted into its red, green and blue components. In line with [58/67], the OD was most evident in the red plane. To further make the contrast prominent, the extracted red channel image was converted into a negative image as shown in Figure 5.5.

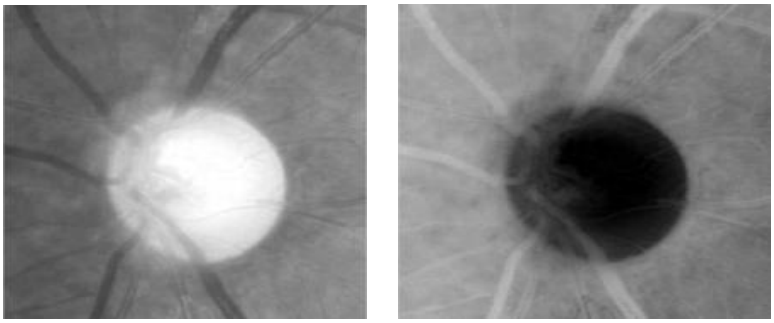

Figure 5.5: Grayscale and Negative images of red channel.

Adaptive thresholding [26/11] was applied to the OD image. Due to artifacts in the fundus images, a number of post-thresholding images contained incorrectly segmented portions other than OD. A connected component algorithm [56/66, 81/68] was utilized to isolate and then remove unnecessary segments while leaving behind the desired OD with minor artifacts. Figure 5.6 depicts before and after conditions of one binary image.

Minor artifacts remained inside OD the region being primarily present on the threshold boundary due to the presence of blood vessels. Using morphological operators [52/69], a binary image was attained after convolving carefully designed structuring elements.

Image processing operation of perimeter determination based on dilation and erosion which determines the perimeter pixels of the object in binary image is used to convert segmented out OD feature into an OD sketch. A pixel is considered as a perimeter pixel if it satisfies essential criteria.

Figure 5.7 shows the segmented out OD and its perimetric representation which we used subsequently for diameter calculation.

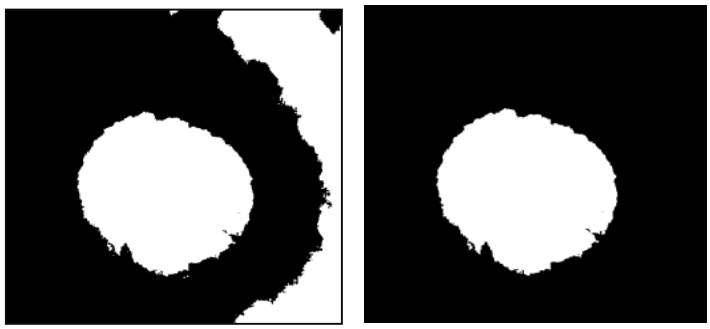

Figure 5.6: Binary image before and after removing major artifacts.

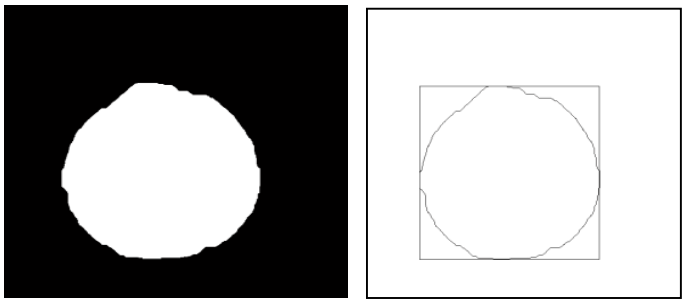

Figure 5.7: Binary and perimeterized optic disc images.

5.2.3.2 Reference Point Detection

Reference point was needed to measure the shifting of blood vessels from middle of the ONH. A rectangle was drawn around segmented out optic disc. Two reference points shown in figure 5.8 were selected at intersection points, one for right eye and other one for left eye. These points were used in subsequently part for measuring distance between centroids of blood vessels in nasal, inferior and superior zones.

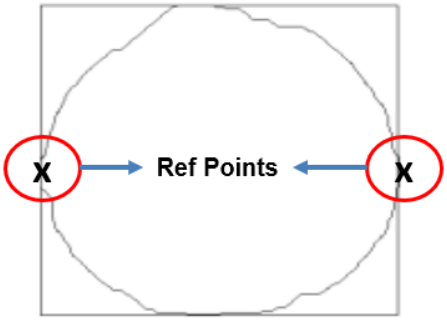

Figure 5.8: Reference points on Optic Disc boundary.

5.3 Vasculature Shift Detection

Method adopted in this part of the study is a bit different technique as compared to those mostly being used by researchers while doing automated assessment of glaucoma. Instead of using cup-to-disc ratio or utilizing ISNT rule, feature of blood vessels shifting from optic nerve head center has been detected and utilized for automated segregation of normal images from glaucomic ones. This morphological alteration of blood vessels is a permanent feature in glaucomic eyes and can prominently be detected and analyzed inside optic disc. These blood vessels displacements can even be visualized in those eyes in which glaucoma is in its initial stages. As the intraocular pressure increases the aqueous humor puts pressure on retina due to which nerve fibers start getting damaged. These nerve fibers are spread all over the retina and taking electrical signals to the brain after passing through neuro retinal rim. Inside neuroretinal rim or in the middle of the optic disc also lies the blood vessels. As the nerve fibers that are surrounding the blood vessels inside optic disc starts getting disappearing which is also known as excavation phenomenon, the inner blood vessels which are already lying little bit on nasal side starts dragging more towards the nasal end.

This approach is although directly linked with enlargement of optic cup or excavation growth [7/2] however in automated detection of glaucoma segmentaton of this very feature is the biggest challenge so far due to multiple reasons few of which include low contrast of optic cup in severly affected glaucomic images, blood vessel occlusion, poor eminence etc. Therefore the involvement of optic cup has kept limited in proposed method to improve efficacy of the system. The proposed method is comprised of below mentioned stages and the flow diagram is depicted in figure 5.9:-

(1) ROI extracted image

(2) OD segmentation

(3) Blood vessel extraction

(4) Dividing OD into ISN zones using masks

(5) Detection, marking and measurement of centroids on OD

ROI extraction and OD segmentation has already carried out in the start of first part. Same ROI and OD segmentation will be utilized as the beginning steps of this second stage i-e blood vessel extraction. The only addition to these processes will be to centeralize the segmented out optic disc so that at the time of segregation of optic disc into different zones all regions will have the same size.

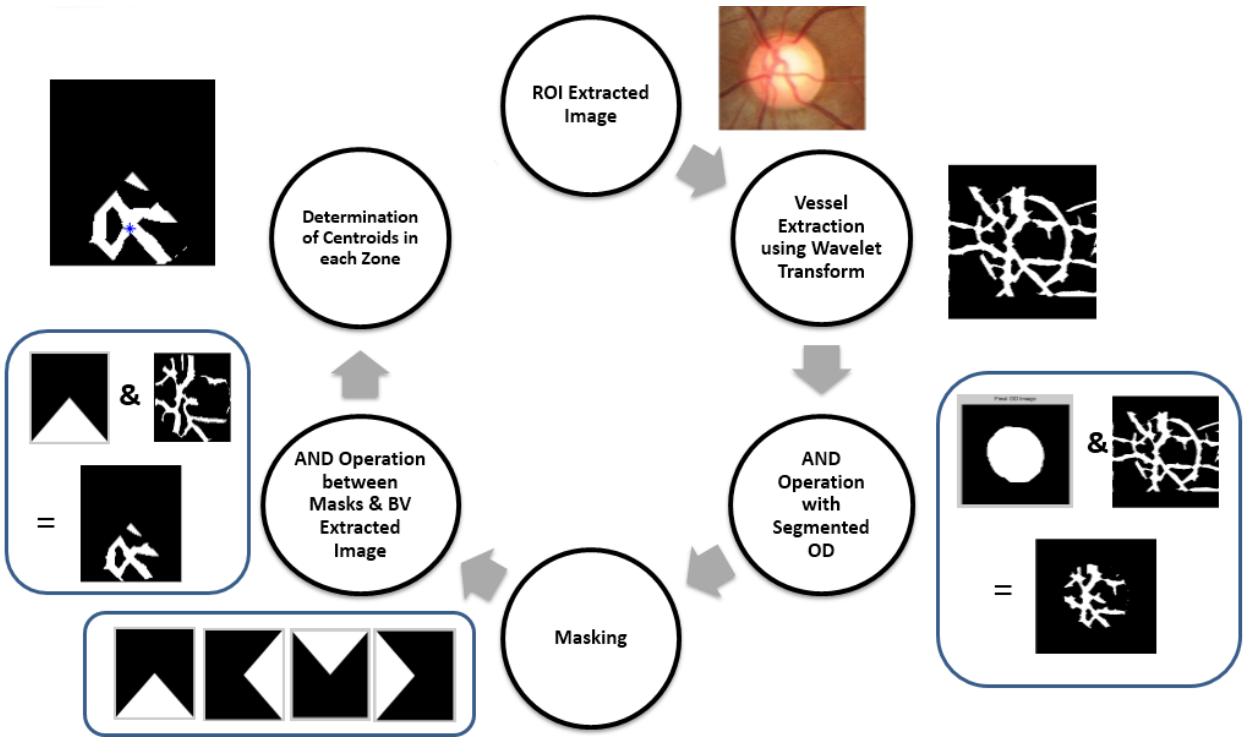

Figure 5.9: Flow diagram of vascular displacement measurement

5.3.1 Blood Vessel Extraction

Correct extraction of blood vessels is an important step before assessing the accurate vasulature shift inside optic disc. A binary image having clear demarkation between background and blood vessels was required to find out the centroids in next part of the proposed method. RGB color image of ROI extracted previously was available as an input image. As the green channel of RGB image gives better contrast between different retinal features hence the same was used in its inverted form in order to get more prominance between blood vessels and background image and enhanced segmentation. Subsequently wavelet transform is applied onto these extracted green mode images for enhavement of blood vessel pattern specifically those part in which very thin vessels are located [82]. Obtained enhanced image of blood vessels of ROI is then processed with multilayered thresholding which resulted in binary images having different level of segmented out blood vessels. To form a binary mask for vessels extraction, adaptive thresholding was utilized. Masking was carried out between the two images which produced an image having more clear view of blood vessels. Figure 5.10 depicts the flow diagram of suggested method.

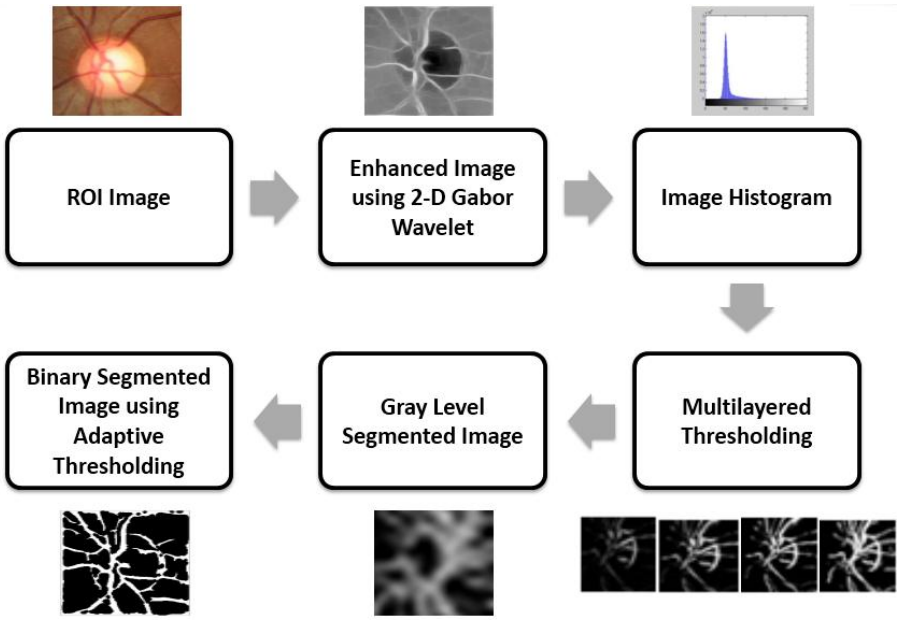

Figure 5.10: Flow chart of blood vessel extraction

5.3.1.1 Blood Vessel Enhancement

Vessel enhancement was carried out to make thin blood vessels more prominent as visisibility always remain an issue for such tiny features. The issue was resolved by implementing 2-D Gabor wavelet on original RGB image of ROI. Due to directional selectiveness ability of Gabor wavelet it act as a good edge distinguisher and reduce image noise. As blood vessels have also possess the directional configuration therefore Gabor wavelet performed well in detecting this feature.

5.3.1.2 Multilayered Thresholding

Multilayered thresholding technique being incorporated for segmentation of blood vessels. As the image contain both thick and thin blood vessels therefore the response of thresholding cannot be optimal due to high intensities in the middle of vessel and low intensities at the edges and in case of tiny vessels. This module takes enhanced image as its input and calculates its threshold value using histogram for the first time. Using this threshold value the initial blood vessel segmented image is found. This segmented image is further processed using morphological operator to convert it into skeletonized image having all vessels with a width of one pixel. This skeletonized image then act as an input to the edge image module in which all those vessels having false edges and disconnected segments are removed. As a last operation acquired edge image is subtracted from edge image obtained in previous iteration. On getting zero output of the difference between edge images the iteration stops and threshold is reduced

by one for next loop repeating the same procedure till the time final segmented image is obtained. This final segmented image is then utilized to generate a gray level image having original intensities of invertedgreen channel for thos pixels only which are segmented out as blood vessels. Finally a binary image is created using adaptive thresholding on graylevel image which is considered as the true blood vessel segmention.

5.3.2 Extraction of OD Portion

Extracted blood vessels image also contain surrounding portion of optic disc which has no role in evaluation of glaucoma in this specific method and in some images the optic disc do not lie exactly in the middle of the ROI. Initially the optic disc was centralized by finding the middle point inside optic disc through sketching a rectangle touching all four sides of optic disc boundary as shown in figure 5.7. Once the rectangle encompassing the OD is made then the mid point of that rectangle was taken as the mid of optic disc. Subsequently the width of portions left outside the rectangle on all four sides was measured. The smallest width was taken as the standard measurement and the image was cropped from all sides as per this minimum reading in order to brin gthe optic disc part right into the middle of the ROI for succeeding steps. Such portion do contain blood vessels which results in increased computational time. As the system entails only central part of optic nerve head ONH for measurement of vasculature shift hence the same was filtered out using AND operation between OD mask and vessel segmented image. Figure 5.11 shows the outcome of this step.

Figure 5.11: Extracted OD portion.

5.3.3 Image Masking and Segregation of OD into ISNT Zones

To proceed further with the proposed method the next requirement is to divide the binary image of optic nerve head into its three zones namely inferior, superior and nasal as shown in figure 5.12.

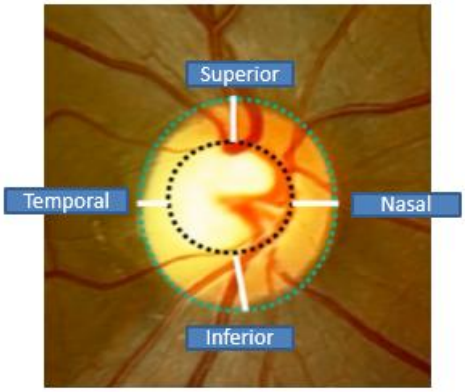

Figure 5.12: ISNT Zones of Optic Nerve Head

These zones are segregated with the help of masking operation carried out between four binary masks made exactly of the same size as of binay image of extracted blood vessels. These masks are shown below in Figure 5.13.

Figure 5.13: Masks used for segmentation of vessels in four zones.

The segmentation of blood vessels in binary image is carried out with the help of AND operation carried out with the corresponding mask of that zone. The resultant images obtained after masking operation is shown in figure 5.14.

Figure 5.14: (a) Inferior zone, (b) Nasal zone, (c) Superior zone

5.3.4 Detection of Centroids

Before evaluating the vessel shift measurement with respect to ref point assessed previously and depicted in figure 5.8 it is mandatory to find the centroid of blood vessels contained inside already extracted zones. Blood vessels extracted zone contain multiple irregular objects of

different sizes for which finding the centroid is a complex task as compared to an object with isotropic region. Image proceesing toolbox function of *regionprops* was used to measure the centroid for each connected component in the binary image. Depending upon the size of each connected component the weighted mean of these multiple centroids was calculated which is the tangible centroid of complete zone. Similarly following the same procedure the centroids of all the three zones were calculated. Figure 5.15 shows the screenshots of zones marked with centroids.

Figure 5.15: Detection of centroids.

Consequently, these calculated centroids were plotted back onto the binary image of extracted optic disc with segmented blood vessels visible inside. After plotting these centroids, the features required to be extracted and marked onto the final binary image i-e three centroids and reference point are complete and shown in figure 5.16

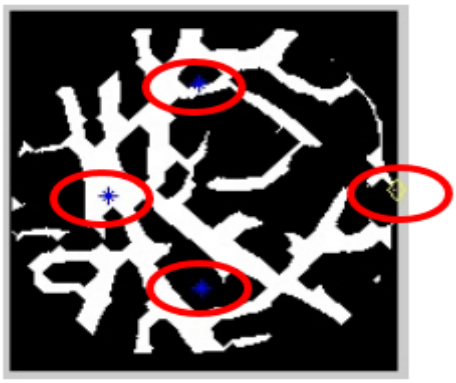

Figure 5.16: OD binary image with plotted reference point and centroids

5.3.5 Vessel Shift Distance Measurement

In this phase of the proposed method, the displacements of blood vessels from original location that is the center of the optic disc however slightly biased towards nasal side are calculated. All of these displacements calculations of three centroids were carried out with

reference to the ***'Ref Pt'*** earmarked towards the temporal side on the boundary of optic disc (shown in figure 5.17).

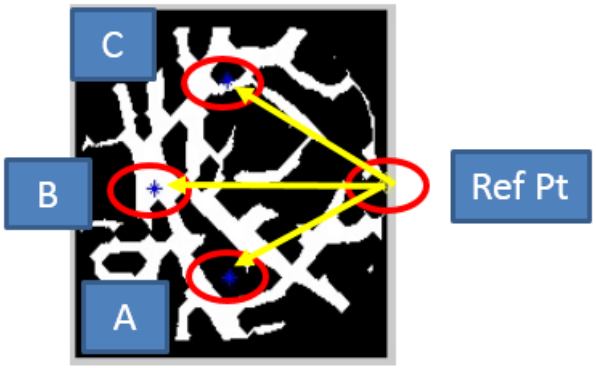

Figure 5.17: Vessel displacments measurement

The distances d_A, d_B and d_C from centroids A, B and C respectively were calculated using chessboard metric defined by Eq. (1) due to the fact that maximum displacement of vessels takes place in horizontal direction.

$$D_{centroid} = \max (| X_2 - X_1 | , | Y_2 - Y_1 |) \quad (1)$$

Where (X_1,Y_1) are the coordinates of ref pt and (X_2,Y_2) are the coordinates of three centroids taken one at a time.

As the proposed method is applied on the retinal images of different sizes and no two optic discs have same shape and diameter therefore the measured distances were normalized after taking the weighted mean of all three centroids. More weightage is given to the nasal centroid due to the reason that displacement is maximum in the horizontal direction. The governing equations are as under:-

$$Disp_{mean} = (0.25 * d_A) + (0.5 * d_B) + (0.25 * d_C) \quad (2)$$

$$Disp_{norm} = (Disp_{mean} / Dia_{hor}) * 100 \quad (3)$$

Where Dia_{hor} in Eq. (3) is the horizontal diameter of the optic disc taken from temporal to nasal direction and $Disp_{mean}$ is the mean distance of centroid required to be normalized.

5.4 Comparative Analysis for Glaucomic Image Sorting

After the assessment of normalized mean displacement there is a requirement of finding the decision point or threshold value in order to make decision between normal and glaucomic images. Total of 42 images were experimented using the matlab code for deciding the threshold point. The threshold was finalized on the basis of the dispersion of the normal and glaucomic

images with respect to the mean value (μ) of the distribution. Using the mean value and results acquired from experiment about the vaculature displacement in both normal and glaucomic images the standard deviation (σ) was calculated. Resultantly the range of dispersion of both the distrbutions were found out. Obtained results are depicted in Table 5.1 below.

TABLE 5.1: VASCULATURE DISPLACEMENT RANGE IN NORMAL AND GLAUCOMIC IMAGES.

	No of Images	Mean (μ)	Std Dev (σ)	μ-σ	μ+σ
Normal Images	16	69	1.99	67.48	71.47
Glaucomic Images	26	73	3.81	69.07	76.69

From table 5.1 it is evident that the dispersion of data comes out to be in the range of 67.48 to 71.47 for normal images and from 69.07 to 76.69 for glaucomic images. Instead of getting the exact value for threshold for deciding the classes of two types of images an overlapping range of 69.07 to 71 .47 was found out. By taking mean of this overlapping range that comes out to be around 70.5 as a threshold value, it caused too many false results hence reduced the system accuracy to approximately 71% as compared to reported method which claimed it around 91.34%. Therefore a new approach was adopted and the available data is segragated into three categories instead of two by taking the overlapping values as the threshold range (T_R) for images classification. A special comparison module was designed which take the calculated values of these images as input and carryout segregation of images as intial result. Figure 5.18 shows the flow of the system.

Calculated mean displacement of images and empirically determined threshold range is used as the main deciding factor for declaring input image as affected or normal. The input value of mean dispalcement is comapred with pre-stored thershold range. If the dispalcement value which is denoted by ‘A’ in flow diagram comes out to be greater than T_R (threshold range) then the image is classified as glaucomic. If this value ‘A’ comes out to be less than T_R then the image is classified as normal image. And if the displacement lie within the threshold range than instead of putting it in one of the categories and increase false positive or false negative result a new category of suspected image has been created which require further confirmation testing hence passed on to novel technique called biometric approach for final assessment and classification on the basis of outcome of this procedure.

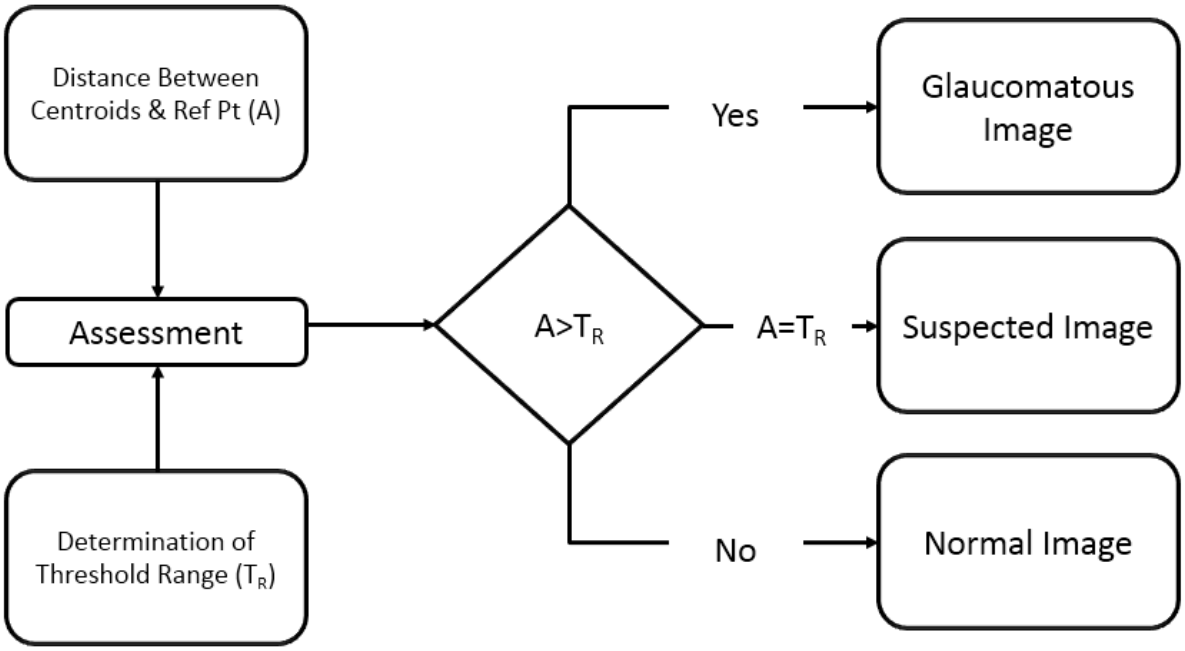

Figure 5.18: Flow diagram of comparison module.

5.5 Classification using Biometric Approach

Blood vessel inside ONH must change orientation in eyes affected with glaucoma. Ophthalmologists therefore recommend periodic screening of eyes to glaucoma patients. Same analogy is used in proposed part to enhance overall accuracy of the mechanism. In this part, the basic concept of personnel recognition through matching distinctive features was utilized and implemented. Multiple glaucomic images were required – at least 5 per person (3 for training / 2 for testing) to implement biometric application with a condition that these images are taken at different point of time. Due to non availability of required number of glaucomic images, an alternate mode of using multiple images of normal eye taken from AFIO was used to validate the efficacy of the system. Image of patient once taken by the system will be stored in its database. If non glaucomatous, it will always match with its new image taken after any interval of time and vice versa. Overall recognition rate / accuracy due to this approach was considerably increased.

5.5.1 Methods

Biometric identification systems work on the principle of matching input data with sample database used as reference. If input data qualifies the matching criteria with sample database only then positive results are generated. At times an input image qualifies the matching criteria with

more than one reference images. In such case more stringent criterion are required to be set so that possibility of false identification can be curtailed. Keeping this in view the proposed method is devised in a way to avoid reliance on only one feature hence increases the reliability of the system. The different steps adopted in proposed method are represented in Figure 5.19.

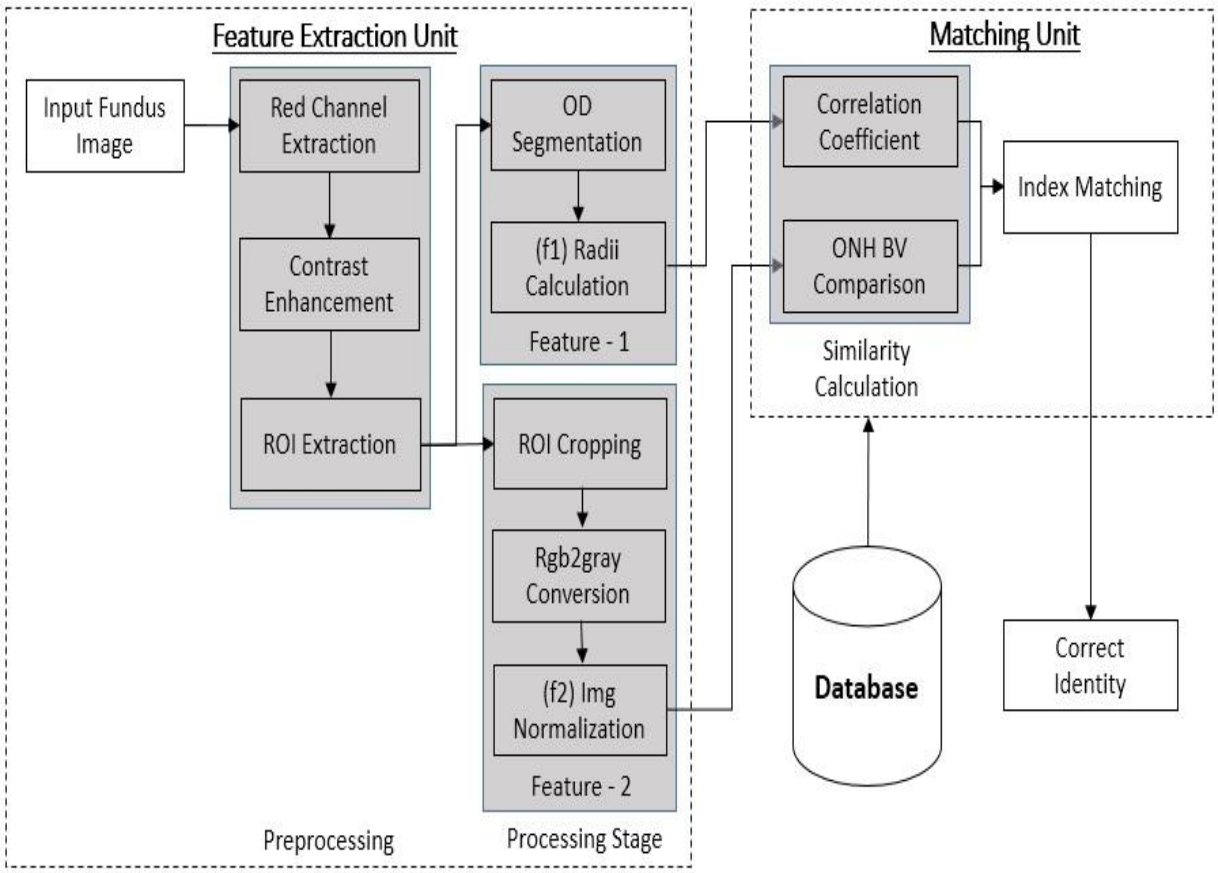

Figure 5.19: Flow diagram of proposed identification system.

5.5.2 Data Acquisition

5.5.2.1 Dataset Collection

Although copious datasets of fundus images are available online however with reference to this study more than one image per individual were required. To fulfill the requirement, 5 digital images per person were arranged from Armed Forces Institute of Ophthalmology (AFIO). Fundus images of different patients were captured with prior consent of patients and institutional ethics committee approval. All images were stored in JPEG format and had a resolution of 1504 x 1000 pixels. In addition to these images, 26 images of fifteen different individuals were included in the study taken from Ibrahim Eye Trust Hospital with a resolution of 3216 x 2136 pixels.

5.5.2.2 Segregation of Acquired Images

Collected images were then segregated into two categories i-e reference and test images. 3 out of 5 images were selected at random to be used as reference image and remaining 2 images were kept to be utilized as test images. Reference images were used to make database of each individual containing two distinct features i-e average of OD radii taken at every 10 degree along the extracted boundary of OD segmented out using adaptive threshold method and gray scale normalized image of the same extracted OD region. Remaining 2 images were kept as test images.

5.5.3 Feature Extraction

Images segregated as test image is taken as the input in this proposed method. All input images passed through same stages for extraction of desired features through which reference images are passed for establishment of database.

5.5.3.1 Preprocessing Stage

Various factors affect the eminence of image during acquisition. Inter technician proficiency, opacities due to disease and large image size could be one of these factors. Preprocessing of image includes contrast enhancement and ROI extraction. Same procedure is adopted for both of these task which has already been discussed in OD segmentation part above.

5.5.3.2 Processing Stage

Extracted ROI image was processed using red channel image due to better prominence of OD followed by conversion of red channel image into negative image for reaching to improved contrast. Adaptive thresholding was applied on grayscale image of red channel for OD segmentation.

5.5.4 Radii Calculation

Radius of OD is measured incorporating multiple directions. A vector based approach has been introduced to calculate multiple radii of the OD. Vector of length equivalent 1.6 times the horizontal radius of OD are drawn at an interval of 10^o starting from 0^o with respect to x-axis covering complete circumference of the disc. Euclidean distance between center of OD and intersection point of drawn vector with perimeter of OD was measured and vector having 36 elements was formed (Figure 5.20).

$$Euclidean\ Distance = d = \sqrt{\sum_{i=1}^{N}(xi - yi)^2} \quad (4)$$

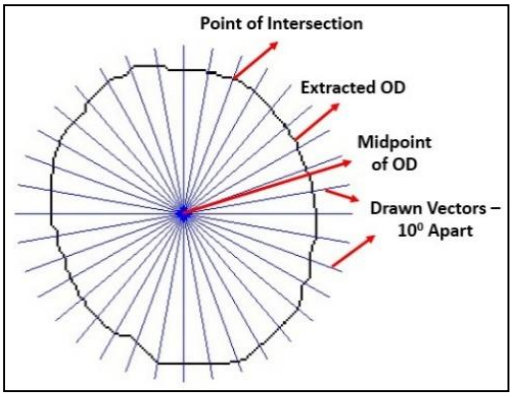

Figure 5.20: Intersection between OD and drawn vectors.

5.5.5 Image cropping and Normalization

Intensity values of colored image is distributed over the range of 0 to 255 in three dimensional planes i-e red, green and blue. In order to make colored images simplified for computational purposes the RGB image of retina is converted into grayscale image by reducing it into two dimensional domain. Intensity values of grayscale image also ranges from 0 to 255 however having only one plane (0 being darkest and 255 being brightest). The purpose behind converting the colored image into grayscale and subsequently normalizing the pixel values was to obtain an *image comparison index* whose value depicts level of similarity between reference and input images. Flow diagram shown in figure 5.19 depicts the procedure adopted for obtaining normalized image.

Input colored image of ROI (Figure 5.21a) was converted into standard grayscale image (Figure 5.21b). Obtained image hold redundant information which increases the computation cost hence get rid of by cropping the ROI extracted image into the one containing only OD segmented out region as depicted in Figure 5.21c.

(a) **(b)** **(c)**

Figure 5.21: (a) Original RGB image, (b) Grayscale image, (c) Cropped ROI.

Resultant image is the one covering only ONH region from where blood vessels originates. Pattern made by these vessels inside ONH differs in every individual hence making it a useful feature to be utilized for personal identification. Variations occur in pixels values of two similar images at same coordinates during acquisition. Various factors like luminance, inter technician variability, individual inconsistency etc. are responsible for such variations and can be condensed through normalization. In proposed method the normalization is implemented on reference as well as input images to reduce the effect of illumination differences. Intensity values of grayscale images ranging from 0-255 are normalized between 0-10. This transformation reduces the sum of differences between pixel values of two images of identical individual taken at different instances to its minimum level hence reducing the computational cost. Following relationship is used to obtain normalized image n(x):-

$$n(x) = \frac{[\{(g(x) - \min(g(x))\} * (10-1)]}{\max g(x) - \min g(x)} \quad (5)$$

Where g(x) is grayscale image and max / min g(x) are the highest and lowest pixel values in grayscale images respectively.

5.5.6 Similarity Calculation

After extracting two distinct features from every test image which include normalized image and radii vector these features are then compared with similar features already extracted from reference images and stored in knowledge base.

5.5.6.1 Correlation Coefficient

Correlation coefficient is calculated using radii vector of test and ref images. The input test image radii vector is compared with all stored radii vectors of reference images and a correlation coefficient is calculated for all images using following formula.

$$`r_{xy} = \frac{\sum_{i=1}^{n}(xi - \overline{x})(yi - \overline{y})}{\sqrt{\sum_{i=1}^{n}(x_i - \overline{x})^2 \sum_{i=1}^{n}(y_i - \overline{y})^2}} \quad (6)$$

Two radii vectors having highest similarity between radii at different angles gives correlation index close to positive 1. All other vectors either give negative values or close to zero depending upon the pattern of values at different angles. Index number of reference image having close correlation coefficient with test image is stored and is subsequently used at indices matching stage for final verification.

5.5.6.2 Image Comparison Index

Image comparison index is the outcome of comparison between test and reference images. Input test image is converted into grayscale image followed by conversion into normalized image having intensity values ranges from 1-10. This normalized image only contain the information about blood vessel pattern formed inside the ONH. This normalized image is then compared with all the ref images already available in the database. Two normalized images having the maximum resemblance give the lowest intensity difference value by adding the difference between individual pixel values. Following mathematical relationship is used for acquisition of image comparison index:

$$C_i = \sum_{i=1}^{n} \sum_{j=1}^{m} \left(X_{ij} - Y_{ij}\right) \tag{7}$$

Where X_{ij} depicts test image and Y_{ij} represents ref image.

5.5.6.3 Indices Matching

In biometric application it is of utmost importance that test sample only matches with true ref sample in order to increase the system reliability. Keeping zero tolerance criteria in view two distinct features have been incorporated in this proposed method. Both features generate separate index on the basis of calculation. Both indices have equal weightage in deciding whether test image matches with ref image or otherwise. Test image which was suspected of glaucoma in previous part is declared as normal only if both the indices give similar results otherwise test image is declared as glaucomic with respect to already stored previous image of same patient. Flow chart of this matching unit is shown in figure 5.22.

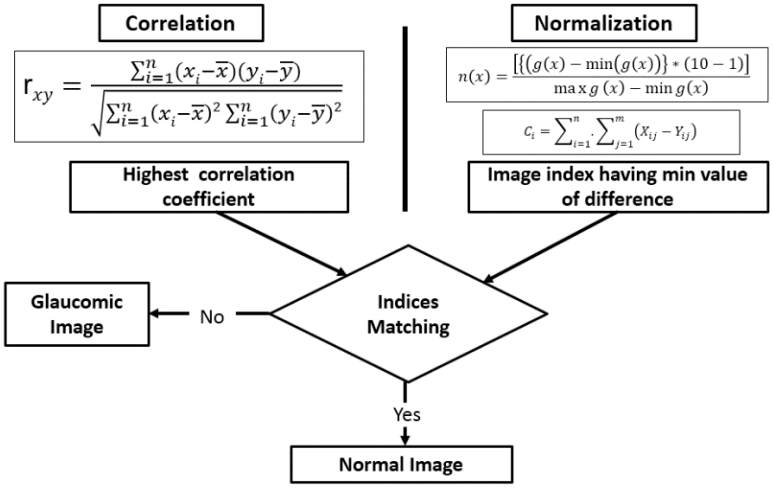

Figure 5.22: Flow diagram - Matching unit of proposed identification system.

CHAPTER - 6

RESULTS AND ANALYSIS

6.1 Experimental Parameters

To assess the efficacy of developed algorithm and implemented Matlab code on available digital retinal fundus images following parameters were fixed at the time of experiments:-

- Visual inspection and concordance of automated results with annotations.
- Computational customization.
- Recognition rate using index matching criteria.

6.2 Employed Datasets

Datasets containing multiple fundus images of both normal as well as glaucomic eyes were required for assessing the usefulness and reliability of implemented code keeping set parameter under consideration. To fulfil this requirement following two datasets were employed which were taken from different hospitals.

6.2.1 Ibrahim Eye Trust Hospital

This dataset were collected from Ibrahim eye trust hospital, Gujranwala with kind courtesy of hospital management. 26 fundus images of 15 glaucomic patients considering both eyes as separate case were collected. All of these images were annotated by two separate ophthalmologists along with assessment of CDR values. These images are in JPG format with a high resolution of 3216x2136 pixels.

6.2.2 AFIO

This dataset was acquired from Armed Forces Institute of Ophthalmology. 100 RGB fundus images of 20 different individuals containing 5 digital fundus images per person of same eye were collected. All of these images were of normal individuals. These images are in JPG format with a resolution of 1504x1000 pixels. These five images were further categorized into two parts. 3 out of 5 available images per person were randomly selected for creation of reference database. Remaining 2 images were used as test images to check the correctness of the system.

6.3 Illustrative Results of Implemented Algorithm

Developed code for automated detection of glaucoma from fundus imagery was sub-divided into three main parts. Illustrative results of all three parts are separately depicted as per sequence in succeeding paragraphs.

6.3.1 Optic Disc (OD) Segmentation

The leading step of this decision support system for automated glaucoma detection was to segment out optic disc from retinal fundus image having other main structures of retina as well. The process adopted for attainment of this feature is as under:-

6.3.1.1 ROI Extraction

Original fundus images of both employed datasets were covering the complete retinal features. Portion of retina required for proposed method included only optic nerve head region. In order to evade redundant data the original image was shrunk to the region of interest by cropping useful part from rest of the image. Figure 6.1 shows the outcome of applied algorithm on original image.

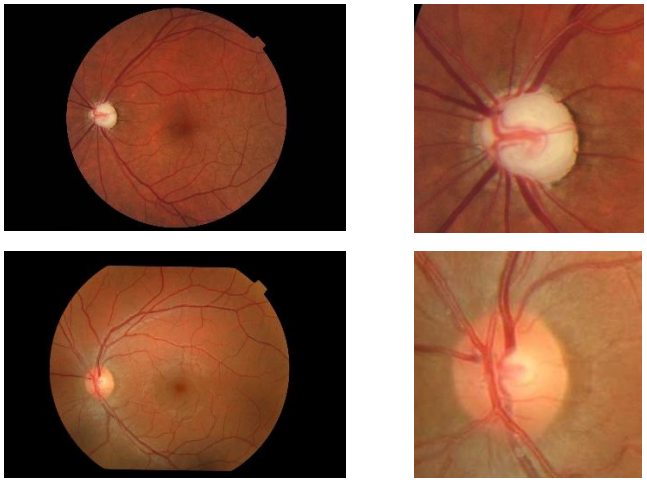

Figure 6.1: ROI extracted regions from original fundus images *(1st row shows images from Ibrahim eye trust hospital. 2nd row shows images from AFIO).*

6.3.1.2 Separation of RGB Image into Color Channels

In order to segment out optic disc, RGB image was segregated into red, green and blue planes to assess the prominence of features in different conditions. Optic cup was most prominent

in green plane however red plane showed the most encouraging contrast result for optic disc hence selected for further processing and segmentation of this required feature. Figure 6.2 shows the result of these three channels.

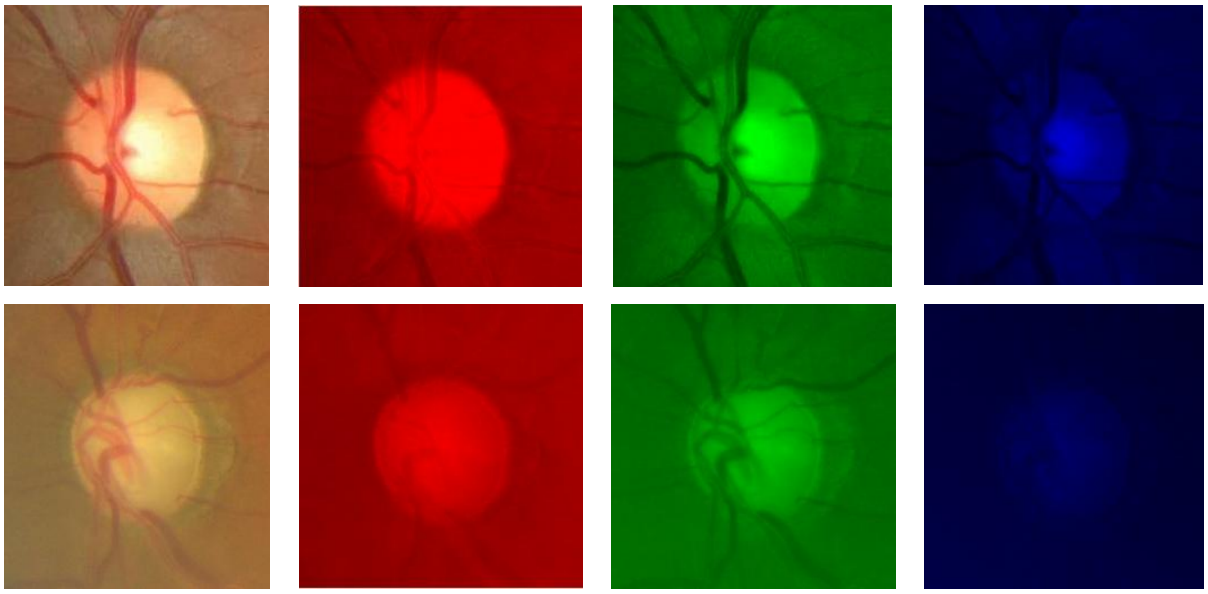

Figure 6.2: Preprocessed images of employed datasets *(1st row normal image from AFIO dataset, 2nd row glaucomic image from Ibrahim eye trust dataset). 1st column shows ROI of original RGB images. 2nd column shows red channel of ROI. 3rd column shows green channel. 4th column shows blue channel.*

6.3.1.3 Adaptive Thresholding & Morphological Operations

Obtained red plane of RGB image was converted into grayscale for application of segmentation techniques. Grayscale image further enhanced the feature of optic disc in the image. Input image was divided into four portion each having both background and some part of desired feature need to be extracted. Adaptive thresholding technique was applied in which threshold of all portions were calculated separately using the histogram and on the basis of that value image was converted into binary image from grayscale image. Few resultant images had some artifacts due to poor contrast and low quality of image therefore another technique of connected component analysis was applied on the binary images. All the pixel with value '1' and connected with each other were labelled and grouped together. The size of each segregated component was then calculated and the one having maximum number of pixels with value '1' was declared as the optic disc as no other feature was bigger than this feature while remaining all were considered as the

artifact and converted into '0'. Final image was acquired after applying morphological operation using disc type structuring element which is shown in 4th column of figure 6.3.

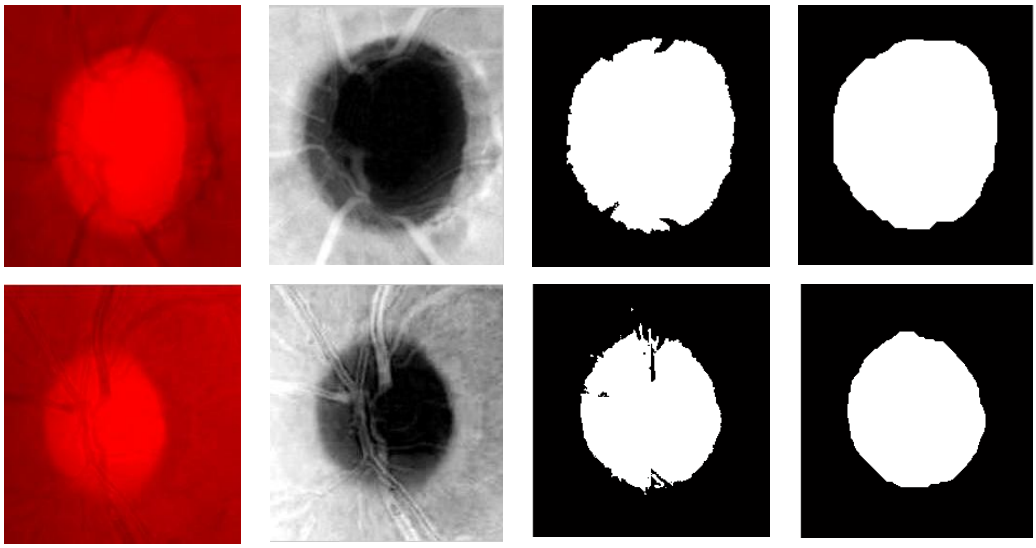

Figure 6.3: OD segmentation result *(1st row dataset of Ibrahim eye trust hospital and 2nd row dataset of AFIO). 1st column shows ROI in red plane. 2nd column shows grayscale images of ROI. 3rd column shows OD segmentation after Adaptive Thresholding. 4th column shows final OD region after Morphological Operation.*

6.3.1.4 Perimeterization

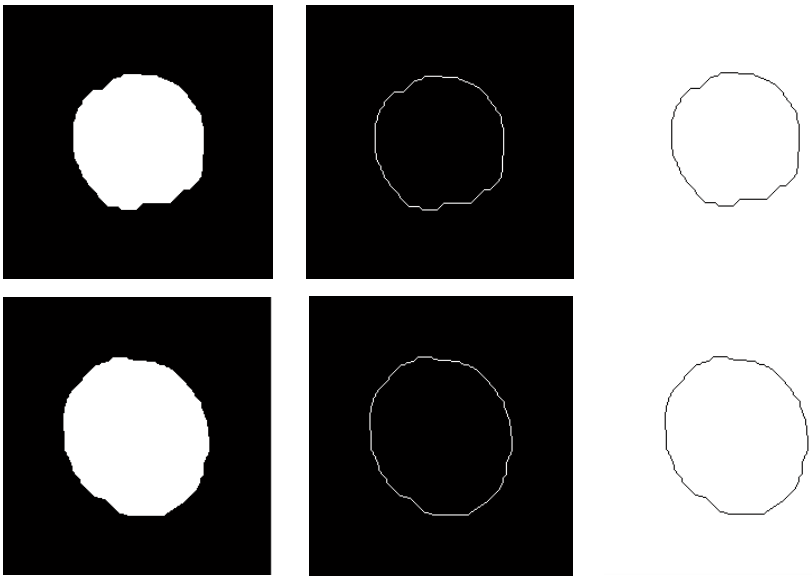

Figure 6.4: Perimeterized binary images. *1st column show binary images of segmented OD of both datasets. 2nd & 3rd columns show perimeterized binary images of OD with black and white backgrounds respectively.*

Perimeterization return a binary image containing only perimeter pixels of object. In this case the same was applied on binary image of segmented OD and an image showing only the boundary of OD is achieved for further assessment. Same is depicted in figure 6.4 above.

6.3.2 Vasculature Displacement Measurement

For assessment of glaucoma method of vasculature shift measurement inside optic disc was adopted. Step wise results of adopted procedure is as under:-

6.3.2.1 Blood Vessels Extraction using Wavelet Transform

Blood vessels in RGB image of ROI was enhanced using wavelet transform and then converted into binary image after undergoing multilayered thresholding technique. Figure 6.5 illustrate the outcome of three main steps involved in extraction of blood vessels.

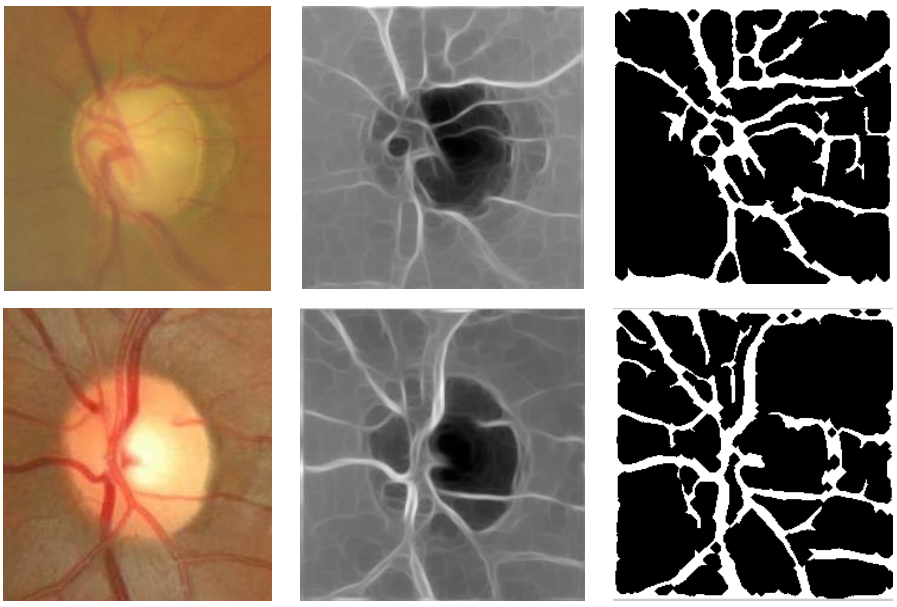

Figure 6.5: Blood vessels extraction using Wavelet Transform. *1st row shows original, enhanced and binary images of ROI from Ibrahim eye trust hospital and 2nd row shows same images from AFIO.*

6.3.2.2 AND Operation between BV Extracted & OD Segmented Images

Redundant information contained in extracted image utilizes extra resources and increase computational time hence required to be removed. AND operation between binary images of segmented OD and vascular bundle fulfilled this requirement and the obtained image is demonstrated in figure 6.6.

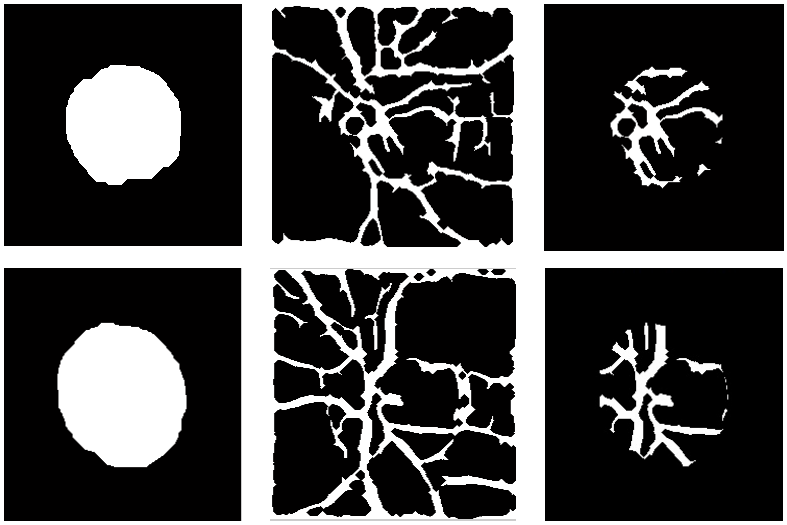

Figure 6.6: Resultant blood vessels extracted image of OD using AND operation. *1st row shows images from Ibrahim eye trust hospital and 2nd row shows images from AFIO.*

6.3.2.3 Masking Operation

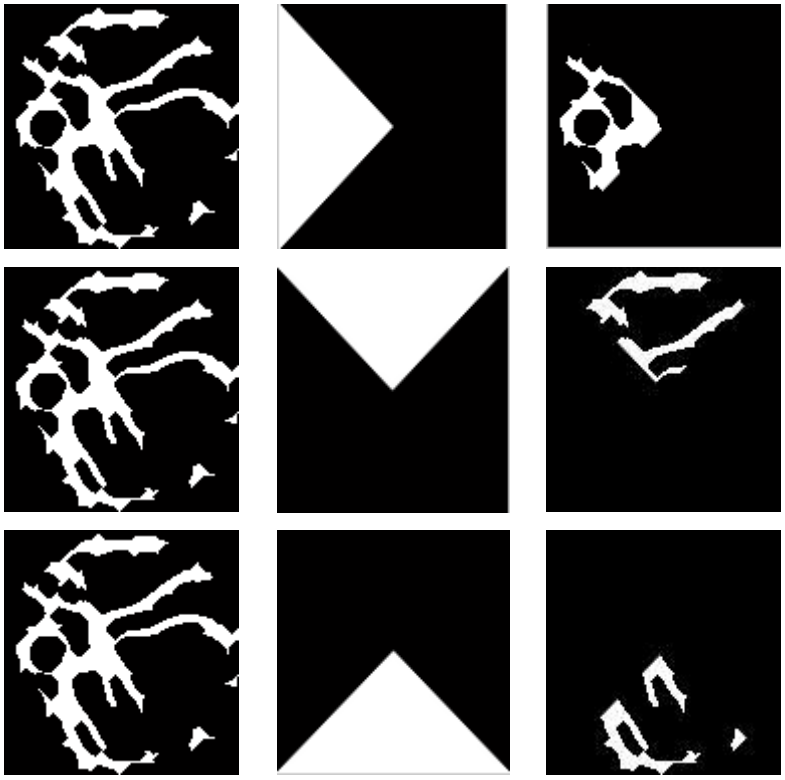

Figure 6.7: Masking Operation. *1st column shows OD segmented image. 2nd column shows three masks and 3rd column shows extracted nasal, superior and inferior zones after AND operation.*

In order to find out the vasculature shift the extracted blood vessels were distributed into three portions i-e nasal, inferior and superior. Centroid of each portion was assessed separately and then weighted mean was calculated. Separate centroids were assessed by segregating each portion first using masks illustrated in figure 6.7.

6.3.2.4 Centroid Detection

Individual centroids were detected using regionprops function of image processing toolbox that measure different properties of image regions. Centroid of Input binary image containing only background and segregated portion of optic disc was assessed and plotted. Figure 6.8 depicts all three centroids plotted on binary image of optic disc extracted image.

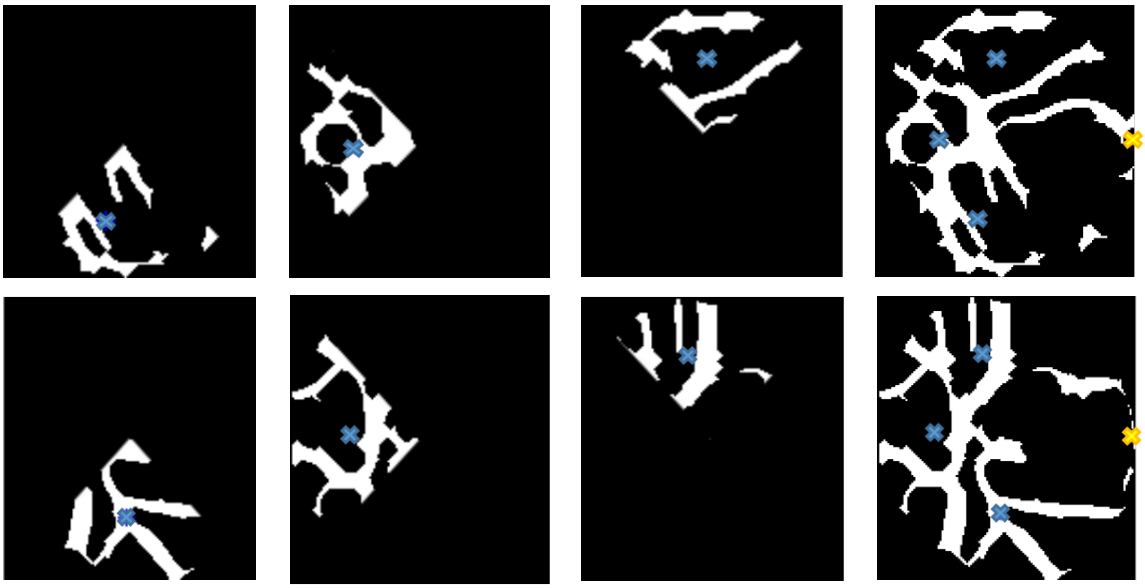

Figure 6.8: Independent centroid detection in inferior, nasal, superior zones respectively and plotting on extracted image of complete OD. *1st row shows glaucomic image from Ibrahim eye trust hospital and 2nd row shows normal image from AFIO.*

6.3.3 Biometric Approach

Large dispersion of BV displacement (Normal images between 67.48 to 71.47 & Glaucoma images between 69.07`to 76.69) with overlapping range of 69.07 to 71 .47 caused too many false results hence reduced system accuracy (approximately 71%). Images lying inside overlapping range were then segregated as suspected glaucoma. Comparison module was designed and these suspected images were passed through another step designed in-line with biometric approach for enhancing accuracy.

6.3.3.1 Image Normalization

Test and reference images had to be compared in this step and declared as the feature one of said approach. Same was implemented by converting only OD portion of ROI into grayscale image and taking the sum of pixel to pixel difference of two images. Images of same eye had the least difference as compared to other images. As grayscale image has intensity values from 0-255 therefore the output value came out to be a bigger figure even for the least difference as well. Consequently images were normalized between 0-10 hence the resultant values reduced to the range of (10000 – 200000) with the threshold fixed at 50000. Figure 6.9 shows screenshot of grayscale and normalized image matrices.

	150	151	152	153	154	155	156	157	158
153	227	231	235	239	245	251	254	255	255
154	223	228	232	236	242	247	251	254	255
155	221	225	230	234	239	244	249	253	255
156	218	222	227	232	237	241	246	252	255
157	216	220	225	230	234	238	243	249	254
158	214	218	223	227	231	235	240	246	251
159	212	216	220	224	229	233	238	243	248
160	209	213	217	221	227	232	237	241	245
161	209	213	217	221	227	232	236	240	242
162	211	215	218	222	227	232	237	240	243
163	214	217	220	224	229	233	237	241	243
164	218	220	223	226	230	235	238	242	244
165	220	223	226	229	233	237	240	242	244
166	224	226	230	233	236	238	241	243	245

(a)

	150	151	152	153	154	155	156	157	158
153	8	9	9	9	9	9	9	10	10
154	8	9	9	9	9	9	9	9	10
155	8	8	9	9	9	9	9	9	10
156	8	8	8	9	9	9	9	9	10
157	8	8	8	9	9	9	9	9	9
158	8	8	8	8	9	9	9	9	9
159	8	8	8	8	9	9	9	9	9
160	8	8	8	8	8	9	9	9	9
161	8	8	8	8	8	9	9	9	9
162	8	8	8	8	8	9	9	9	9
163	8	8	8	8	9	9	9	9	9
164	8	8	8	8	9	9	9	9	9
165	8	8	8	9	9	9	9	9	9
166	8	8	9	9	9	9	9	9	9

(b)

Figure 6.9: Screenshots of matrices showing (a) Grayscale image (b) Normalized image.

6.3.3.2 Radii Calculation through Vector Based Method

Second feature need to be obtained was the radii vector of segmented OD. At every 10^0 a vector was drawn and Euclidean distance between midpoint of OD and intersection point of drawn vector and OD boundary was calculated. An array of multiple entries was obtained which will

always be a unique entity in every particular case. Figure 6.10 shows the perimeterized optic disc with vectors drawn over regular intervals.

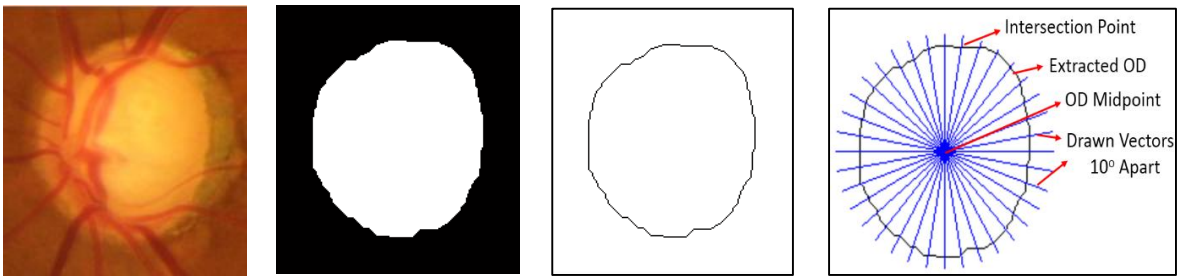

Figure 6.10: Novel vector based approach for radii calculation.

6.4 Experimental Results

6.4.1 OD Segmentation & Diameter Calculation

One of the main objective of OD segmentation was to assess the horizontal diameters of OD calculated through an automated vector based method and comparing it with annotated image shown in figure 6.11. Diameter of the marked OD was measured by taking the average of number of pixels from four different directions. Obtained accuracies varied from 84.67% to 99.75% depending on the direction chosen. The overall accuracy of proposed method was found to be 97.32%. Table 6.1 shows the accuracies of selected images.

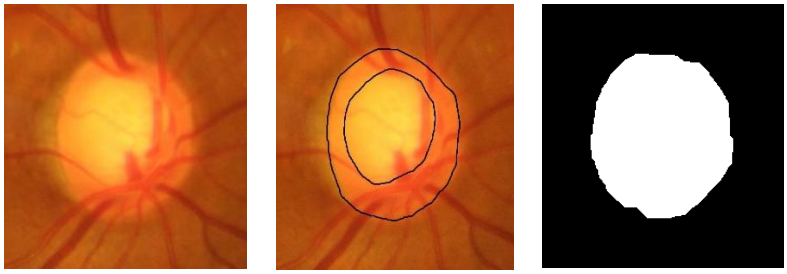

Figure 6.11: Annotated image and automated extraction result of OD segmentation.

TABLE 6.1: ACCURACY CHART OF DIAMETER READINGS.

IMAGE	DIAMETER READINGS		ACCURACY%
	ANNOTATED	AUTOMATED	
IMAGE 8	266	225.2	84.67
IMAGE 9	308.5	307.7	99.75
IMAGE	354	346.3	97.83

IMAGE	348.5	369.5	93.99
IMAGE	325	323.1	99.41
IMAGE	327	309.0	94.51
IMAGE	271	269.6	99.47
IMAGE	381	392.5	96.97
IMAGE	313.5	320.2	97.85
IMAGE	296	281.2	95.00
		Average	**97.32**

6.4.2 Evaluation of Blood Vessels Centroid Displacement

Table 6.2 & 6.3 demonstrate the normalized mean displacement of glaucomic and normal images respectively. Table includes OD horizontal diameter, three distances measured between detected reference point on OD boundary and zonal centroids, weighted mean displacement of blood vessels shift and normalized mean displacement as different images have different OD sizes and required to be standardized.

TABLE 6.2: NORMALIZED MEAN DISPLACEMENT OF VASCULAR BUNDLE – GLAUCOMIC IMAGES

Ser	Image Name	OD Hor Dia	Dist A	Dist B	Dist C	Mean Disp	Norm Mean Disp
Glaucomic Images - Ibrahim Eye Trust Hospital, Gujranwala							
1	L_roi1	170	111.99	132.80	104.51	122.98	**72.3**
2	L_roi2	110	81.40	84.77	69.88	81.12	**73.7**
3	L_roi4	150	102.00	114.04	89.52	106.73	**71.2**
4	L_roi5	132	81.11	102.08	77.86	93.04	**70.5**
5	L_roi6	159	98.60	120.13	90.57	109.91	**69.1**
6	L_roi7	130	86.98	104.28	103.12	100.59	**77.4**
7	L_roi8	114	69.79	86.12	76.91	81.01	**71.1**
8	L_roi9	128	81.42	101.73	81.59	93.64	**73.2**
9	L_roi10	106	68.52	79.31	73.98	76.08	**71.8**
10	L_roi11	189	148.56	170.38	122.20	156.38	**82.7**
11	L_roi12	130	76.34	99.23	79.97	90.80	**69.8**
12	L_roi13	141	88.09	105.33	83.95	97.60	**69.2**
13	L_roi14	168	116.96	135.35	109.92	126.59	**75.3**
14	R_roi2	112	69.37	83.28	69.93	77.83	**69.5**
15	R_roi4	139	86.73	104.20	84.74	96.81	**69.7**
16	R_roi5	146	83.44	114.74	87.00	102.93	**70.5**
17	R_roi6	128	81.31	96.79	102.29	94.79	**74.1**

18	R_roi7	138	90.85	104.71	88.29	98.65	**71.5**
19	R_roi8	117	75.48	83.61	74.96	80.25	**68.6**
20	R_roi9	128	92.64	102.64	76.55	95.42	**74.5**
21	R_roi10	150	97.03	122.95	91.64	111.50	**74.3**
22	R_roi12	119	77.73	92.68	75.56	86.27	**72.5**
23	R_roi13	136	83.84	102.23	82.54	94.61	**69.6**
24	R_roi14	152	120.31	127.25	108.43	122.10	**80.3**
25	R_roi15	132	88.83	97.23	90.83	94.27	**71.4**
26	R_roi16	165	112.55	145.48	118.99	133.59	**81.0**

TABLE 6.3: NORMALIZED MEAN DISPLACEMENT OF VASCULAR BUNDLE - NORMAL IMAGES

Ser	Image Name	OD Hor Dia	Dist A	Dist B	Dist C	Mean Disp	Norm Mean Disp
Normal Images – AFIO							
27	set2	125	80.96	93.93	82.12	88.97	**71.2**
28	set3	133	78.89	94.00	79.65	88.11	**66.2**
29	set5	127	80.82	92.86	74.55	86.79	**68.3**
30	set6	124	85.8401	91.3457	76.336	87.2426	**70.4**
31	set8	129	83.59	95.25	84.97	90.86	**70.4**
32	set9	144	85.46	109.56	86.56	100.14	**69.5**
33	set10	143	81.26	105.07	88.85	97.06	**67.9**
34	set12	132	76.80	96.90	86.62	90.82	**68.8**
35	set13	129	82.74	88.82	83.35	86.51	**67.1**
36	set14	127	80.47	92.20	77.79	86.97	**68.5**
37	set15	135	88.09	105.02	92.48	99.13	**73.4**
38	set16	145	87.72	110.86	95.36	103.13	**71.1**
39	set17	131	84.85	100.12	85.08	94.06	**71.8**
40	set18	126	73.07	89.08	79.36	83.93	**66.6**
41	set19	131	75.02	100.59	86.14	92.59	**70.7**
42	set20	124	79.77	91.22	78.14	86.31	**69.6**

Dispersion range of vascular bundles in normal and glaucomic images was calculated by taking mean of complete distribution and subsequently calculating its standard deviation. Table 6.4 show the dispersion ranges of both datasets.

TABLE 6.4: DISPERSION RANGE OF VESSELS DISPLACEMENT

	No of Images	Mean (μ)	Std Dev (σ)	μ-σ	μ+σ
Normal Images	16	69	1.99	67.48	71.47
Glaucomic Images	26	73	3.81	69.07	76.69

Threshold value of 70.5 was fixed as the cut-off point after taking mean of dispersion range. Images having BV displacement below threshold value were categorized as normal and vice versa.

On the basis of this threshold images were classified and sensitivity, specificity and accuracy of attained number of true positives, true negatives, false positives and false negatives were calculated using following equations and shown in table 6.5.

$$Sensitivity = \frac{True\ Positive}{True\ Positive + False\ Negative} \quad (1)$$

$$Specificity = \frac{True\ Negative}{True\ Negative + False\ Positive} \quad (2)$$

$$Accuracy = \frac{True\ Positive + True\ Negative}{True\ Positive + False\ Negative + True\ Negative + False\ Positive} \quad (3)$$

TABLE 6.5: RESULTS OF PROPOSED METHOD APPLIED ON 42 IMAGES.

Results - Proposed Method	
Threshold	70.5
TP	19
FN	7
TN	11
FP	5
Sensitivity	73.08
Specificity	68.75
Accuracy	71.43

6.4.3 Evaluation of Accuracy Enhancement using Biometric Approach

In this part, the basic concept of personnel recognition through matching ***distinctive features*** was utilized and implemented. Multiple glaucomic images were required (at least 5 per person - 3 for training / 2 for testing) to implement biometric approach. Due to non-availability of required number of glaucomic images, an alternate mode of using multiple images of normal eye taken from AFIO was used to validate the efficacy of the system. Image of patient once taken by

the system would be stored in its database. If non glaucomatous, it will always match with its new image taken after any interval of time and vice versa. Overall recognition rate / accuracy of this approach found out to be 94%.

6.4.3.1 Assessment of Correlation Coefficient

Table 6.6 shows the radii vectors of five images per patient taken from AFIO. Average of first 3 three images of all patients was calculated and stored in database. Remaining two images were used as test images and correlation was found which is given in table 6.7. All the test images have correlation close to '1' with images of same patient only.

TABLE 6.6: RADII VECTORS OF REFERENCE IMAGES STORED IN DATABASE.

	Angle	**0**	**10**	**20**	**30**	**40**	**50**	**60**	**70**	**110**	**120**	**130**	**140**	**150**	**160**	**170**	**180**	**190**	**200**	**210**	**220**	**230**	**240**	**250**	**290**	**300**	**310**	**320**	**330**	**340**	**350**
Set1	roi1	62	64	65	65	67	67	70	67	67	64	64	64	65	63	62	62	63	63	62	64	65	66	67	64	64	61	60	60	61	60
	roi2	62	64	64	65	67	67	64	64	67	64	64	64	62	63	61	62	63	61	64	64	64	66	67	64	64	64	61	61	61	60
	roi3	61	63	64	65	65	64	60	56	67	66	65	65	64	63	62	61	60	59	61	64	64	64	67	61	62	59	57	58	57	57
	roi4	60	61	63	64	65	65	66	64	70	68	64	64	64	62	60	60	60	59	61	61	62	64	70	61	62	59	57	58	57	57
	roi5	64	65	65	67	68	68	70	67	67	66	64	65	65	64	62	63	63	63	64	65	65	66	67	67	64	62	61	62	63	61
Set2	roi1	65	65	64	64	60	61	62	64	67	70	68	67	67	67	65	65	66	65	65	64	64	66	64	67	68	65	65	67	68	66
	roi2	67	67	68	66	57	58	66	67	70	70	70	69	67	68	66	66	67	67	66	67	67	68	67	67	68	67	67	68	69	68
	roi3	67	68	68	67	63	62	68	70	70	70	70	68	67	67	66	66	67	67	66	65	67	68	64	67	68	68	67	69	69	68
	roi4	67	68	69	67	61	62	68	70	70	72	70	69	69	69	67	67	68	67	66	67	67	68	67	70	68	68	68	69	70	68
	roi5	66	67	67	67	63	62	66	67	70	70	68	67	67	66	64	65	66	65	65	65	65	66	64	67	68	67	67	69	69	67
Set3	roi1	65	65	64	66	64	64	66	67	70	68	67	67	66	66	64	64	64	64	65	67	65	66	64	70	72	70	69	66	65	64
	roi2	63	63	63	64	63	62	66	70	70	68	67	65	65	64	62	62	62	63	63	65	64	64	64	70	70	70	67	66	63	63
	roi3	62	62	63	65	61	62	66	67	67	68	67	65	65	65	63	62	62	63	64	65	64	64	64	67	70	68	67	64	64	63
	roi4	63	63	63	66	63	64	66	70	70	68	67	65	65	64	63	63	62	63	64	65	64	64	64	70	70	68	67	65	62	61
	roi5	64	63	63	64	61	62	64	67	70	68	67	65	65	64	63	63	63	64	65	67	67	68	70	73	72	70	67	65	63	64
Set4	roi1	62	63	63	65	68	68	70	73	61	62	62	60	59	59	59	60	62	65	66	67	67	70	70	64	64	64	61	61	61	61
	roi2	61	61	62	64	67	67	70	67	61	62	62	61	60	60	60	59	61	64	66	65	67	70	70	64	64	62	61	61	61	61
	roi3	64	65	64	67	69	70	70	73	61	60	62	61	61	61	62	62	64	66	68	68	68	70	70	67	66	64	64	64	63	63
	roi4	60	60	61	64	67	67	68	70	64	60	62	61	59	60	59	59	61	63	66	67	68	70	70	64	64	62	61	61	60	59
	roi5	61	62	63	65	68	68	70	73	61	60	59	59	58	59	59	60	61	64	66	67	68	68	70	67	64	64	63	61	62	61
Set5	roi1	63	63	64	65	65	65	66	67	67	62	62	67	69	66	63	60	61	63	64	68	68	68	70	64	68	67	65	64	63	63
	roi2	63	63	64	64	64	64	64	64	67	62	61	67	67	64	63	60	61	62	65	69	68	70	73	64	68	67	65	65	64	64
	roi3	62	62	63	64	64	65	66	67	67	62	61	64	65	64	62	59	59	62	64	68	67	68	70	61	68	67	65	64	63	63
	roi4	64	65	64	64	64	64	64	64	67	60	56	63	65	65	64	61	60	62	65	68	70	70	70	64	72	68	68	66	66	65
	roi5	65	64	64	65	64	64	66	67	67	64	61	68	69	67	66	63	64	66	69	72	72	72	70	70	72	70	69	67	67	65
Set6	roi1	71	71	70	69	68	68	68	64	70	72	73	74	75	75	72	71	72	70	70	70	70	70	70	64	68	72	72	74	75	72
	roi2	71	71	70	69	68	68	64	61	70	70	72	72	74	73	71	71	71	69	69	70	70	68	70	64	70	72	72	73	76	73
	roi3	71	71	71	69	69	68	64	64	70	72	72	74	75	73	72	72	72	69	69	70	70	68	73	67	70	72	72	72	76	73

	roi4	71	71	71	69	69	70	68	64	70	72	73	73	75	75	72	71	71	69	68	70	70	68	70	67	68	72	72	73	76	73
	roi5	71	70	71	69	69	68	66	61	70	70	72	72	74	72	71	70	70	68	68	69	70	68	70	67	68	72	72	72	73	72
Set7	roi1	72	73	73	74	74	73	72	73	70	70	68	68	66	68	71	72	69	71	69	71	73	72	73	70	72	72	72	70	69	72
	roi2	72	72	73	74	74	75	72	73	70	72	70	68	67	69	72	71	69	71	70	70	72	70	70	73	72	72	72	70	69	72
	roi3	72	73	73	74	74	75	72	73	70	70	68	68	67	69	72	71	69	69	69	70	72	70	73	70	72	73	73	72	70	71
	roi4	70	71	72	73	72	72	70	70	64	70	67	67	65	67	69	69	67	68	68	68	70	70	73	67	72	72	71	69	68	71
	roi5	69	69	72	70	71	72	70	70	67	70	68	68	67	68	69	69	69	70	68	69	68	70	73	67	70	70	69	67	67	69
Set8	roi1	65	64	67	69	68	70	70	64	79	74	72	64	66	65	66	65	67	70	72	72	73	76	79	76	74	72	69	72	69	67
	roi2	63	64	64	67	67	68	68	59	76	72	68	61	64	64	64	63	64	67	68	70	72	76	79	76	72	70	68	68	67	64
	roi3	64	65	64	66	64	65	62	53	76	70	67	59	61	61	61	62	64	66	69	70	72	76	79	79	76	72	71	72	68	65
	roi4	66	67	68	69	69	72	70	64	79	72	68	64	66	65	65	65	65	67	69	70	73	76	76	76	76	72	71	72	70	67
	roi5	65	65	66	67	67	68	68	58	76	72	68	63	66	65	65	64	65	68	69	69	73	76	79	76	72	70	69	70	68	66
Set9	roi1	64	64	66	65	67	68	72	73	73	72	72	69	67	64	62	64	64	64	64	64	67	68	70	73	74	68	69	68	67	64
	roi2	65	66	66	66	67	70	72	76	76	74	72	69	67	64	63	64	65	64	62	63	65	68	70	73	74	68	69	69	68	65
	roi3	64	64	65	66	65	68	74	76	76	72	72	69	67	64	63	64	64	64	64	64	67	68	70	73	74	68	68	67	66	64
	roi4	63	64	64	65	65	67	72	76	73	72	70	68	66	64	63	63	64	64	64	65	67	70	73	73	74	70	71	68	66	64
	roi5	64	65	65	65	67	67	72	73	73	72	72	69	67	65	64	64	65	66	65	65	68	72	73	76	76	70	71	68	67	65
Set10	roi1	62	63	63	60	59	58	56	58	61	62	59	60	61	61	61	61	60	62	59	59	61	60	61	56	58	58	57	57	57	60
	roi2	62	63	63	59	57	58	58	58	59	62	59	60	62	61	62	62	62	63	60	61	61	62	64	59	60	59	59	58	57	62
	roi3	60	61	62	59	57	56	56	56	61	60	59	60	61	61	61	60	61	61	60	59	61	60	61	59	58	56	57	57	55	59
	roi4	61	61	62	58	57	56	56	56	59	60	58	59	60	60	61	60	61	61	60	59	61	62	61	59	58	58	59	58	57	60
	roi5	61	62	63	59	57	58	56	56	59	60	58	60	61	60	60	60	60	61	59	57	61	60	61	59	58	58	59	58	57	61
Avg of 3	set2	62	64	64	65	66	66	65	62	67	65	64	64	64	63	62	62	62	61	62	64	64	65	67	63	63	61	59	60	60	59
	set3	66	67	67	66	60	60	65	67	69	70	69	68	67	67	66	66	67	66	66	65	66	67	65	67	68	67	66	68	69	67
	set5	63	63	63	65	63	63	66	68	69	68	67	66	65	65	63	63	63	63	64	66	64	65	64	69	71	69	68	65	64	63
	set6	62	63	63	65	68	68	70	71	61	61	62	61	60	60	60	60	62	65	67	67	67	70	70	65	65	63	62	62	62	62
	set8	63	63	64	64	64	65	65	66	67	62	61	66	67	65	63	60	60	62	64	68	68	69	71	63	68	67	65	64	63	63
	set9	71	71	70	69	68	68	65	63	70	71	72	73	75	74	72	71	72	69	69	70	70	69	71	65	69	72	72	73	76	73
	set10	72	73	73	74	74	74	72	73	70	71	69	68	67	69	72	71	69	70	69	70	72	71	72	71	72	72	72	71	69	72
	set12	64	64	65	67	66	68	67	59	77	72	69	61	64	63	64	63	65	68	70	71	72	76	79	77	74	71	69	71	68	65
	set13	64	65	66	66	66	69	73	75	75	73	72	69	67	64	63	64	64	64	63	64	66	68	70	73	74	68	69	68	67	64
	set20	61	62	63	59	58	57	57	57	60	61	59	60	61	61	61	61	61	62	60	60	61	61	62	58	59	58	58	57	56	60

TABLE 6.7: EVALUATED CORRELATION COEFFICIENTS BETWEEN TEST AND REFERENCE IMAGES

	Set	**1**	**2**	**3**	**4**	**5**	**6**	**7**	**8**	**9**	**10**
Set1	**roi1**	**0.85**	-0.35	0.09	0.63	0.40	-0.61	0.25	0.14	0.48	-0.02
	roi2	**0.88**	-0.37	0.18	0.56	0.47	-0.46	0.31	0.42	0.41	-0.02
	roi3	**0.88**	-0.11	-0.01	0.03	0.31	0.02	-0.03	0.32	0.12	0.45
	roi4	**0.91**	-0.10	0.21	0.34	0.40	-0.34	0.09	0.31	0.55	0.15
	roi5	**0.83**	-0.37	0.11	0.62	0.31	-0.65	0.29	0.18	0.49	-0.15
Set2	**roi1**	-0.27	**0.90**	0.43	-0.60	-0.16	0.49	-0.62	0.19	0.23	0.13
	roi2	-0.25	**0.95**	0.38	-0.41	0.02	0.34	-0.52	0.16	0.21	0.27

	roi3	-0.27	**0.89**	0.47	-0.32	-0.15	0.11	-0.30	-0.02	0.43	-0.06
	roi4	-0.21	**0.94**	0.49	-0.39	-0.07	0.21	-0.46	0.09	0.41	0.08
	roi5	-0.20	**0.87**	0.56	-0.44	-0.10	0.26	-0.31	0.15	0.47	-0.13
Set3	**roi1**	0.00	0.43	**0.97**	-0.08	0.31	-0.16	-0.10	0.43	0.68	-0.33
	roi2	0.04	0.43	**0.96**	0.07	0.31	-0.32	-0.02	0.39	0.82	-0.39
	roi3	0.01	0.52	**0.96**	0.00	0.33	-0.16	-0.15	0.38	0.74	-0.31
	roi4	0.19	0.32	**0.94**	0.13	0.29	-0.45	0.04	0.38	0.84	-0.37
	roi5	0.13	0.41	**0.82**	0.16	0.50	-0.23	-0.09	0.73	0.64	-0.07
Set4	**roi1**	0.39	-0.47	0.05	**0.98**	0.46	-0.76	0.47	0.25	0.29	-0.22
	roi2	0.49	-0.47	0.02	**0.97**	0.54	-0.67	0.37	0.40	0.29	-0.18
	roi3	0.26	-0.57	-0.05	**0.97**	0.41	-0.75	0.52	0.20	0.16	-0.29
	roi4	0.50	-0.43	0.14	**0.95**	0.61	-0.70	0.33	0.42	0.35	-0.21
	roi5	0.30	-0.50	0.09	**0.96**	0.47	-0.78	0.52	0.29	0.29	-0.32
Set5	**roi1**	0.41	-0.13	0.36	0.47	**0.97**	-0.14	-0.01	0.36	0.33	-0.04
	roi2	0.34	-0.06	0.26	0.43	**0.96**	0.01	-0.02	0.57	0.20	0.06
	roi3	0.35	-0.15	0.38	0.59	**0.96**	-0.21	0.18	0.46	0.37	-0.15
	roi4	0.04	-0.10	0.24	0.35	**0.83**	-0.02	0.21	0.48	0.07	-0.05
	roi5	-0.02	0.07	0.41	0.34	**0.79**	-0.07	-0.16	0.52	0.13	-0.05
Set6	**roi1**	-0.30	0.38	-0.25	-0.71	-0.15	**0.95**	-0.59	-0.22	-0.41	0.22
	roi2	-0.34	0.32	-0.23	-0.73	-0.12	**0.98**	-0.45	-0.08	-0.45	0.21
	roi3	-0.27	0.36	-0.20	-0.73	-0.11	**0.96**	-0.49	-0.10	-0.37	0.28
	roi4	-0.28	0.30	-0.23	-0.76	-0.21	**0.94**	-0.48	-0.22	-0.35	0.11
	roi5	-0.23	0.26	-0.21	-0.75	-0.12	**0.93**	-0.41	-0.04	-0.39	0.23
Set7	**roi1**	0.16	-0.51	-0.15	0.54	0.18	-0.52	**0.94**	0.08	0.00	-0.04
	roi2	0.11	-0.50	0.00	0.38	-0.12	-0.62	**0.92**	0.00	0.13	-0.25
	roi3	0.11	-0.55	-0.09	0.40	0.16	-0.39	**0.95**	0.02	0.06	-0.27
	roi4	0.05	-0.43	-0.13	0.44	0.19	-0.26	**0.84**	0.04	-0.04	-0.08
	roi5	0.37	-0.53	-0.20	0.53	0.22	-0.37	**0.65**	0.05	0.03	0.17
Set8	**roi1**	0.38	0.12	0.45	0.34	0.46	-0.20	0.00	**0.98**	0.48	-0.07
	roi2	0.42	0.04	0.39	0.34	0.50	-0.17	0.06	**0.98**	0.41	-0.01
	roi3	0.16	0.16	0.39	0.17	0.40	-0.01	0.03	**0.97**	0.28	0.00
	roi4	0.37	0.05	0.49	0.33	0.53	-0.22	0.18	**0.94**	0.53	-0.18
	roi5	0.37	0.08	0.32	0.25	0.48	-0.06	0.01	**0.98**	0.34	0.06
Set9	**roi1**	0.32	0.25	0.79	0.28	0.32	-0.41	0.04	0.45	**0.98**	-0.44
	roi2	0.31	0.27	0.74	0.20	0.22	-0.39	0.12	0.34	**0.99**	-0.45
	roi3	0.35	0.28	0.79	0.30	0.33	-0.48	0.04	0.39	**0.99**	-0.41
	roi4	0.25	0.25	0.81	0.39	0.46	-0.44	0.09	0.50	**0.94**	-0.41
	roi5	0.26	0.27	0.81	0.34	0.42	-0.41	0.03	0.59	**0.92**	-0.35
Set10	**roi1**	0.26	0.13	0.46	-0.32	-0.09	0.28	-0.04	-0.21	-0.42	**0.90**

Set10	**roi2**	0.06	0.17	0.38	-0.20	0.01	0.25	-0.13	-0.01	-0.42	**0.93**
	roi3	0.26	0.23	-0.31	-0.32	-0.04	0.23	-0.29	0.02	-0.36	**0.94**
	roi4	-0.03	0.25	-0.38	-0.29	-0.02	0.33	-0.21	0.09	-0.51	**0.91**
	roi5	0.01	0.18	-0.44	-0.39	-0.09	0.37	-0.08	-0.06	-0.44	**0.87**

6.4.3.2 Image Comparison using Normalization

Intensity values of each reference image is normalized from (0-255) to (1-10) and stored in database. Heuristic threshold of 50,000 was selected for image comparison. Only that test image which is similar to the one already saved gave the result of difference less than this threshold otherwise difference between test image and remaining all reference images were found out to be well above threshold.

6.4.4 Matching Unit and Recognition Rate

In order to verify the effectiveness of proposed algorithm dataset of 20 different individuals containing 5 digital fundus images per individual was utilized. 3 out of 5 available images per person were randomly selected for creation of reference database. Remaining 2 images were used as test images to check the correctness of the system.

Proposed algorithm was initially applied on sample of 60 randomly selected reference images for extraction of desired features. Two features per image were extracted and both were stored in database to be used subsequently for testing input images. Subsequently remaining 40 images for which no feature was previously extracted and stored in the database were given as input to the system to check whether system recognizes that image and declare as ‘matched’ with correct reference image already stored in database or otherwise.

Out of 40 unknown images 38 were correctly matched with reference images which were already available in database (true positive). 2 images were wrongly matched by the system with reference images which belonged to other individuals (false positive). With this much number of true positives the overall accuracy of the system comes out to be 95%.

In addition to these 40 images, 26 images of another dataset were also tested on the same code with little modification to cater for the variance in image resolution. The purpose was to assess the code for its efficacy. These 26 images were taken from Ibrahim eye trust for which no matching

reference image was stored in database. On applying the proposed code on these images, except 2 all test images were declared as “not matched” with the images already stored in database producing 92.3% true negative result.

Keeping both these results in view it can be easily assessed that recognition rate of proposed method is satisfactory i-e 94%. Table 6.8 shows the recognition rate of both datasets. Statistics illustrates that system is reasonably effective to be used for automated detection of glaucoma using digital retinal fundus image.

TABLE 6.8: RECOGNITION RATE OF DEVELOPED ALGORITHM ON AVAILABLE DATASETS.

DATA SET	TOTAL IMAGES	CORRECTLY RECOGNIZED	WRONGLY RECOGNIZED	RECOGNITION RATE (%)
AFIO	40	38	2	95
IBRHM	26	24	2	92.3
TOTAL	66	62	4	93.9

6.5 Summary

Vasculature displacement is one of the accepted physiological parameters used for diagnosing glaucoma. The accuracy of evaluating correct vascular shift depends upon correct segmentation of optic disc and blood vessels contained inside OD boundary. Automated detection of these features using digital fundus images is not a new approach however still needs improvement. This study was aimed at automated detection of glaucoma in digital retinal fundus images while employing novel biometric approach. Adaptive thresholding technique augmented with a connected component algorithm and morphological operations was used for OD segmentation. Furthermore, a vector based approach coupled with normalized grayscale image comparison was utilized for automated evaluation of OD radii vector and segregation of glaucomic images from normal ones. A dataset of 66 images including 40 normal and 26 glaucomic images annotated by certified ophthalmologists was used to assess the performance of developed algorithm. Global accuracy of 93.9% was achieved. This approach is worthy of incorporating more features that can contribute towards more accurate evaluation of morphological changes occur in eyes that leads towards glaucoma.

CHAPTER – 7

CONCLUSION AND FUTURE WORK

7.1 Conclusion

Automated detection of glaucoma using digital fundus imagery is implemented in proposed methodology. Locally collected dataset of fundus images were utilized for obtaining results. Proposed technique was further sub-divided into three different stages including 1) Feature extraction and segmentation of OD, 2) Vasculature displacement measurement, and 3) Biometric approach. Multimodalities including basic adaptive thresholding, connected component algorithm and morphological operations form the basis of first stage. Blood vessel extraction using wavelet transform and detection of centroids using AND operation with triangular masks remained focal areas in second stage. Novel vector-based approach for obtaining radii vector and image comparison method using normalized images were used in third stage to bring further improvement in acquired results. Better performance of suggested methodology adds a new procedure to already existing automated detection techniques for glaucoma at mass screening level which mainly rely on CDR, ISNT rule and RNFL analysis.

7.2 Future Work

The final accuracy of proposed method for the automated detection of glaucoma is evaluated using digital fundus images of normal patients using biometric approach due to non-availability of required number of images collected with a gap of at least 3 months. In future it would be endeavored to implement the same algorithm on more glaucomic images vis-à-vis dovetailing more physiological features associated with glaucoma like RNFL texture, ISNT rule and CDR for more reliable automated detection of the disease.

Appendix A

MATLAB CODE

GLAUCOMA DETECTION

```
clc
clear all
close all
%%
[FileName,PathName] = uigetfile('nonmydriatic1\*.*','Select A Fundus Image');
img1 = imread([PathName FileName]);
%% This portion gets input from user about left or right eye
prompt='Enter 1 for RIGHT EYE & 2 for LEFT EYE = ';
side=input(prompt);
[r c v] = size(img1);
if(c > 251)
   img1=imresize(img1,[251 251]);
end
%img = imresize(img1,[round((rr/cc)*1600) 1600]);
%img = imresize(gimgcolor1,[round((r/c)*r) c]);

discimg=img1;
[cc,gimgcolor1]=contrast1(discimg); %this function gives contrast enhanced image with OD in center
[k]=contrast11(discimg); %this function gives contrast enhanced image with OD in center
[perimetricimg,disk2]=diskextraction(cc); %This Func gives outline and binary image of OD
figure, imshow(disk2), title('Final OD Image'),impixelinfo;
%-----Finding radius of an OD------
figure, imshow(perimetricimg), title('Image for OD Radius'),impixelinfo;
radius=ODradius1(perimetricimg); %This func calculates radius of OD at different angles
%-----end--------
img=gimgcolor1;
figure,imshow(img);
%% Vessel
[vessel_wavelet, vessel_seg] = vessel_segmentation(img);
figure, imshow(vessel_wavelet,[]),title('figure-1');
% impixelinfo;
figure,imshow(vessel_seg),title('Salman');
% impixelinfo;
%% This portion multiply Final OD image and blood vessel extracted image to get only middle portion of OD
visible however remaining part wl get black
finalimg=vessel_seg.*disk2;
figure, imshow(finalimg),title('OD With Black Margins'),impixelinfo;
[rr cc] = size(finalimg);
%% This portion crop finalimg and the output is only OD portion while undesired black portion is cropped
ymin=k;      % Starting pt y
xmin=k;      % Starting pt x
ymax=cc-2*k; % width of image
xmax=rr-2*k; % Height of image

finalimg1=imcrop(finalimg,[ymin xmin ymax xmax]);
figure,imshow(finalimg1),title('Only OD w/o Margins'),impixelinfo;
%hold on;
%% This portion will find out the reference pt
[r3 c3] = size(finalimg1);
%% This portion divide finalimg1 into 4x parts using 4x triangular masks
```

```
% 1) Making of masks
[mask1,mask2,mask3,mask4]=mask(r3,c3); % this comd call fn that makes 4x masks
mask_size=size(mask1); %original code
if(side==2)% means image selected is of left eye so ref pt will b on right edge
   refpt_x = floor(mask_size(1)/2);
   refpt_y = mask_size(2);
   Ref_Pt=[refpt_y;refpt_x]
   %plot(refpt_y,refpt_x,'yd');
else % means image selected is of right eye so ref pt will b on left edge
   refpt_x = floor(mask_size(1)/2);
   refpt_y = 1;
   Ref_Pt=[refpt_y;refpt_x]
   %plot(refpt_y,refpt_x,'yd');
end
%% This portion segregates inferior, superior and temporal regions and save it in current folder
% 1) First identify type of img whether left eye or right eye img
% 2) On this basis select three out of four masks
% 3) Multiply each mask with finalimg1 to get bloodvessels of that region only

if(side==2)% means image selected is of left eye so mask4,mask1 and mask2 will be selected
   sup=mask4.*finalimg1;
   nas=mask1.*finalimg1; % trial only
   inf=mask2.*finalimg1;
   figure,imshow(sup),title('Superior Region of Left Eye'),impixelinfo;
   figure,imshow(nas),title('Nasal Region of Left Eye'),impixelinfo;
   figure,imshow(inf),title('Inferior Region of Left Eye'),impixelinfo;
   imwrite(sup,'supzone.jpg');%save suprr zone image in current folder
   imwrite(nas,'naszone.jpg'); % save nasal zone image in current folder
   imwrite(inf,'infzone.jpg'); % save infr zone image in current folder
else % means image selected is of right eye so mask4,mask3 and mask2 will be selected
   sup=mask4.*finalimg1;
   nas=mask3.*finalimg1;
   inf=mask2.*finalimg1;
   figure,imshow(sup),title('Superior Region of Right Eye')
   impixelinfo;
   figure,imshow(nas),title('Nasal Region of Right Eye'),impixelinfo;
   figure,imshow(inf),title('Inferior Region of Right Eye')
   impixelinfo;
   imwrite(sup,'supzone.jpg'); % save sup zone image in current folder
   imwrite(nas,'naszone.jpg'); % save sup zone image in current folder
   imwrite(inf,'infzone.jpg'); % save sup zone image in current folder
end
%% This part calculate centroids of all three regions
centroid1=centroid_sup(sup) % this comd calc centroid of superior zone
centroid2=centroid_nas(nas) % this comd calc centroid of nasal zone
centroid3=centroid_inf(inf) % this comd calc centroid of inferior zone

%% this part plot centroids on blood vessel extracted image finalimg1 or
figure, imshow(finalimg1);
hold on
plot(centroid1(1),centroid1(2), 'b*') % Plotting centroid1 on SUPERIOR ZONE of finalimg1
plot(centroid2(1),centroid2(2), 'b*') % Plotting centroid2 on NASAL ZONE of finalimg1
plot(centroid3(1),centroid3(2), 'b*') % Plotting centroid3 on INFERIOR ZONE of finalimg1
plot(refpt_y,refpt_x,'yd') % Plotting ref pt
hold off
%% This portion calculate distance between ref pts and centroids
```

```
req_angle=[0 180];
% manually selecting two opp angles against which dimensions are req to calc horizontal radius of OD
angle_row=radius(1,:);% will pick row of angles from radius matrix
salman=ismember(angle_row,req_angle);
% this comd will replace entries 0 & 180 with '1' and remaining with '0'
indexes=find(salman);
% this comd will only give the index value of entries having value '1'
rad_row=radius(2,:);% radius row will be segregated from radius matrix
rad_values=rad_row(indexes);% values against 0 & 180 deg will b picked up
Horizontal_Radius=sum(rad_values)% calc sum of two values
%% This portion calc mean and normalized displacement of blood vessels in Optic disc
[distA,distB,distC,mean_displacement,normalized_displacement]=norm_disp(Ref_Pt,centroid1,centroid2,centroid3,
Horizontal_Radius)%without temporal factor
Results=[Horizontal_Radius;distA;distB;distC;mean_displacement;normalized_displacement]
```

Functions

(1) contrast1 Function

```
function [cc,gimgcolor1]=contrast1(discimg)
%++++++++This potion segregate r,g and b channels from original image and
%carryout contrast enhancement of grayscale ROI
%clc;
%clear all;
%close all;

%[filename,path]=uigetfile({'*.jpg; *.png; *.gif; *.bmp','Picture files(*.jpg,*.png,*.gif,*.bmp)'},'Pick a file');  %get
file and divide it into path and filename
%discimg=imread(strcat(path,filename)); % read image after concatenating path and filename
gimg1=rgb2gray(discimg);
gimg2=imadjust(gimg1);
red = discimg(:,:,1); % Red channel
green = discimg(:,:,2); % Green channel
blue = discimg(:,:,3); % Blue channel
a = zeros(size(discimg, 1), size(discimg, 2));
just_red = cat(3, red, a, a);
just_green = cat(3, a, green, a);
just_blue = cat(3, a, a, blue);
back_to_original_img = cat(3, red, green, blue);

%cc=imadjust(red,[0 1], [1 0]); %taking negative of red portion of an image
%---Alternate of above line
red=imadjust(red); %contrast enhancement of red portion
cc=imadjust(red,[0 1], [1 0]);%taking negative of contrast enhanced image

%---try
%cc=imadjust(red); %contrast enhancement of red portion

%figure, imshow(just_red), title('justred');
%figure, imshow(red), title('red Image');
%impixelinfo;
%figure, imshow(cc), title('Contrast Enhanced Image');
d = blkproc(cc,[125 125], @adapt_thresh);
%d = blkproc(cc,[225 225], @adapt_thresh);
%%figure;
%subplot(1,2,1), imshow(cc), title('Original  image');
```

```
%subplot(1,2,2), imshow(d), title('Adaptive Thresholding');
dcompl=~d;  % taking compliment of image 'd'

%---removing unneccessary connected components other than disk
dcompl1=bwconncomp(dcompl,4);
diskdata=regionprops(dcompl1,'basic');
disk_area=[diskdata.Area];
[max_area, idx]=max(disk_area);
disk = false(size(dcompl));
disk(dcompl1.PixelIdxList{idx})=true;
%figure, imshow(disk), title('Conn comp other than disc removed');

%---removing small conn comps lying inside disc using closing
%morphological op

se2=strel('disk',5);
disky=imclose(disk,se2);
%figure, imshow(disky), title('Closed dic');

%----Morphological operation 'opening, for removing small white holes' fol by 'closing, for removing black portions
from disc'----
%se1=strel('disk',30);
se1=strel('disk',15);
intrep=disky;
disk1=imopen(intrep,se1);
%figure, imshow(disk1), title('Opened disc');
%se3=strel('disk',30);
se3=strel('disk',15);
disk2=imclose(disk1,se3);
%disk2=~disk2; %temporaryline
%%figure, imshow(disk2), title('Again Closed disc');

img1 = bwperim(disk2);    % Very imp step---Matrix containing perimeter of OD
%img1=edge(dcompl,'canny');
img1compl = ~img1;  % taking complement of img1 i-e optic disc so that reactangle around OD remain visible

% ---finding starting point, width and height of rectangle
[x,y] = find(img1);
xmin = min(x);
xmax = max(x);
ymin = min(y);
ymax = max(y);
x1 = xmax-xmin;
y1 = ymax-ymin;

%----finding mid point of rectangle
midpt_x = floor((x1/2)+xmin);
midpt_y = floor((y1/2)+ymin);

%figure, imshow(red), title('Original Image');
%figure, imshow(cc), title('Adjusted Image');
%impixelinfo;
%figure, imshow(dcompl), title('Binary Image');
%figure, imshow(disk1), title('Opened Image');
%figure, imshow(disk2), title('Closed Image');
%figure, imshow(img1compl), title('Skeleton Image');
```

```
%hold on
%rectangle('Position',[ymin,xmin,y1,x1],'LineWidth',1);  % drawing rectangle around optic disc
%impixelinfo;

%---Recalculate OD bdry using sub-cropped image
[totalx, totaly]=size(cc);
k1=[xmin,ymin,(totalx-xmax),(totaly-ymax)];
k=min(k1);
%k=20; %constant
cc=imcrop(cc,[(ymin-k) (xmin-k) (y1+(2*k)) (x1+(2*k))]);
%gimg=imcrop(cc,[(ymin-k) (xmin-k) (y1+(2*k)) (x1+(2*k))]);
gimg=imcrop(gimg2,[ymin xmin y1 x1]);
%%
gimgcolor1=imcrop(discimg,[(ymin-k) (xmin-k) (y1+(2*k)) (x1+(2*k))]);
gimgcolor=imcrop(discimg,[ymin xmin y1 x1]);
figure, imshow(gimgcolor1), title('Colored Contrast Enhanced Cropped Image-cc');
figure, imshow(gimgcolor), title('Colored Only OD Cropped Image-gimg');

%%
figure, imshow(cc), title('Contrast Enhanced Cropped Image-cc');
figure, imshow(gimg), title('Only OD Cropped Image-gimg');
%%impixelinfo;
return
end
```

---

(2) contrast11 Function

```
function [k]=contrast11(discimg)
%+++++++This potion segregate r,g and b channels from original image and
%carryout contrast enhancement of grayscale ROI
%clc;
%clear all;
%close all;

%[filename,path]=uigetfile({'*.jpg; *.png; *.gif; *.bmp','Picture files(*.jpg,*.png,*.gif,*.bmp)'},'Pick a file');  %get
file and divide it into path and filename
%discimg=imread(strcat(path,filename)); % read image after concatenating path and filename
gimg1=rgb2gray(discimg);
gimg2=imadjust(gimg1);
red = discimg(:,:,1); % Red channel
green = discimg(:,:,2); % Green channel
blue = discimg(:,:,3); % Blue channel
a = zeros(size(discimg, 1), size(discimg, 2));
just_red = cat(3, red, a, a);
just_green = cat(3, a, green, a);
just_blue = cat(3, a, a, blue);
back_to_original_img = cat(3, red, green, blue);

%cc=imadjust(red,[0 1], [1 0]); %taking negative of red portion of an image
%---Alternate of above line
red=imadjust(red); %contrast enhancement of red portion
cc=imadjust(red,[0 1], [1 0]);%taking negative of contrast enhanced image
%---try
%cc=imadjust(red); %contrast enhancement of red portion
```

```
%figure, imshow(just_red), title('justred');
%figure, imshow(red), title('red Image');
%impixelinfo;
%figure, imshow(cc), title('Contrast Enhanced Image');
d = blkproc(cc,[125 125], @adapt_thresh);
%d = blkproc(cc,[225 225], @adapt_thresh);
%%figure;
%subplot(1,2,1), imshow(cc), title('Original  image');
%subplot(1,2,2), imshow(d), title('Adaptive Thresholding');
dcompl=~d;  % taking compliment of image 'd'

%---removing unneccessary connected components other than disk
dcompl1=bwconncomp(dcompl,4);
diskdata=regionprops(dcompl1,'basic');
disk_area=[diskdata.Area];
[max_area, idx]=max(disk_area);
disk = false(size(dcompl));
disk(dcompl1.PixelIdxList{idx})=true;
%figure, imshow(disk), title('Conn comp other than disc removed');

%---removing small conn comps lying inside disc using closing
%morphological op

se2=strel('disk',5);
disky=imclose(disk,se2);
%figure, imshow(disky), title('Closed dic');

%----Morphological operation 'opening, for removing small white holes' fol by 'closing, for removing black portions
from disc'----
%se1=strel('disk',30);
se1=strel('disk',15);
intrep=disky;
disk1=imopen(intrep,se1);
%figure, imshow(disk1), title('Opened disc');
%se3=strel('disk',30);
se3=strel('disk',15);
disk2=imclose(disk1,se3);
%disk2=~disk2; %temporaryline
%%figure, imshow(disk2), title('Again Closed disc');

img1 = bwperim(disk2);    % Very imp step---Matrix containing perimeter of OD
%img1=edge(dcompl,'canny');
img1compl = ~img1;  % taking complement of img1 i-e optic disc so that reactangle around OD remain visible

% ---finding starting point, width and height of rectangle
[x,y] = find(img1);
xmin = min(x);
xmax = max(x);
ymin = min(y);
ymax = max(y);
x1 = xmax-xmin;
y1 = ymax-ymin;

%----finding mid point of rectangle
midpt_x = floor((x1/2)+xmin);
midpt_y = floor((y1/2)+ymin);
```

```
%figure, imshow(red), title('Original Image');
%figure, imshow(cc), title('Adjusted Image');
%impixelinfo;
%figure, imshow(dcompl), title('Binary Image');
%figure, imshow(disk1), title('Opened Image');
%figure, imshow(disk2), title('Closed Image');
%figure, imshow(img1compl), title('Skeleton Image');

%hold on
%rectangle('Position',[ymin,xmin,y1,x1],'LineWidth',1);  % drawing rectangle around optic disc
%impixelinfo;

%---Recalculate OD bdry using sub-cropped image
[totalx, totaly]=size(cc);
k1=[xmin,ymin,(totalx-xmax),(totaly-ymax)];
k=min(k1);
%k=20; %constant
cc=imcrop(cc,[(ymin-k) (xmin-k) (y1+(2*k)) (x1+(2*k))]);
%gimg=imcrop(cc,[(ymin-k) (xmin-k) (y1+(2*k)) (x1+(2*k))]);
gimg=imcrop(gimg2,[ymin xmin y1 x1]);
%%
gimgcolor1=imcrop(discimg,[(ymin-k) (xmin-k) (y1+(2*k)) (x1+(2*k))]);
gimgcolor=imcrop(discimg,[ymin xmin y1 x1]);
figure, imshow(gimgcolor1), title('Colored Contrast Enhanced Cropped Image-cc');
figure, imshow(gimgcolor), title('Colored Only OD Cropped Image-gimg');

%%
figure, imshow(cc), title('Contrast Enhanced Cropped Image-cc');
figure, imshow(gimg), title('Only OD Cropped Image-gimg');
impixelinfo;
return
end
```

---

(3) diskextraction Function

```
function [img1,disk2]=diskextraction(cc)
%---This code calc adaptive threshold using blkproc function

[sizex sizey]=size(cc);
d = blkproc(cc,[floor(sizex/2) floor(sizey/2)], @adapt_thresh);
dcompl=~d;  % taking compliment of image 'd'
%---removing unneccessary connected components other than disk
dcompl1=bwconncomp(dcompl,4);
diskdata=regionprops(dcompl1,'basic');
disk_area=[diskdata.Area];
[max_area, idx]=max(disk_area);
disk = false(size(dcompl));
disk(dcompl1.PixelIdxList{idx})=true;
%----removing small conn comps lying inside disc using closing
%morphological op

se2=strel('disk',5);
disky=imclose(disk,se2);

%----Morphological operation 'opening, for removing small white holes' fol by 'closing, for removing black portions
```

```
from disc'----
se1=strel('disk',15);
intrep=disky;
disk1=imopen(intrep,se1);
se3=strel('disk',15);
disk2=imclose(disk1,se3);

%-----Changed for testing
figure, imshow(disk2), title('Final OD Image');
impixelinfo;

%-----
img1 = bwperim(disk2);    % Very imp step---Matrix containing perimeter of OD
img1compl = ~img1;  % taking complement of img1 i-e optic disc so that reactangle around OD remain visible
figure, imshow(img1compl), title('Perimetric Image-2');

return
end
```

---

(4) ODradius1 Function

```
function xy_plane=ODradius1(img1)
%This func stretch the circular disc into a straight line form (xy plane) and
%calculate radius of OD at an angle of 0 to 360 degree at interval of 10 degree

% ---finding starting point, width and height of rectangle
[x,y] = find(img1);
xmin = min(x);
xmax = max(x);
ymin = min(y);
ymax = max(y);
x1 = xmax-xmin;
y1 = ymax-ymin;

% ----finding mid point of rectangle
midpt_x = floor((x1/2)+xmin);
midpt_y = floor((y1/2)+ymin);

img1compl=~img1;
figure, imshow(img1compl), title('Skeleton Image');

midpt_xx=midpt_y;
midpt_yy=midpt_x;   % finding midpoint of optic disc
r=.6*((x1+y1)/2);           % radius of circle will be 0.6 times horizontal dia of OD
th_deg=0:10:350;    % Dividing circle into 24 equal parts (15 deg each)
th_rad=th_deg*(0.005555*pi);    % converting degrees into radians
[x_circle y_circle]=pol2cart(th_rad,r); % convert polar coord into cartesian (x,y)

%----This portion stretch the circular disc into a straight form (xy plane) and
%calculate radius of OD at an angle of 0 to 345 degree at interval of 15
%degree

nn=0;
for i=1:1:36
x_act_cir=x_circle(i)+midpt_xx;
y_act_cir=y_circle(i)+midpt_yy;
```

```
plot([midpt_xx,x_act_cir],[midpt_yy,y_act_cir]);
bb=[midpt_xx;x_act_cir];
aa=[midpt_yy;y_act_cir];
[yii,xii]=polyxpoly(x,y,aa,bb);
if((xii(1)==midpt_xx)&&(yii(1)==midpt_yy))
   x_disc=xii(end);
   y_disc=yii(end);
   y_dist=round(sqrt((midpt_xx-x_disc)^2+(midpt_yy-y_disc)^2));
else
   x_disc=xii(1);
   y_disc=yii(1);
   y_dist=sqrt((midpt_xx-x_disc)^2+(midpt_yy-y_disc)^2);
   y_dist=round(y_dist);
end
nn=nn+1;
xy_plane(:,nn)=[th_deg(i);y_dist];
end
%---picking up values from 1-70, 120-250, 290-350
th_deg=th_deg([1:8,12:26,30:end]);
y_dist=xy_plane(2,:);
y_dist=y_dist([1:8,12:26,30:end]);
xy_plane=[th_deg;y_dist];
```

---

(5) vessel_segmentation Function

```
function [img_wavelet img_seg] = vessel_segmentation(img);
[r c v] = size(img);
if (r>1100); ... for Shifa Images.
   scales = 9;
else
   scales = 2.5;
end
epsi = 2.5;
k_y  = 2.5;
k_x  = 0;
img_seg=0;
img = double(img) / 255;
green = img(:,:,2);
green=imcomplement(green);
im = green;
img_gr = im;
se = strel('disk',6);
img_gr = imclose(img_gr,se);
fimg = fft2(img_gr);
k0x = k_x;
k0y = k_y;
a = scales;
epsilon = epsi;
[img_wavelet]= maxwavlet(fimg, a, epsilon, [k0x k0y], 10);
img_wavelet = img_wavelet;%.*bg_mask(:,:,1);
im = img_wavelet;
im=im-min(im(:));
im=im/max(im(:));
im=uint8(im*255);
if (r > 1100)
```

```
    imf = medfilt2(im,[35 35]);
    BndBox=200;
    MjrLn=55;
    T=8;
else
    imf = medfilt2(im,[21 21]);
    BndBox=120;
    MjrLn=40;
    T=7;
end
vess=(im-imf)>T;
while (mean(mean(vess))<0.05)
    T=T-1;
    vess=(im-imf)>T;
end
imo = (bwareaopen((imclose(vess,strel('diamond',3))),160));
lbl=bwlabel(imo);
prps=regionprops(imo,'BoundingBox','MajorAxisLength','MinorAxisLength');
v=zeros(1,length(prps));
for i=1:length(prps)
    if (max(prps(i).BoundingBox(3:4))<BndBox)
        if(prps(i).MajorAxisLength/prps(i).MinorAxisLength<3 || prps(i).MajorAxisLength<MjrLn);
        v(i)=i;
        end
    end
end
[~, ~ ,objs] = find(v);
imo = (~ismember(lbl,objs).*imo) > 0;
img_seg = imo;
```

---

(6) maxwvlet Function

```
function [wtmodmax] = maxwavlet(fimg,  a, epsilon, k0, step)
[r c] = size(fimg);
largelins = r + 1 + mod(r, 2);
largecols = c + 1 + mod(c, 2);
%%variable to store max response
wtmodmax = - Inf * ones(r,c);
for t = 0:step:179
  theta= t * (pi/180);
% Calculates wavelet
  wvlt = wavlet([largelins largecols], theta, a, epsilon, k0);
  wvlt = wvlt(1:r, 1:c);
% Takes the complex conjugate.
  cwvlt = conj(wvlt);
% Shifts.
  cwvlt = fftshift (cwvlt);
% Transfers to the frequency domain.
  fcwvlt = fft2 (cwvlt);
% Multiplies image by wavelet conjugate in freq domain. The
% conjugate below indicates correlation in space, instead of
% convolution.
  fimgwv = fimg .* conj (fcwvlt);
% Back to space domain.
  imgwv = ifft2 (fimgwv);
% Normalization (only by scale a)
```

```
  imgwv = imgwv / a;
% Get the modulus of the result.
  modimgwv = abs (imgwv);
% Updates the maximum.
  wtmodmax = max( modimgwv, wtmodmax );
end
figure, imshow(wtmodmax,[]);
```

---

(7) mask Function

```
function [mask11,mask22,mask33,mask44]=mask(r3,c3)
val=max(r3,c3); %checking no of rows and cols
mid=val/2;
mid1=floor(mid);
%checking whether row or cols are odd or even (even is req) for easy distr of mask in 4 parts
dif_mid=mid-mid1;
if(dif_mid==0)
   a=ones(val);
else
   val=val+1;
   mid=val/2;
   a=ones(val);
end
% dividing mask into 4 regions
a1=a(1:mid,1:mid);
a2=a(mid+1:end,1:mid);
a3=a(1:mid,mid+1:end);
a4=a(mid+1:end,mid+1:end);
% making white triangular shapes in balck mask
aa1=tril(a1);
aa2=flipud(aa1);
a3(a3==1)=0;
aa3=a3;
a4(a4==1)=0;
aa4=a4;
aa=vertcat(aa3,aa4);
aaa=vertcat(aa1,aa2);
mask11=horzcat(aaa,aa);% original code
mask11=imresize(mask11,[r3 c3]);
%figure(1),imshow(mask11),impixelinfo;
mask33=fliplr(mask11);
mask33=imresize(mask33,[r3 c3]);
%figure(2),imshow(mask33),impixelinfo;
mask44=rot90(mask33);
mask44=imresize(mask44,[r3 c3]);
%figure(3),imshow(mask44),impixelinfo;
mask22=flipud(mask44);
mask22=imresize(mask22,[r3 c3]);
%figure(4),imshow(mask22),impixelinfo;
return
end
```

---

(8) centroid_nas Function

```
function [centroid2] = centroid_nas(nas)
%% This portion finds the centroid of Nasal zone and mark it in blue on the image
```

```
%Code also take care of portionswhich are very small in size hence reduce accuracy of centroid
N = nas;
Ibw = im2bw(N);
Ilabel1 = bwlabel(Ibw);
% This part detect white portion which are very small in size and reduce accuracy of centroid
i=max(max(Ilabel1));
for y=1:i
a=find(Ilabel1==y);
if numel(a)<100
Ilabel1(a)=0;
y=y+1;
else
y=y+1;
end
end
Ilabel = bwlabel(Ilabel1);
stat = regionprops(Ilabel,'centroid');
imshow(N); hold on;
for x = 1: numel(stat)
   plot(stat(x).Centroid(1),stat(x).Centroid(2),'ro');
end
centroids_nas = cat(1,stat.Centroid);
if x<2
   imshow(N);
   hold on
   plot(centroids_nas(1), centroids_nas(2), 'b*')
   hold off
   centroid2=centroids_nas';
else
%_____________ This part calc weighted mean of centroids
j=1;
for j = 1:x
   aa=find(Ilabel==j);
   bb(j)=numel(aa);
end
wt=bb/sum(bb);
mean_centroids_nas=centroids_nas'*wt';
imshow(N);
hold on
plot(mean_centroids_nas(1), mean_centroids_nas(2), 'b*')
hold off
centroid2=mean_centroids_nas;
end
return
end
```

MATLAB CODE

BIOMETRIC APPROACH

% **Main file.** This Code takes test Fundus Image, match it with reference images stored in database and give result

```
close all;
clear all;
clc;

[filename,path]=uigetfile({'*.jpg; *.png; *.gif; *.bmp','Picture files(*.jpg,*.png,*.gif,*.bmp)'},'Pick a file');  %get file and divide it into path and filename
discimg=imread(strcat(path,filename)); % read image after concatenating path and filename

[cc gimg]=contrast1(discimg); %this function gives contrast enhanced image with OD in center

[perimetricimg,disk2]=diskextraction(cc); %This Func gives outline and binary image of OD

radius=ODradius(perimetricimg); %This func calculates radius of OD at different angles

radius=(radius(2,:));
correlidx=correlation(radius);

imgcompidx=img_comparison1(gimg);

%--Extracted Features of Input Fundus Image
[maxval maxind]=max(correlidx);
matchingimg=maxind;

if imgcompidx==matchingimg
   fprintf('Matching successful with sample %d \n',matchingimg);
else
   display('No match found');
end
```

Functions

(1) contrast1 function

```
function [cc,gimg]=contrast1(discimg)
%This potion segregate r,g and b channels from original image and
%carryout contrast enhancement of grayscale ROI

gimg1=rgb2gray(discimg);
gimg2=imadjust(gimg1);
red = discimg(:,:,1); % Red channel
green = discimg(:,:,2); % Green channel
blue = discimg(:,:,3); % Blue channel
a = zeros(size(discimg, 1), size(discimg, 2));
just_red = cat(3, red, a, a);
just_green = cat(3, a, green, a);
just_blue = cat(3, a, a, blue);
back_to_original_img = cat(3, red, green, blue);

red=imadjust(red); %contrast enhancement of red portion
cc=imadjust(red,[0 1], [1 0]);%taking negative of contrast enhanced image
```

```
d = blkproc(cc,[125 125], @adapt_thresh);
dcompl=~d;  % taking compliment of image 'd'

%---removing unneccessary connected components other than disk
dcompl1=bwconncomp(dcompl,4);
diskdata=regionprops(dcompl1,'basic');
disk_area=[diskdata.Area];
[max_area, idx]=max(disk_area);
disk = false(size(dcompl));
disk(dcompl1.PixelIdxList{idx})=true;
%figure, imshow(disk), title('Conn comp other than disc removed');

%---removing small conn comps lying inside disc using closing
%morphological op

se2=strel('disk',5);
disky=imclose(disk,se2);
%figure, imshow(disky), title('Closed dic');

%----Morphological operation 'opening, for removing small white holes' fol by 'closing, for removing black portions
from disc'----
se1=strel('disk',15);
intrep=disky;
disk1=imopen(intrep,se1);
%figure, imshow(disk1), title('Opened disc');
se3=strel('disk',15);
disk2=imclose(disk1,se3);
%figure, imshow(disk2), title('Again Closed disc');

img1 = bwperim(disk2);    % Very imp step---Matrix containing perimeter of OD
img1compl = ~img1;  % taking complement of img1 i-e optic disc so that reactangle around OD remain visible

%----finding starting point, width and height of rectangle
[x,y] = find(img1);
xmin = min(x);
xmax = max(x);
ymin = min(y);
ymax = max(y);
x1 = xmax-xmin;
y1 = ymax-ymin;

%----finding mid point of rectangle
midpt_x = floor((x1/2)+xmin);
midpt_y = floor((y1/2)+ymin);

%figure, imshow(img1compl), title('Skeleton Image');

%hold on
%rectangle('Position',[ymin,xmin,y1,x1],'LineWidth',1);  % drawing rectangle around optic disc
%impixelinfo;

%---Recalculate OD bdry using sub-cropped image
[totalx, totaly]=size(cc);
k1=[xmin,ymin,(totalx-xmax),(totaly-ymax)];
k=min(k1);
cc=imcrop(cc,[(ymin-k) (xmin-k) (y1+(2*k)) (x1+(2*k))]);
```

```
gimg=imcrop(gimg2,[ymin xmin y1 x1]);

figure, imshow(cc), title('Contrast Enhanced Cropped Image-cc');
figure, imshow(gimg), title('Only OD Cropped Image-gimg');
%%impixelinfo;
return
end
```

(2) diskextraction function

```
function [img1,disk2]=diskextraction(cc)
%---This code calc adaptive threshold using blkproc function

[sizex sizey]=size(cc);
d = blkproc(cc,[floor(sizex/2) floor(sizey/2)], @adapt_thresh);
dcompl=~d;  % taking compliment of image 'd'
%figure, imshow(dcompl), title('Binary Image-2');
%---removing unneccessary connected components other than disk
dcompl1=bwconncomp(dcompl,4);
diskdata=regionprops(dcompl1,'basic');
disk_area=[diskdata.Area];
[max_area, idx]=max(disk_area);
disk = false(size(dcompl));
disk(dcompl1.PixelIdxList{idx})=true;
%figure, imshow(disk), title('Conn comp other than disc removed');
%----removing small conn comps lying inside disc using closing
%morphological op

se2=strel('disk',5);
disky=imclose(disk,se2);
%figure, imshow(disky), title('Closed dic');

%----Morphological operation 'opening, for removing small white holes' fol by 'closing, for removing black portions
from disc'----
se1=strel('disk',15);
intrep=disky;
disk1=imopen(intrep,se1);
%figure, imshow(disk1), title('Opened disc');
se3=strel('disk',15);
disk2=imclose(disk1,se3);

%-----Changed for testing
figure, imshow(disk2), title('Final OD Image');
impixelinfo;

img1 = bwperim(disk2);    % Very imp step---Matrix containing perimeter of OD
img1compl = ~img1;  % taking complement of img1 i-e optic disc so that reactangle around OD remain visible
figure, imshow(img1compl), title('Perimetric Image-2');

return
end
```

(3) ODradius function

```
function xy_plane=ODradius(img1)
%This func stretch the circular disc into a straight line form (xy plane) and
```

```
%calculate radius of OD at an angle of 0 to 360 degree at interval of 10 degree

% ---finding starting point, width and height of rectangle
[x,y] = find(img1);
xmin = min(x);
xmax = max(x);
ymin = min(y);
ymax = max(y);
x1 = xmax-xmin;
y1 = ymax-ymin;

% ----finding mid point of rectangle
midpt_x = floor((x1/2)+xmin);
midpt_y = floor((y1/2)+ymin);

img1compl=~img1;
figure, imshow(img1compl), title('Skeleton Image');

hold on
%rectangle('Position',[ymin,xmin,y1,x1],'LineWidth',1);  % drawing rectangle around optic disc
%p2=circle([midpt_y, midpt_x],(0.6*y1));     % draw circle around OD for plotting lines from middle of OD to
circle
%circle([midpt_y, midpt_x],(0.6*y1));     % draw circle around OD for plotting lines from middle of OD to circle
%impixelinfo;

midpt_xx=midpt_y;
midpt_yy=midpt_x;   % finding midpoint of optic disc
r=.6*((x1+y1)/2);           % radius of circle will be 0.6 times horizontal dia of OD
th_deg=0:10:350;    % Dividing circle into 24 equal parts (15 deg each)
th_rad=th_deg*(0.005555*pi);    % converting degrees into radians
[x_circle y_circle]=pol2cart(th_rad,r); % convert polar coord into cartesian (x,y)

%----This portion stretch the circular disc into a straight form (xy plane) %and calculate radius of OD at an angle of
0 to 345 degree at interval of 15
%Degree.

nn=0;
for i=1:1:36
x_act_cir=x_circle(i)+midpt_xx;
y_act_cir=y_circle(i)+midpt_yy;

plot([midpt_xx,x_act_cir],[midpt_yy,y_act_cir]);
bb=[midpt_xx;x_act_cir];
aa=[midpt_yy;y_act_cir];
[yii,xii]=polyxpoly(x,y,aa,bb);

if((xii(1)==midpt_xx)&&(yii(1)==midpt_yy))
   x_disc=xii(end);
   y_disc=yii(end);
   y_dist=round(sqrt((midpt_xx-x_disc)^2+(midpt_yy-y_disc)^2));
else
   x_disc=xii(1);
   y_disc=yii(1);
   y_dist=sqrt((midpt_xx-x_disc)^2+(midpt_yy-y_disc)^2);
   y_dist=round(y_dist);
end
```

```
nn=nn+1;
xy_plane(:,nn)=[th_deg(i);y_dist];

end

%---picking up values from 1-70, 120-250, 290-350
th_deg=th_deg([1:8,12:26,30:end]);
y_dist=xy_plane(2,:);
y_dist=y_dist([1:8,12:26,30:end]);
xy_plane=[th_deg;y_dist];

figure, plot(xy_plane(1,:),xy_plane(2,:)), title('OD in xy plane');
axis([0 350 0 300]);
```

(4) correlation function

```
function correlidx=correlation(radius)
%---Feature-1
input=radius;
test=[62 64 64 65 66 66 65 62 67 65 64 64 64
      63 62 62 62 61 62 64 64 65 67 63 63
      61 59 60 60 59
66    67 67 66 60 60 65 67 69 70 69 68 67
      67 66 66 67 66 66 65 66 67 65 67 68
      67 66 68 69 67
63    63 63 65 63 63 66 68 69 68 67 66 65
      65 63 63 63 63 64 66 64 65 64 69 71
      69 68 65 64 63
62    63 63 65 68 68 70 71 61 61 62 61 60
      60 60 60 62 65 67 67 67 70 70 65 65
      63 62 62 62 62
63    63 64 64 64 65 65 66 67 62 61 66 67
      65 63 60 60 62 64 68 68 69 71 63 68
      67 65 64 63 63
71    71 70 69 68 68 65 63 70 71 72 73 75
      74 72 71 72 69 69 70 70 69 71 65 69
      72 72 73 76 73
72    73 73 74 74 74 72 73 70 71 69 68 67
      69 72 71 69 70 69 70 72 71 72 71 72
      72 72 71 69 72
64    64 65 67 66 68 67 59 77 72 69 61 64
      63 64 63 65 68 70 71 72 76 79 77 74
      71 69 71 68 65
64    65 66 66 66 69 73 75 75 73 72 69 67
      64 63 64 64 64 63 64 66 68 70 73 74
      68 69 68 67 64
61    62 63 59 58 57 57 57 60 61 59 60 61
      61 61 61 61 62 60 60 61 61 62 58 59
      58 58 57 56 60];

%---step#1--this portion calculate mean of test dataset and input dataset
meaninput=mean(input);
for i=1:size(test,1)
   meantest(i)=mean(test(i,:));
end
```

```
%---step#2--this portin subtract indl values of both datasets from their mean values
a=input-meaninput;

for i=1:size(test,1)
   for j=1:size(test,2)
      b(i,j)=test(i,j)-meantest(i);
   end
end

%---step#3--this portin calculate axb, a^2, b^2
ab=zeros(size(test,1),size(test,2));
for i=1:size(test,1)
   ab(i,:)=a.*b(i,:);
end
aa=a.*a;
bb=b.*b;

%---step#4--Take summation of ab, aa, bb calculated in step#3(do it again)
ab=ab';
sum_ab=sum(ab);
sum_ab=sum_ab';

bb=bb';
sum_bb=sum(bb);
sum_bb=sum_bb';

sum_aa=sum(aa);

%---step#5--calculate correlation
correlidx=zeros(1,10);
for i=1:size(test,1)
correlidx(i)=sum_ab(i)/sqrt(sum_aa*sum_bb(i));
end

return
end
```

---

(5) img_comparison1 function

```
function imgcompidx=img_comparison1(gimg)
%---Feature-2
%---This func normalize the intensity values of an image from 0-255 to 0-10.
%Then take sum of difference between the input and already saved images.
%Smallest difference shows max matching criteria is used in this func.

for i=1:27
%a(:,:,i)=double(imread(strcat('od',sprintf('%d',i),'.jpg')));
a(:,:,i)=double(imread(strcat('E:\ref_img\od',sprintf('%d',i),'.jpg')));
end

A=min(min(a(:,:,:)));
%A=min(min(a(:,:,1)));
B=max(max(a(:,:,:)));
A=double(A);
B=double(B);
aa=double(1);
```

```
bb=double(10);
b=zeros(size(a,1),size(a,2),size(a,3));
for k=1:size(a,3)
   b(:,:,k)=floor(aa+((a(:,:,k)-A(:,:,k)).*(bb-aa))/(B(:,:,k)-A(:,:,k))); %converting intensity values of all images stored
in matrix 'a'
end                                                    %into normalized values b/w 1-10

I=imresize(gimg,[300 300]); %Input image containing OD portion only along with blood vessels
I=double(I);
A=min(min(I));
B=max(max(I));
A=double(A);
B=double(B);
aa=1;
bb=10;
aa=double(aa);
bb=double(bb);
I2=zeros(size(I,1),size(I,2));
I2(:,:)=floor(aa+((I(:,:)-A).*(bb-aa))/(B-A));
for k=1:size(a,3)
   result(k)=sum(sum(abs(I2-b(:,:,k))));
end

[minval minind]=min(result);
if minval<50000
   minindex=(minind/3);
   minindex=ceil(minindex);
   imgcompidx=minindex;
   %fprintf('Matching successful with sample %d \n',minindex);
else
   imgcompidx=0;
   %fprintf('No Match');
end
end
```

REFERENCES

[1] www.healthpartners.com.au/optical/products/eye-examinations/OCT

[2] www.chemistryinmedicine.wordpress.com/2012/04/

[3] www.wisegeek.org/what-are-x-rays.htm

[4] webvision.med.utah.edu/book/part-i-foundations/simple-anatomy-of-the-retina/

[5] "Medical Imaging for Improved Patient Care" presented in European science foundation policy briefing on 28 September 2007.

[6] Chrástek, Radim, Matthias Wolf, Klaus Donath, Heinrich Niemann, Dietrich Paulus, Torsten Hothorn, Berthold Lausen, Robert Lämmer, Christian Y. Mardin, and Georg Michelson. "Automated segmentation of the optic nerve head for diagnosis of glaucoma." Medical Image Analysis 9, no. 4 (2005): 297-314.

[7] de la Fuente-Arriaga, José Abel, Edgardo M. Felipe-Riverón, and Eduardo Garduño-Calderón. "Application of vascular bundle displacement in the optic disc for glaucoma detection using fundus images." Computers in biology and medicine 47 (2014): 27-35.

[8] www.allaboutvision.com/resources/anatomy.htm

[9] www.asrs.org/patients/retinal-diseases

[10] www.cheyennevisionclinic.com

[11] www.merckmanuals.com/home/eye-disorders/retinal-disorders/age-related-macular-degeneration-amd-or-armd

[12] www.merckmanuals.com/home/eye-disorders/retinal-disorders/hypertensive-retinopathy

[13] Robert L Stamper, Marc F Lieberman, Michael V Drake. "Becker – Shaffer's Diagnosis and Therapy of the Glaucomas."(2009).

[14] www.glaucoma.org/glaucoma/types-of-glaucoma.php

[15] Rupert RA Bourne "Glossary The optic nerve head in glaucoma". Community eye health journal, vol 19 No.59, pp 44-45, 2006.

[16] www.dotmed.com/listing/ophthalmoscope/frigitronics/2-x-indirect/2264245

[17] Andrew Jackson "Understanding and living with glaucoma". American academy of ophthalmology. ISBN 978-0-9621579-0-2. 2012

[18] cheshuntopticians.co.uk/fundus-photography

[19] www.ophthalmologyweb.com/5740-Digital-Retinal-Camera/10177822-VISUCAM-500/

[20] www.opsweb.org/?page=fundusphotography

[21] Haleem, Muhammad Salman, Liangxiu Han, Jano van Hemert, and Baihua Li. "Automatic extraction of retinal features from colour retinal images for glaucoma diagnosis: a review." Computerized medical imaging and graphics 37, no. 7 (2013): 581-596.

[22] Chaudhuri, S., S. Chatterjee, N. Katz, M. Nelson, and M. Goldbaum. "Automatic detection of the optic nerve in retinal images." In Proceedings of the IEEE International Conference on Image Processing, vol. 1, pp. 1-5. 1989.

[23] Sinthanayothin, Chanjira, James F. Boyce, Helen L. Cook, and Thomas H. Williamson. "Automated localisation of the optic disc, fovea, and retinal blood vessels from digital colour fundus images." *British Journal of Ophthalmology* 83, no. 8 (1999): 902-910.

[24] Lowell, James, Andrew Hunter, David Steel, Ansu Basu, Robert Ryder, Eric Fletcher, and Lee Kennedy. "Optic nerve head segmentation." IEEE Transactions on medical Imaging 23, no. 2 (2004): 256-264.

[25] Sekhar, Sribalamurugan, Waleed Al-Nuaimy, and Asoke K. Nandi. "Automated localisation of retinal optic disk using Hough transform." In 2008 5th IEEE International Symposium on Biomedical Imaging: From Nano to Macro, pp. 1577-1580. IEEE, 2008.

[26] Gonzalez, Rafael C., and Richard E. Woods. "Digital image processing." (2002).

[27] Rizon, Mohamed, Yazid Haniza, Saad Puteh, Ali Yeon, Md Shakaff, Saad Abdul Rahman, Masanori Sugisaka, Yaacob Sazali, Mamat M Rozailan, and M. Karthigayan. "Object detection using circular Hough transform." (2005).

[28] Li, Huiqi, and Opas Chutatape. "Automatic location of optic disk in retinal images." In Image Processing, 2001. Proceedings. 2001 International Conference on, vol. 2, pp. 837-840. IEEE, 2001.

[29] Osareh, Alireza, Majid Mirmehdi, Barry Thomas, and Richard Markham. "Classification and localisation of diabetic-related eye disease." In European Conference on Computer Vision, pp. 502-516. Springer Berlin Heidelberg, 2002.

[30] Youssif, Aliaa Abdel-Haleim Abdel-Razik, Atef Zaki Ghalwash, and Amr Ahmed Sabry Abdel-Rahman Ghoneim. "Optic disc detection from normalized digital fundus images by means of a vessels' direction matched filter." IEEE Transactions on Medical Imaging 27, no. 1 (2008): 11-18.

[31] Usman, Anam, Sarmad Abbas Khitran, M. Usman Akram, and Yasser Nadeem. "A robust algorithm for optic disc segmentation from colored fundus images." In International

Conference Image Analysis and Recognition, pp. 303-310. Springer International Publishing, 2014.

[32] Hoover, Adam, and Michael Goldbaum. "Locating the optic nerve in a retinal image using the fuzzy convergence of the blood vessels." IEEE transactions on medical imaging 22, no. 8 (2003): 951-958.

[33] Park, Jonghyun, Nguyen Trung Kien, and Gueesang Lee. "Optic disc detection in retinal images using tensor voting and adaptive mean-shift." In 2007 IEEE International Conference on Intelligent Computer Communication and Processing, pp. 237-241. IEEE, 2007.

[34] Khalid, Noor Elaiza Abdul, Noorhayati Mohamed Noor, and Norharyati Md Ariff. "Fuzzy c-Means (FCM) for Optic Cup and Disc Segmentation with Morphological Operation." Procedia Computer Science 42 (2014): 255-262.

[35] Walter, Thomas, and Jean-Claude Klein. "Segmentation of color fundus images of the human retina: Detection of the optic disc and the vascular tree using morphological techniques." In International Symposium on Medical Data Analysis, pp. 282-287. Springer Berlin Heidelberg, 2001.

[36] Zhu, Xiaolu, Rangaraj M. Rangayyan, and Anna L. Ells. "Detection of the optic nerve head in fundus images of the retina using the hough transform for circles." Journal of digital imaging 23, no. 3 (2010): 332-341.

[37] Aquino, Arturo, Manuel Emilio Gegúndez-Arias, and Diego Marín. "Detecting the optic disc boundary in digital fundus images using morphological, edge detection, and feature extraction techniques." IEEE transactions on medical imaging 29, no. 11 (2010): 1860-1869.

[38] Carmona, Enrique J., Mariano Rincón, Julián García-Feijoó, and José M. Martínez-de-la-Casa. "Identification of the optic nerve head with genetic algorithms." Artificial Intelligence in Medicine 43, no. 3 (2008): 243-259.

[39] Babu, TR Ganesh, and S. Shenbagadevi. "Automatic detection of glaucoma using fundus image." European Journal of Scientific Research 59, no. 1 (2011): 22-32.

[40] Welfer, Daniel, Jacob Scharcanski, and Diane Ruschel Marinho. "A morphologic two-stage approach for automated optic disk detection in color eye fundus images." Pattern Recognition Letters 34, no. 5 (2013): 476-485.

[41] Xu, Chenyang, and Jerry L. Prince. "Snakes, shapes, and gradient vector flow." IEEE Transactions on image processing 7, no. 3 (1998): 359-369.

[42] Kass, Michael, Andrew Witkin, and Demetri Terzopoulos. "Snakes: Active contour models." *International journal of computer vision* 1, no. 4 (1988): 321-331.

[43] Xu, Juan, Opas Chutatape, Eric Sung, Ce Zheng, and Paul Chew Tec Kuan. "Optic disk feature extraction via modified deformable model technique for glaucoma analysis." Pattern recognition 40, no. 7 (2007): 2063-2076.

[44] Mittapalli, Pardha Saradhi, and Giri Babu Kande. "Segmentation of optic disk and optic cup from digital fundus images for the assessment of glaucoma." Biomedical Signal Processing and Control 24 (2016): 34-46.

[45] Joshi, Gopal Datt, Jayanthi Sivaswamy, and S. R. Krishnadas. "Optic disk and cup segmentation from monocular color retinal images for glaucoma assessment." IEEE Transactions on Medical Imaging 30, no. 6 (2011): 1192-1205.

[46] Li, Huiqi, and Opas Chutatape. "Boundary detection of optic disk by a modified ASM method." Pattern Recognition 36, no. 9 (2003): 2093-2104.

[47] FENGSHOU, YIN. "Extraction of features from fundus images for glaucoma assessment." PhD diss., National University of Singapore, 2011.

[48] Roerdink, Jos BTM, and Arnold Meijster. "The watershed transform: Definitions, algorithms and parallelization strategies." Fundamenta informaticae 41, no. 1, 2 (2000): 187-228.

[49] Kim, Sun Kwon, Hyoun-Joong Kong, Jong-Mo Seo, Bum Joo Cho, Ki Ho Park, Jeong Min Hwang, Dong-Myung Kim, Hum Chung, and Hee Chan Kim. "Segmentation of optic nerve head using warping and RANSAC." In 2007 29th Annual International Conference of the IEEE Engineering in Medicine and Biology Society, pp. 900-903. IEEE, 2007.

[50] Zhao, Wenyi, Rama Chellappa, P. Jonathon Phillips, and Azriel Rosenfeld. "Face recognition: A literature survey." ACM computing surveys (CSUR) 35, no. 4 (2003): 399-458.

[51] Wong Wing Kee Damon, Jimmy Liu, Tan Ngan Meng, Yin Fengshou, Wong Tien Yin. “Automatic detection of the optic cup using vessel kinking in digital retinal fundus images.” ISBI (2012): pp. 1647-1650.

[52] O. Marques, “Practical image and video processing using Matlab,” IEEE press.

[53] Pardha Saradhi Mittapalli, Giri Babu Kande. “Segmentation of optic disk and optic cup from digital fundus images for the assessment of glaucoma.” Biomedical Signal Processing and Control (2016): pp. 34–46.

[54] Kande Giri Babu, P.V. Subbaiah, T. Satya Savithri. “Unsupervised fuzzy based vessel segmentation in pathological digital fundus images.” J. Med. Syst. (2010): pp. 849–858.

[55] S. Kavitha, K. Duraiswamy. “An efficient decision support system for detection of glaucoma in fundus images using ANFIS.” International Journal of Advances in Engineering & Technology, (2012): vol. 2, pp. 227-240.

[56] K. Narasimhan, Dr. K. Vijay Arekha, “An efficient automated system for glaucoma detection using fundus image”. Journal of Theoretical and Applied Information Technology, vol. 33, pp. 104-110, 2011.

[57] Y. Hatanaka, A. Noudo, C. Muramatsu. “Automatic measurement of cup to disc ratio based on line profile analysis in retinal images.” 33rd Annual International Conference of the IEEE EMBS, USA. (2011): pp. 3387-3390.

[58] S. Kavitha, S. Karthikeyan, Dr. K. Duraiswamy,”Early detection of glaucoma in retinal images using cup to disc ratio.” Second International Conference on Computing, Communication and Networking Technologies, 2010.

[59] A. Poshtyar, J. Shanbehzadeh, H. Ahmadieh. ”Automatic measurement of cup to disc ratio for diagnosis of glaucoma on retinal fundus images.” 6th International Conference on Biomedical Engineering and Informatics BMEI (2013): pp. 24-27.

[60] Fingeret M, Medeiros FA, Susanna Jr R, Weinreb RN. “Five rules to evaluate the optic disc and retinal nerve fiber layer for glaucoma.” Optometry (2005): Vol 76: pp. 661-668.

[61] Tan N, Liu J, Lim J, Zhang Z, Lu S, Li H. “Automatic detection of pathological myopia using variational level set.” 31st Annual International Conference of the IEEE Engineering in Medicine and Biology Society. (2009): pp.3609–12.

[62] Muramatsu C, Hatanaka Y, Sawada A, Yamamoto T, Fujita H. “Computerized detection of peripapillary chorioretinal atrophy by texture analysis.” Conference Proceedings IEEE Engineering in Medicine and Biology Society. (2011): pp. 5947–50.

[63] Smola A, Vishwanathan S. Introduction to Machine Learning. Cambridge, United Kingdom: Cambridge University Press; (2008).

[64] Prageeth, P.G, David J, and A. Sukesh Kumar. "Early Detection of Retinal Nerve Fiber Layer Defects Using Fundus Image Processing." *2011 IEEE Recent Advances in Intelligent Computational Systems* (2011): p. 930-935.

[65] Dua S, Acharya UR, Chowriappa P, Sree SV. Wavelet-based energy features for glaucomatous image classification. IEEE Transactions on Information Technology in Biomedicine 2012: pp. 80–87.

[66] Jan Odstrcilik, Radim Kolar, Ralf-Peter Tornow, Jiri Jan, Attila Budai.” Thickness related textural properties of retinal nerve fiber layer incolor fundus images.” Computerized Medical Imaging and Graphics 38 (2014): 508–516.

[67] Dharmanna lamani, T. C. Manjunath, Mahesh M., Y. S. Nijagunarya.” Early detection of glaucoma through retinal nerve fiber layer analysis using fractal dimension and texture feature.” International Journal of Research in Engineering and Technology, vol 03 (2014): p. 158-163.

[68] Bock, Rüdiger, Jörg Meier, László G. Nyúl, Joachim Hornegger, and Georg Michelson. "Glaucoma risk index: automated glaucoma detection from color fundus images." Medical image analysis 14, no. 3 (2010): 471-481.

[69] Meier, Jörg, Rüdiger Bock, Georg Michelson, László G. Nyúl, and Joachim Hornegger. "Effects of preprocessing eye fundus images on appearance based glaucoma classification." In International Conference on Computer Analysis of Images and Patterns, pp. 165-172. Springer Berlin Heidelberg, 2007.

[70] Bock, Rüdiger, Jörg Meier, Georg Michelson, László G. Nyúl, and Joachim Hornegger. "Classifying glaucoma with image-based features from fundus photographs." In Joint Pattern Recognition Symposium, pp. 355-364. Springer Berlin Heidelberg, 2007.

[71] M. Ortega, M.G. Penedo, J. Rouco, N. Barreira, and M.J. Carreira, “Retinal verification using a feature points-based biometric pattern”, EURASIP J. Adv. Signal Process, pp. 1-13, 2009.

[72] Z.W. Xu, X.X. Guo, X.Y. Hu, X. Chen, and Z.X. Wang, “The identification and recognition based on point for blood vessel of ocular fundus”, In Proc. ICB 2006 LNCS 3832, pp. 770-776, 2006.

[73] K. Fukuta, T. Nakagawa, Y. Hayashi, Y. Hatanaka, T. Hara, H. Fujita, "Personal Identification Based on Blood Vessels of Retinal Fundus Images", Proc. of SPIE 6914, 2008.

[74] Sana Qamber, Zahra Waheed, Usman Akram, "Personal Identification System Based on Vascular Pattern on Human Retina", Biomedical Engineering Conference, pp. 64-67, 2012.

[75] L. Gagnon, M. Lalonde, M. Beaulieu, "Fast and robust optic disc detection using pyramidal decomposition and Hausdorff-based template matching," IEEE Trans. Med. Imaging 11, pp.1193–1200, 2011.

[76] N. M. Noor, N. E. A. Khalid, N. M. Arif, "Optic cup and disc color channel multi thresholding segmentation," IEEE International Conference on Control System, Computing and Engineering, pp. 530-534, 2013.

[77] Sushma G. Thorat, Prof Savita Raut, "Detecting the optic disc and optic cup boundary for glaucoma screening: A review" IJRITCC, vol. 2, pp. 372-375, 2014.

[78] S. Liu, J. Chen, "Detection of the optic disc on retinal fluorescein angiograms," J. Med. Biol. Eng, pp. 405–412, 2011.

[79] A. Issac, M. Parthasarthi, M. K. Dutta, "An adaptive threshold based algorithm for optic disc and cup segmentation in fundus images," 2nd International Conference on Signal Processing and Integrated Networks (SPIN), pp. 144-147, 2015.

[80] T. Yu, Y. M. Ma, W. Li, "Automatic localization and segmentation of optic disc in fundus image using morphology and level set," 9th International Symposium on Medical Information and Communication Technology (ISMICT), pp. 195-199, 2015.

[81] Matlab user's guide on "Image processing toolbox," Matlab ver. 7.12.0.635 (R2011a).

[82] Akram, M. Usman, and Shoaib A. Khan. "Multilayered thresholding-based blood vessel segmentation for screening of diabetic retinopathy." Engineering with computers 29.2 (2013): 165-173.

[83] McInerney, Tim, and Demetri Terzopoulos. "Deformable models in medical image analysis." In *Mathematical Methods in Biomedical Image Analysis, 1996., Proceedings of the Workshop on*, pp. 171-180. IEEE, 1996.

[84] Mendels, F., C. Heneghan, P. Harper, R. Reilly, and J. Thiran. "Extraction of the optic disk boundary in digital fundus images." Proceedings BMES/EMBS 1999 2, no. EPFL-CONF-86620 (1999): 1139.